The University of Manchester
School of Mechanical, Aerospace and Civil Engineering

EXPERIMENTAL INVESTIGATIONS ON SOOTY FLAMES AT ELEVATED PRESSURES

A thesis submitted to the University of Manchester for the degree of

Doctor of Philosophy

in the Faculty of Engineering and Physical Sciences

2010

Hamidreza Gohari Darabkhani

School of Mechanical, Aerospace and Civil Engineering

LIST OF CONTENTS

Final Word Count: 52,340

LIST OF FIGURES

LIST OF TABLES

ABSTRACT

This study addresses the influence of elevated pressures, fuel type, fuel flow rate and co-flow air on the flame structure and flickering behaviour of laminar oscillating diffusion flames. Photomultipliers, high speed photography and schlieren, accompanied with digital image processing techniques have been used to study the flame dynamics. Furthermore, the effects of pressure on the flame geometry and two-dimensional soot temperature distribution in a laminar stable diffusion flame have been investigated, utilising narrow band photography and two-colour pyrometry technique in the near infra-red region. This study provides a broad dataset on the diffusion (sooty) flame properties under pressures from atmospheric to 16 bar for three gaseous hydrocarbon fuels (methane, ethylene and propane) in a co-flow burner facility.

It has been observed that the flame properties are very sensitive to the fuel type and flow rate at elevated pressures. The cross-sectional area of the stable flame shows an average inverse dependence on pressure to the power of n, where n was found to be 0.8 ± 0.2 for ethylene flame, 0.5 ± 0.1 for methane flame and 0.6 ± 0.1 for propane flame. The height of a flame increases firstly with pressure and then decreases with further increase of pressure. It is observed that the region of stable combustion was markedly reduced as pressure was increased. An ethylene flame flickers with at least three dominant modes, each with corresponding harmonics at elevated pressures. In contrast, methane flames flicker with one dominant frequency and as many as six harmonic modes at elevated pressures. The increase in fuel flow rate was observed to increase the magnitude of oscillation. The flickering frequency, however, remains almost constant at each pressure. The dominant flickering frequency of a methane diffusion flame varies with the chamber pressure as $f=15.7P^{0.17}$.

It has been observed that the flame dynamics and stability are also strongly affected by the co-flow air velocity. When the co-flow velocity reached a certain value, the buoyancy driven flame oscillation was completely suppressed. The schlieren imaging has revealed that the co-flow of air is able to push the initiation point of outer toroidal vortices beyond the visible flame to create a very stable flame. The oscillation frequency was observed to increase linearly with the air co-flow rate, a, as $f=0.33a+11$.

The soot temperature results obtained by applying the two-colour method in the near infra-red region shows that in diffusion flames the overall temperatures decrease with increasing pressure. It is shown that the rate of temperature drop is greater for a pressure increase at lower pressures in comparison with higher pressures.

DECLARATION

No portion of the work referred to in the dissertation has been submitted in support of an application for another degree or qualification of this or any other university or other institute of learning;

COPYRIGHT STATEMENT

i. The author of this thesis (including any appendices and/or schedules to this thesis) owns certain copyright or related rights in it (the “Copyright”) and s/he has given The University of Manchester certain rights to use such Copyright, including for administrative purposes.

ii. Copies of this thesis, either in full or in extracts and whether in hard or electronic copy, may be made only in accordance with the Copyright, Designs and Patents Act 1988 (as amended) and regulations issued under it or, where appropriate, in accordance with licensing agreements which the University has from time to time. This page must form part of any such copies made.

iii. The ownership of certain Copyright, patents, designs, trade marks and other intellectual property (the “Intellectual Property”) and any reproductions of copyright works in the thesis, for example graphs and tables (“Reproductions”), which may be described in this thesis, may not be owned by the author and may be owned by third parties. Such Intellectual Property and Reproductions cannot and must not be made available for use without the prior written permission of the owner(s) of the relevant Intellectual Property and/or Reproductions.

iv. Further information on the conditions under which disclosure, publication and commercialisation of this thesis, the Copyright and any Intellectual Property and/or Reproductions described in it may take place is available in the University IP Policy in any relevant Thesis restriction declarations deposited in the University Library, The University Library’s regulations and in The University’s policy on presentation of Theses.

THE AUTHOR

The author graduated from Amirkabir University of Technology in 1997 with a first-class Bachelor of Science (B.Sc.) honours degree in Mechanical Engineering (Thermo-Fluids). His final project was industry-based, working on design and optimisation of the cooling towers with contra-flow. The author then started a Master of Science (M.Sc.) at the same university in 1998 and obtained his degree with Distinction in Aerospace Engineering (Propulsion Systems) in 2001. Through his Master courses and the final project, he gained a broad knowledge of combustion in gas turbines and propulsion systems. Since obtaining his first degree, the author has also greatly benefited from more than 7 years work experience in industry.

He was awarded a fully funded PhD research scholarship in 2006 from the School of Mechanical, Aerospace and Civil Engineering (MACE), the University of Manchester. He has successfully investigated the effects of elevated pressures, fuel type and flow rate and also co-flow air on combustion dynamics and instabilities, as well as soot temperature and concentration. The author received the Best Research Presentation Award and the Runner-up Research Poster Prize, awarded by the School of MACE and British Petroleum (BP), at the Postgraduate Research Conference in 2009.

The present PhD research is directly related to problems currently faced by the energy industry and in combustion systems; where elevated pressures and variable fuel and air flow rates lead to combustion instabilities and enhancement in soot formation, which are yet to be fully understood.

DEDICATION

*"Have you considered the **fire** which you kindle? Is it you who made the tree therefore to grow (for firewood), or are We the Grower? We have granted it as reminder and an article of use for the travellers in the wilderness (and all the others, in this world). Then glorify with praises the Name of your Lord, the Most Great."*

Holly Quran, Chapter 56 - Verses 71 to 74

Dedicated To My Lovely Family

ACKNOWLEDGEMENTS

First and foremost, I thank almighty Allah for answering my every prayer and for granting me the grace to see this research work to complete fruition.

I would also like to thank my supervisor, Prof. Yang Zhang for his encouragement, patience and invaluable advice during the course of this programme. I am also thankful for the moral courage and financial assistance, which I received from him during last four years.

The PhD research scholarship awarded by the School of Mechanical, Aerospace and Civil Engineering, the University of Manchester is gratefully acknowledged. I would also like to thank all those academic and support staff in the School of MACE who helped me with my questions and problems.

I especially want to thank my dear wife, Arezoo, for all her love, friendship, never-ending patience and for believing in me. My daughter, Zahra, and my son, Ali, you have truly been my motivation for achieving a better life full of prosperity, happiness and spirituality.

I am deeply indebted to my parents Mr. & Mrs. Gohari Darabkhani for their continued prayers and patronage all through my study years. Indeed, your self-sacrifice and support opened up the path of learning to me. Also I would like to thank my father and mother in law Mr. & Mrs. Akhoundzadeh for their continuous support and prayers.

My warm appreciation goes to my brother, Mohammadreza, and my sisters, Leila and Narges, for their heartening words and well wishes. One important thing I've learnt in my educational years and would like to share with you is that success is not a result of spontaneous combustion. You must set yourself on fire!

Last but not least, special thanks must also go to my colleagues who have been very helpful over the course completing this research, amongst whom are: Dr. Jason Bassi, Dr. Anthony Ehi-Uujamhan, Dr. Sarmad Yaqub, Dr. Kenny Cheung, Dr. Kevin Huang, Dr. Zoe Yoka, Dr. Bassam Rakhshani, Dr. Parham Momeni, Dr. Ahmed Zaki, Dr. Mark Jabbal, Jizhao, Qian, Amr, Robert, Amir, Hossein, Craig, Tohid, Rasool, Mahyar and Sadiq. Thanks a lot mates.

NOMENCLATURE

Roman Symbols:

a	Co-flow air flow rate (standard litres per minute, slpm)
A_{cs}	Cross-sectional area of the flame
b	Flame width
C	Parameter which is defined as; $C=16m^2R^2T^2/\pi^2d^5$
C_1	Planck's first constant ($C_1=3.74177\times10^{-16}$ W m^2)
C_2	Planck's second constant ($C_2=1.438775\times10^{-2}$ K m)
D	Burner diameter (in meters)
d_a	Air exit diameter (mm)
Da	Damköhler number (reaction rate/convective mass transport rate)
d_f	Fuel nozzle exit diameter (mm)
D_H	Hydraulic diameter (for an annulus geometry is equal with the subtraction of outer and inner diameters (Do-Di)
dI	The differences between maximum and minimum of mean pixel intensity in a full cycle of high speed images.
D_{ij}	Binary diffusion coefficient (molecular diffusivity)
f	Frequency of flame flicker or frequency of vortex shedding
Fr	Froude number
fv	Soot volume fraction
g	Gravitational acceleration (9.81 m/s^2)
H_f	Flame height (length) or height of stabilised flame (mm)
$I_\lambda{}^b$	Monochromatic blackbody radiant intensity (W/m^2/μm)
I_λ	Monochromatic radiant intensities at wavelength λ (W/m^2/μm)
I_780	Intensity of flame images taken by applying 780 nm filter
I_1064	Intensity of flame images taken by applying 1064 nm filter
k	Instrument constant
L	Optical path length
L_f	Flame oscillation magnitude
m	Fluid (fuel or air) mass flow rate
m_{air}	Air mass fraction
m_{fuel}	Fuel mass fraction
P	Pressure (ambient or chamber)
R	Gas constant

R	The ratio of intensities at two wavelengths ($I_{\lambda 2}/ I_{\lambda 1}$)
Re	Reynolds number
S	Instrument factor ($S_{\lambda 1}/ S_{\lambda 2}$), for calibration of the optical setup
S_λ	Spectral sensitivity of the imaging system
St	Strouhal number
T	Soot temperature (K)
T_{FS}	Maximum temperature at flame surface (K)
U	Fuel or air mean jet exit velocity (m/s)
Y_F	Mass fraction of fuel
Y_{Ox}	Mass fraction of oxidiser
Y_{Pr}	Mass fraction of combustion products
z	Height above the fuel nozzle exit

Greek Symbols:

ε_λ	Emissivity of soot at wavelength of λ ($0 \leq \varepsilon_\lambda \leq 1$)
ε_λ^b	Emissivity blackbody as a perfect emitter (is equal one)
σ	Standard deviation of mean pixel intensity obtained from high speed images
λ	Wavelength of the radiation (µm)
λ	Flame oscillation wavelength (mm)
γ	Air to fuel velocity ratio (stability controlling parameter)
ρ	Fluid (fuel or air) density
Φ	Equivalence ratio

Subscripts

a	Air stream
ave	Average value of a quantity
b	Blue part of a flame
cs	Cross-section
f	Fuel stream / Flame
FS	Flame Surface
i,j	Binary coefficient
max	Maximum value of a quantity
min	Minimum value of a quantity
Ox	Oxidiser

Pr	Combustion Products
stoic	Stoichiometric conditions
v	Volume fraction

Superscripts

b	Blackbody
n	Pressure exponent (dependence on pressure to the power of *n*)

Abbreviations:

a.u.	Arbitrary unit
BS	Beam Splitter
CCD	Charge-Coupled Device
CEAS	Council of European Aerospace Societies
CH_4	Chemical formula of Methane fuel
C_2H_4	Chemical formula of Ethylene fuel
C_3H_8	Chemical formula of Propane fuel
C_2*	C_2 combustion free radical (spectral wavelength of 516 nm)
CH*	CH combustion free radical (spectral wavelength of 430 nm)
CMOS	Complimentary Metal-Oxide Semiconductor
CN*	Carbon-Nitrogen free radical
CO	Chemical formula of carbon monoxide
CO_2	Chemical formula of carbon dioxide
CST	Combustion Science and Technology (Journal)
D	Dimension (One, 2 or 3 dimensional)
DAQ	Data Acquisition (card)
DC	Direct Current
DF	Diffusion Flame
F	Filter (narrow-band interference type)
FFT	Fast Fourier Transform
H_2O	Chemical formula of water vapour
HCO	hydrogen/carbon monoxide
HRFZ-Si	High-resistivity Float-zone silicon
HSV	Hue, Saturation and Value
Hz	Hertz (standard unit of frequency)
ISO	Camera light sensitivity

LADF	Laminar Annular Diffusion Flame
LCDF	Laminar Co-flow Diffusion Flame
LDA	Laser Doppler Anemometry
LDV	Laser Doppler Velocimetry
LIF	Laser Induced Fluorescence
LII	Laser Induced Incandescence
LOSA	Line Of Sight Attenuation
LSM	Laser Scattering of Molecules
LST	Laser Sheet Tomography
MPa	Megapascal (SI unit of pressure, 1 MPa is equal to 10 bar)
MPI	Mean Pixel Intensity of high-speed images
ms	Millisecond (1/1000 of a second)
NH_3	Chemical formula of Ammonia
NH_x	Gaseous Compounds of Nitrogen and Hydrogen
NIR	Near Infera-Red spectrum
OH*	OH (hydroxyl) combustion active radical (at wavelength of 308 nm)
PD	Photodiode
PIV	Particle Image Velocimetry
PLIF	Planar Laser Induced Fluorescence
PM	Photomultiplier
ppm	Part per million
psia	Pounds-force per square inch absolute (14.7 psia=1.01 bar)
Re	Reynolds number
RGB	Red, Green and Blue (the primary colour intensities)
rms	Root mean square of fluctuations
scc/s	Standard cubic centimetres per second
slpm	Standard litres per minute (L/min)
SLR	Single-Lens Reflex
SSE	Soot Spectral Emission
STP	Standard conditions for Temperature and Pressure
THz-TDS	Terahertz Time-domain Spectroscopy
VI	Virtual Instrument (LabVIEW software)

PUBLICATIONS

Journal Papers

1. Gohari Darabkhani, H., and Zhang, Y., "Methane Diffusion Flame Dynamics at Elevated Pressures," *Journal of Combustion Science and Technology (CST)*, Vol. 182, No. 3, pp. 231-251, 2010.
2. Gohari Darabkhani, H., Bassi, J., Huang, H. W., and Zhang, Y., "Fuel Effects on Diffusion Flames at Elevated Pressures," *Journal of Fuel*, Vol. 88, No. 2, pp. 264-271, 2009.
3. Gohari Darabkhani, H., Wang, Q. and Zhang, Y., "Impact of Co-flow Air on Buoyant Diffusion Flames Flicker," Submitted to the journal of *Energy Conversion and Management (ECM)*, 2010 (under review).
4. Wang, Q., Gohari Darabkhani, H., and Zhang, Y., "Schlieren and Laser Sheet Investigation of Methane-air Co-flow Flames," submitted to the journal of *Experiments in Fluids*, 2010 (under review).

Conference Papers

1. Gohari Darabkhani, H., and Zhang, Y., "Suppression Dynamics of a Laminar Oscillating Diffusion Flame with Co-flow Air," accepted for publication in the *Proceedings of the World Congress on Engineering (WCE 2010)*, Imperial College London, UK, 30 June - 2 July, 2010 (The paper has also been recommended by reviewers for the special issue of IAENG Journal and the Best Paper Awards competition).
2. Gohari Darabkhani, H., and Zhang, Y., "Pressure Effects on Structure and Temperature Field of Laminar Diffusion Flames," *Proceedings of 48th AIAA Aerospace Sciences Meeting*, Paper No.: AIAA-2010-779, No. of Pages: 17, Orlando, Florida, USA, 4-7 January 2010.
3. Gohari Darabkhani, H., and Zhang, Y., "Impact of Pressure and Fuel Flow Rate on Flame Dynamics in a High Pressure Combustor," *Proceedings of CEAS 2009 European Air and Space Conference*, Conference DVD, Day2-Propulsion Session, Manchester, UK, 26-29 October 2009.
4. Gohari Darabkhani, H., and Zhang, Y., "Methane Diffusion Flame Dynamics at Elevated Pressures," *PGR-MACE09 Conference*, Book of Abstracts, pp. 12-13, The University of Manchester, UK, 11th June 2009, (Winner of the best presentation award).

5. Bassi, J., Gohari Darabkhani, H., Huang, H.W., and Zhang, Y., "Diffusion Flame Dynamics at Elevated Pressures," *32nd International Symposium on Combustion*, Abstracts of Accepted Papers, pp. 82, Montreal, Canada, 3-8 August 2008.
6. Gohari Darabkhani, H., and Zhang, Y., "Experimental Investigation on Sooty Flames at Elevated Pressures,"*PGR-MACE08 Conference*, Book of Abstracts, pp. 22, The University of Manchester, UK, 27th June 2008.

Poster presentations

1. Gohari Darabkhani, H., and Zhang, Y., "Impact of Pressure on Diffusion Flame Structure," *PGR-MACE09 Conference*, Book of Abstracts, pp. 75, The University of Manchester, UK, 11th June 2009, (Winner of the 2nd poster prize).
2. Gohari Darabkhani, and Zhang, Y., "Diffusion Flame Dynamics at Elevated Pressures," *PGR-MACE08 Conference*, Book of Abstracts, pp. 30, The University of Manchester, UK, 27th June 2008.
3. Gohari Darabkhani, H., and Zhang, Y., "Experimental Investigation of Sooty Flames at High Pressure," *School of MACE Research Showcase*, The University of Manchester, UK, 21st February 2007.

Other Contributions

1. MACE Research Image Competition, Gohari Darabkhani, H., and Zhang, Y., "Diffusion Flame Dynamics at Elevated Pressures," School of Mechanical, Aerospace and Civil Engineering, The University of Manchester, 11th June 2009.
2. MACE Internal Research Seminars in Fluid Mechanics, Gohari Darabkhani, H., and Zhang, Y., "Fuel Effects on Diffusion Flames at Elevated Pressures," School of Mechanical, Aerospace and Civil Engineering, The University of Manchester, 6th May 2009.
3. MACE Internal Research Seminars in Fluid Mechanics, Gohari Darabkhani, H., and Zhang, Y., "Experimental Investigations on Sooty Flames at Elevated Pressures," School of Mechanical, Aerospace and Civil Engineering, The University of Manchester, 6th February 2008.

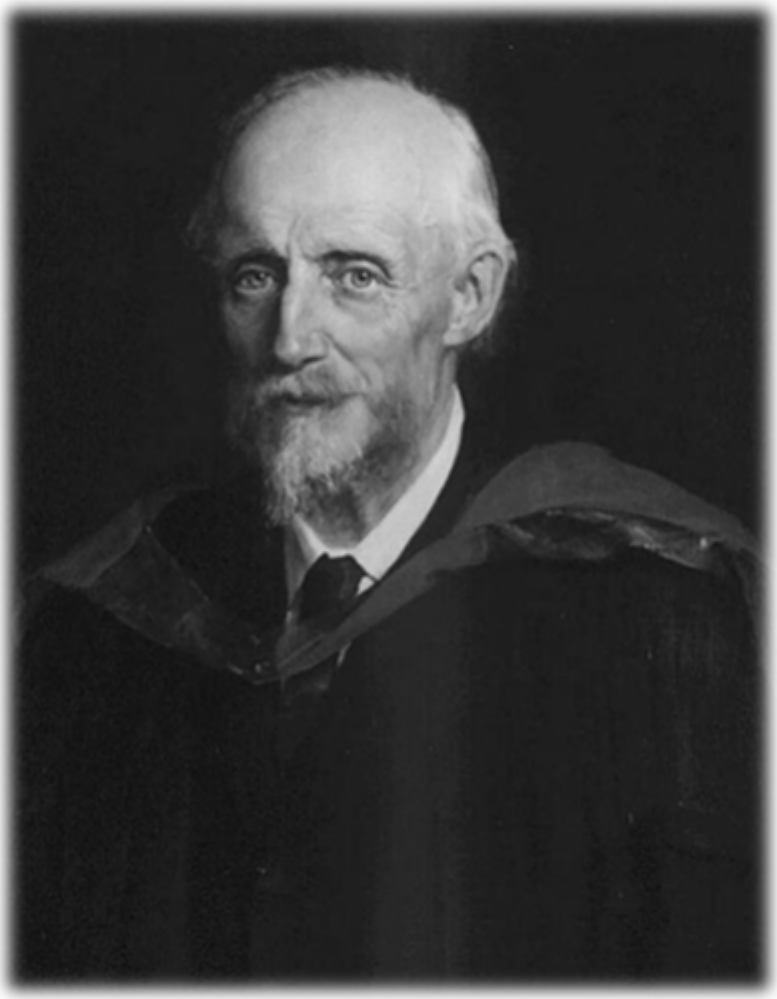

Osborne Reynolds (1842-1912)

"Diffusion flames have received less attention than premixed flames in fundamental research, despite the fact that diffusion flames are more frequently used industrially."

A. G. Gaydon (1911–2004)

CHAPTER 1

INTRODUCTION

1.1 BACKGROUND

Today, combustion still provides most of the energy consumed in the world. Despite the continuing search for alternative energy, the use of combustion fuels will remain important for a considerable time to come. This is especially the case where energy is required in the form of “compact energy”, as in transport; from the jet engine to the internal combustion engine [1]. Thus, there is an urgent need to understand the subtle processes of combustion to increase the efficiency of combustors and to control their pollutants specifically, soot particles and carbon dioxide. The study of combustion processes is difficult because of the complex interactions between the fluid dynamics and the chemistry [2]. However, the understanding of combustion has been enhanced considerably by studies on laminar diffusion flames based on atmospheric conditions.

Diffusion flames are desirable in practical systems from the safety aspects, but they generally have inferior pollutant emission characteristics. This is due to the

stoichiometric combustion and long residence times involved [3]. In combustion, a diffusion (non-premixed) flame is a flame in which the oxidiser combines with the fuel by diffusion. As a result, the burning rate is limited by the rate of diffusion. Diffusion flames tend to produce more soot because there may not be sufficient oxidiser for the reaction to go to completion. In contrast, a premixed flame is a flame in which the oxidiser has been mixed with the fuel before it reaches the flame front. In comparison with diffusion flames, the clear premixed flames have a higher effective temperature and are relatively free from sooting troubles [4]. The soot particles typically produced in a diffusion flame become incandescent from the heat of the flame and provide the readily identifiable orange-yellow colour of these flames. The formation and emission of soot by combustion processes pose problems which have long concerned scientist and engineer alike. Soot emission from engines and turbines reflects poor combustion conditions and a loss of efficiency. However, it has to be noted that soot could also be beneficial in the case of furnaces and boilers where the mechanism of propagation often involves radiant transfer from hot soot particles to the circulating fluids. In such cases, soot particles should be oxidised before they leave the furnace [5]. Soot is also purposefully created in the form of carbon black for use in the manufacturing of paints, tires, and other goods [6]. It means soot can be both beneficial and problematic; therefore, a complete understanding of soot formation and oxidation is crucial for a better control of its presence, from which combustion systems can greatly improve [7].

Since increasing efficiency in modern turbines and internal combustion engines requires the need for higher operating pressures it becomes all the more apparent to further investigate combustion at higher pressures. However, increasing pressure increases the formation of soot particles and enhances the flame instabilities. Current understanding of the influence of pressure on instability behaviour and thermo-physical properties of sooty diffusion flames is still limited [8-10].

The first systematic scientific observations of flame phenomena date back to the early 19th century. Michael Faraday made observations of a candle flame, which were published in his famous book entitled “The Chemical History of a Candle” [11]. Faraday believed that everything could be well understood if it could be directly observed. It is this train of thought which drives the current motivation to understand the array of combustion related problems through direct observation by optical diagnostic techniques. Optical diagnostics are divided into two major categories: active and passive diagnostics; the former rely on self illumination (such as the flame) and the latter requires an illumination source (such as light or laser) [12].

Since the early 1980s laser diagnostic methods have been developed, and are still under development, as tools which can be used to obtain information on the physical and chemical structure of various types of flame. Classical experimental methods which are invasive in nature, such as the use of thermocouple and gas-sampling probes are unlike the laser diagnostic methods which provide quantitative information without physical intrusion and disturption to the combustion process. Laser diagnostic methods also have their limits under high pressure conditions, when soot density increases up to a point where a laser beam cannot penetrate [13]. In addition these methods are complex to use and much more expensive than the direct imaging and light emission measurement techniques.

Using active optical diagnostics methods such as; direct imaging, high speed imaging and schlieren photography accompanied with image processing techniques, in addition to light emission measurements (e.g. Chemiluminescence) enable us to study the structure and dynamics of the flame. Narrow band photography and two-colour pyrometry also provide quantitative data on the soot temperature distribution. These non-intrusive techniques provide us with the properties of sooty flames at different flow and pressure conditions, with high reliability and comparatively low cost.

Chemiluminescence (using photomultipliers) is the generation of electromagnetic radiation in the form of light, by release of energy from a chemical reaction, e.g. in flame. The amount of radiation observed in the flame at a particular wavelength is proportional to the concentration of the associated excited molecule. Thus, the measurement of the radiation can be directly related to the concentration of the excited molecule. Concentration and light emission of combustion species are also linked to the oscillation (flickering) behaviour of the flame. Therefore, a reliable well understood measurement of chemiluminescence could provide quantitative insight into the details of the diffusion flame combustion process and dynamics. It has therefore received renewed attention recently as a possible means of measuring oscillation frequency in unstable combustion systems [10, 14].

1.2 MOTIVATION

The knowledge about steady-state laminar diffusion flames has progressed rapidly over the last few years. This includes the modelling and measurement of different aspects, like soot concentration and temperature distribution. Practical combustion devices, however, often operate under unsteady conditions. Laminar oscillating flames provide an opportunity to take advantage of the repeatability of the oscillations from cycle to cycle in investigating the phenomena of unsteady combustion [15]. They also demonstrate a wide range of time-dependent flame/vortex sheet interactions. The flickering of a laminar diffusion flame is known to be caused by the interaction of the flame and the vortices both inside and surrounding the flame. An elementary flame-vortex interaction is typically periodic and regular in nature and can therefore be easily characterised. Furthermore, laminar oscillating flames keep their rotational symmetry, which simplifies data analysis and reduces the expenditure of time in numerical studies.

In-depth knowledge of the simultaneous pressure, fuel type and flow rate as well as the co-flow air dependence of laminar diffusion flames are of significant relevance to understanding of the flames behaviour and properties. Many systems, such as diesel engines and gas turbine combustors, operate at high pressures to increase their thermodynamic efficiency and decrease their physical size [16]. Research on laminar diffusion flames at high pressures has been limited to a number of studies focused on the soot and temperature profiles within a stable laminar flame [8, 9, 16-22]. However, only a few experimental studies have been carried out on diffusion flame dynamics at sub-atmospheric and at elevated pressures [23, 24].

Through funding provided by the EPSRC, a high pressure burner facility has been developed over the last few years at the University of Manchester, by Bassi and Zhang [1], offering many research opportunities. The burner is designed for the working pressures up to 20 bar. A laminar co-flow diffusion flame can be produced and stabilised on a nozzle with an exit diameter of 4.5 mm. The gaseous hydrocarbon fuels (methane, ethylene and propane) are supplied from a compressed gas cylinder, regulated by a needle valve and measured by calibrated mass flow meters. The burner has two standard quartz windows for access to the visible and near infra-red (NIR) spectrum and two pure silicone windows which are transparent to the far-infrared spectrum and beyond.

Accurate and reliable measurements of soot temperature in the flame by nonintrusive means are highly desirable to achieve an in-depth understanding of combustion and pollutant formation processes. This study therefore, was initially aimed at investigating the effects of elevated pressure on soot temperature distribution within the stable region, utilising a simple and reliable non-intrusive optical diagnostic method. During the experiments a very marked change was observed in the shape, structure and instability behaviour of the diffusion flame as pressure was increased. The lack of

literature in this field motivated the study of these properties. The major part of this research has, therefore, been focused on the study of oscillating laminar co-flow diffusion flames at elevated pressures and at different co-flow conditions.

A laminar flame may oscillate due to buoyancy induced instabilities and interaction with the outer toroidal vortices. These vortices can be modified by pressure, fuel type, and fuel/air flow rates. The effects of air co-flow velocity are found to be very pronounced on flame dynamics and stabilisation mechanism of an oscillating flame. Interestingly, the literature on the co-flow effects is mainly focused on lifted and turbulent flames. Therefore, the study of co-flow air effects on non-lifted methane laminar oscillating flame was found to be of great interest. Experimentally, the results of changes in the flame structure, oscillation wavelength and magnitude as well as the flickering frequencies are able to present a comprehensive dataset of flickering characteristics of sooty flames.

Moreover, the changes in shape and geometry of the stable laminar flames by pressure can be observed and the empirical relationships between pressure and the cross sectional area of the flame according to the fuel type (methane, ethylene and propane) can be proposed. This information improves our understanding on the effect of pressure on the flame structure in the burners working with the laminar flames at elevated pressures. In order to find the distribution of soot temperature, two-colour pyrometry method in the NIR spectrum is also employed. Although two-colour pyrometry is widely used for luminance material temperature measurements, to the best knowledge of the author, applying two-colour method in the NIR region utilising a commercial camera has not been reported in the existing literature. The soot temperature measurement results will provide qualitative information about the influence of pressure on soot concentration and oxidation since soot emission is linked to soot concentration and soot temperature.

Narrowband and high-speed photography accompanied with image processing techniques, in addition to flame emission measurements and high speed schlieren, will help to enhance the understanding of steady, intermittent and oscillating modes of diffusion flames. An experimental investigation is pursued to gain better understanding on combustion instabilities and soot temperature distribution in diffusion flames at atmospheric and elevated pressures.

1.3 STUDY OBJECTIVES

The present research aims to provide a comprehensive investigation on the effects of elevated pressure, fuel type and flow rate and also co-flow of air on diffusion flame dynamics and stabilities in laminar oscillating diffusion flames. The pressure effects on soot temperature distribution of laminar stable diffusion flame are also investigated utilising a commercial digital camera and two-colour pyrometry in NIR region. The high pressure facility is a gaseous co-flow burner which produces a radially axisymmetric diffusion flame with demonstrated stability at high pressures. The main optical diagnostic techniques applied in this research are as follows: direct imaging, narrow band photography, high-speed photography and schlieren, image processing techniques, photomultipliers (chemiluminescence emission of two important radical, e.g. CH* and C_2* or CH* and OH*), and two-colour pyrometry.

The main objectives of this PhD research study in greater detail have been stated below:

1. To investigate the change in the physical appearance of sooty diffusion flames at elevated pressures. The changes in the general shape of a stable flame (e.g. flame height and cross-sectional area) as pressure increases from atmospheric conditions were aiming to be observed and discussed carefully according to the fuel type: Methane (CH_4), Ethylene (C_2H_4) and Propane (C_3H_8).

2. To critically examine, discuss and trace the effects of elevated pressures on the stability region and flickering behaviour of the laminar co-flow diffusion flames for two fuels; methane and ethylene. The flickering frequencies (f) have been measured at elevated pressures up to 16 bar in order to gain a better understanding of the pressure effects on the flame dynamics.

3. To investigate and analyse the coupling effects of chamber pressure and fuel flow rate on the flickering behaviour of a methane-air diffusion flame. To explore the application of flame subtraction technique and definition of the flame scale parameters in order to measure and discuss the change in the flame boundaries, as well as the flame oscillation wavelength (λ) and magnitude (L_f). Furthermore, analysis of the flickering flame luminosity (emission) parameters, obtained from high-speed images (e.g. mean pixel intensity (MPI) and standard deviation (σ) of MPI), and finally to present an empirical formulation for flickering frequency change by pressure.

4. To examine, discuss and trace the effects of co-flow air velocity on the flickering behaviour of laminar methane diffusion flames. This investigation provides a comprehensive dataset on suppression dynamics of diffusion flames by co-flow air, which was found to be an intact area of research on non-lifted diffusion flames. In this part of the study, high speed schlieren photography is utilised in addition to the chemiluminescence and high speed photography in order to study the interaction locations of the outer toroidal vortices with the visible flame and the surrounding hot plume of gases. The study of the flame oscillation wavelength (λ) and magnitude (L_f) as well as the flickering frequencies can help gain a better insight into the effects of co-flow air on unstable and stabilised flames.

5. To determine two-dimensional soot temperature distribution in a stable ethylene laminar diffusion flame based on two-colour measurement of the emission of NIR radiation by soot particles. Theoretical background, discreet considerations in the choice of two narrow band filters and calibration of the instrument factor needs to be described. NIR region has been chosen due to less gas molecules or free radicals radiation in the selected wavelengths in this spectrum, as well as non-saturated photos and the relative novelty of the approach. Study of temperature distribution plays a significant role in understanding the flame properties at elevated pressures.

It is expected that a significant understanding of combustion at high pressure and sooty conditions could be gained from cross-correlating the obtained data through this PhD research study.

1.4 OUTLINE OF THESIS

This thesis consists of seven chapters with a nomenclature at the beginning and list of references and the appendix at the end. The majority of the results in this research study have been published in peer-reviewed journals and conference proceedings or are presently under peer review.

Chapter 1 delineates the background, motivation, objectives and the outlines of the thesis.

Chapter 2 is the literature review, which first reviews the high-pressure studies of sooty diffusion flames and then the literature on the flame dynamics due to change in pressure, fuel type and flow rate and also changes in the co-flow. Finally the related literature on two-colour pyrometry method is summarised. The literatures on flame dynamics and two-colour pyrometry are mainly the reviewed literatures in the published journal or conference papers.

Chapter 3 addresses the experiments and the results of study on the influence of elevated pressures up to 16 bar on the flame geometry and the flickering behaviour of laminar diffusion flames, with particular attention to the effect of fuel type. Methane (CH_4) and Ethylene (C_2H_4) up to 16 bar pressure and Propane (C_3H_8) up to 7 bar pressure were examined and results have been discussed in details. These set of results have been published in the *Journal of Fuel* (Vol. 88, No. 2, pp. 264-271, 2009).

Chapter 4 presents the latest study of the coupling effects of the chamber pressure and fuel flow rate on the flickering behaviour of methane-air diffusion flames over the pressure range of 1 to 10 bar. Photomultipliers and high speed imaging techniques have been used to study the frequency of the flame oscillation. The flame oscillation magnitude (L_f) and oscillation wavelength (λ) were obtained from the high speed imaging database. The standard deviation (σ) of mean pixel intensity (MPI), measured from the flame high speed images, is introduced as a general indicator of the trends of L_f and λ. Finally an empirical formulation for flickering frequency change by pressure was obtained, which was of much interest to the peer reviewers of the published paper in *Journal of Combustion, Science and Technology* (Vol. 182, No. 3, pp. 231-251, 2010) and also in the *proceedings of CEAS 2009 European Air and Space Conference*, (Conference DVD, Day2- Propulsion Session).

Chapter 5 describes the experimental investigation of co-flow air velocity effects on the flickering behaviour of laminar methane-air diffusion flames. In this chapter, high speed schlieren photography was incorporated with high speed photography and chemiluminescence to study the suppression dynamics of diffusion flames with co-flow of air. In four cases of methane flow rates at different co-flow air velocities the global flame shape, the instability initiation point and the frequency and magnitude of the flame oscillation have been characterised. The main set of results with a comprehensive

discussion has been submitted to journal of *Energy Conversion and Management, (ECM),* 2010 (under review). Another part of the results has also been accepted for publication in the *Proceedings of the World Congress on Engineering (WCE),* 2010.

Chapter 6 focuses on the influence of elevated pressures up to 10 bar on two dimensional soot temperature distribution of ethylene-air laminar co-flow diffusion flame. Experimental work was carried out in a high-pressure combustion chamber and two-colour pyrometry technique has been applied in the Near-infrared (NIR) region by utilising a commercial CMOS (Complimentary metal-oxide semiconductor) digital camera. The theoretical background and considerations in the choice of wavelengths and calibration of the instrument factor are also described. The results presented in this chapter have been published in the *Proceedings of 48th AIAA Aerospace Sciences Meeting*, (Paper No.; AIAA-2010-779, No. of Pages; 17).

Chapter 7 broadly summarises the research effort and provides recommendations for future work.

"Everything could be well understood if it could be directly observed."

M. Faraday (1791-1867)

CHAPTER 2

LITERATURE REVIEW

2.1 INTRODUCTION

Considerable amount of literature has been published on laminar diffusion flames at atmospheric pressure but many practical combustion devices operate at high pressures to increase thermodynamic efficiency and to decrease their physical size [16]. Research on laminar diffusion flames at high pressures has been limited to a number of studies focused on the soot and temperature profiles within a stable laminar flame [8, 9, 16-22]. However, only a few experimental studies have been carried out on diffusion flame dynamics and instabilities at sub-atmospheric [23, 24] and at elevated pressures [15].

Since a laminar diffusion sooty flame will be used in this research, some of its fundamental features must be highlighted. Diffusion flame is produced when the fuel and oxidant are not mixed homogeneously prior to the ignition event. Therefore it involves the burning of pure fuel, in the form of a gaseous stream, or liquid or solid surface, along the flame fronts which is in direct contact with the surrounding air. For

small laminar diffusion flame, the burning rate of the combustion process depends on the rate of inter-diffusion between fuel and oxidant. This is to achieve the necessary proportion for reaction to occur along the reaction boundary. Turbulence plays a major role, for large scale diffusion flame, where the additional entrenchment of air due to flame movement would have further impact on the rate of combustion.

The generic shape of a stable laminar annular diffusion flame (LADF) issuing from a standard co-flow burner is depicted in Figure 2-1. The combustion process in the diffusion flame occurs within a very narrow reaction zone. The model of such narrow burning plane is highly idealised. Because of the transfer of heat as well as of mass, considerable amount of reaction occurs on each side of the luminous flame boundary. The general effect is the pyrolysis of fuel and for oxidant to form reactive radicals. Therefore the reactants entering the reaction zone does not correspond to their initial gaseous compositions and states. For this reason, the composition of the gases is non-homogeneous and varies from region to region. The flame front reaction zone, or flame surface, is defined as the surface on which the equivalence ratio is equal to one:

$$\Phi = \frac{(\frac{m_{air}}{m_{fuel}})_{stoic}}{(\frac{m_{air}}{m_{fuel}})} = 1 \qquad 2.1$$

The numerator represents the air-to-fuel mass ratio under stoichiometric conditions and the denominator represents the local air-to-fuel mass ratio. In other words, the flame surface can be described as the locus of points where the fuel and oxidiser meet in stoichiometric conditions. When observing a LADF with the naked eye, the luminous flame boundaries do not exactly correspond to this surface [25].

As fuel flows upwards along the flame axis, it has a tendency to diffuse radially outwards, while the oxidiser has a tendency to diffuse radially inwards [25]. Figure 2-1 (a) shows the radial temperature profile at the indicated height z_1. The flame

is annular in shape, with the maximum temperature (T_{FS}) occurring at the flame surface ($\Phi = 1$). The mass fractions of fuel (Y_F), oxidiser (Y_{Ox}), and combustion products (Y_{Pr}) at the same height are depicted in Figure 2-1 (b). It should be noted that at any radius the sum of the mass fractions must equal unity. Also at the flame surface, the concentration of the combustion products must be at its maximum.

In the upper regions of a vertical flame, buoyancy forces increase the flow velocities; the conservation of mass, therefore, requires the flow streamlines to converge. This causes the flame surface to narrow towards the flame tip [25]. Consequently, the diffusion rate increases in the upper regions of the flame due to the fuel concentration gradient increase (dY_F/dr). This effect can be seen in the differences between Figures 2-1 (b) and (d). Once the tip of the flame surface is reached at height z_3, the maximum temperature occurs on the flame centreline as seen in Figure 2-1 (e). The concentration of fuel in this region is almost zero, as seen in Figure 2-1 (f). For hydrocarbon flames, soot is formed on the fuel side of the reaction zone and is consumed when it flows to the oxidising region [25].

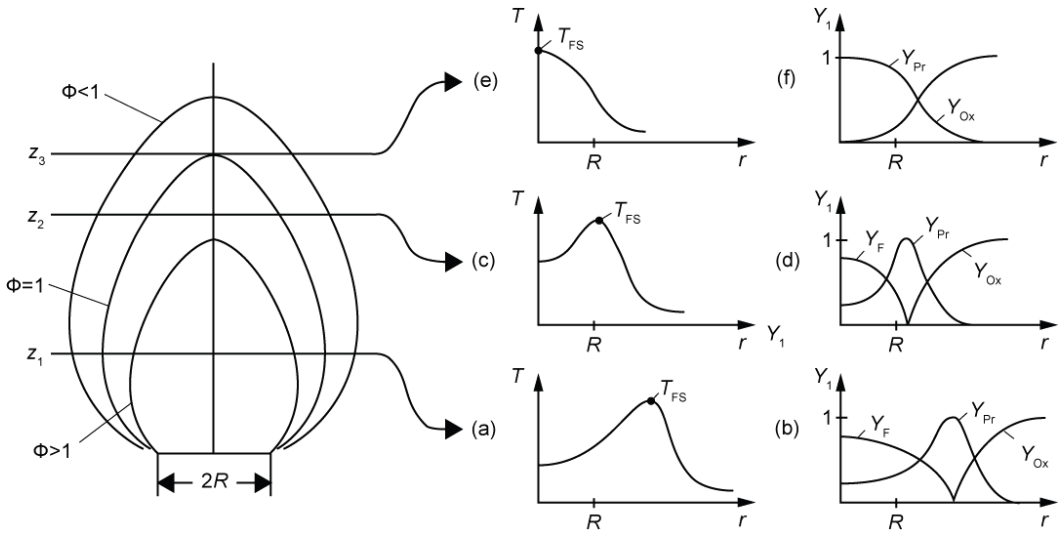

Figure 2-1: Laminar annular diffusion flame characteristics. Profiles of the mass fractions of fuel (Y_F), oxidiser (Y_{Ox}), and combustion products (Y_{Pr}) as well as the maximum temperature at flame surface (T_{FS}), are shown at different heights (z) [25].

This study is aiming to investigate the coupling effects of pressure and fuel type and flow rate and also co-flow effects on laminar diffusion flames (sooty flames) characteristics, utilising the non-intrusive and non-laser optical based techniques. All the non-intrusive optical based combustion diagnostic techniques use almost the same underlying process. Current established based techniques all use electromagnetic radiation in infra-red, visible, or ultraviolet light, which impinges on the molecule or particle under investigation and is scattered or is emitted from the flame itself. For the sake of convenience, most optical techniques for the detection of combustion species have been developed for atmospheric flames. The combustion chambers of many practical devices, however, operate at significantly higher pressures. For high pressure combustion environments, one of the most important limiting factors is the increasing number density of soot. In such environments, modern methods based on optical lasers must contend with broadband absorption and the interference of soot particles [1].

Optical diagnostics are divided into many categories, there are measurements from 1D to 3D also active and passive diagnostics, the former rely on self illumination (such as the flame emission) and the latter requires an illumination source (light or laser). Some of these techniques are matured and commercialised, such as Particle Image Velocimetry (PIV), Laser Doppler Anemometry (LDA) and Laser Induced Fluorescence (LIF) and some of them are in the process of development and maturing, such as Terahertz Time-domain Spectroscopy (THz-TDS) [12].

A summary of the major non-intrusive active and passive optical combustion diagnostic techniques are outlined in Table 2-1. The spectroscopic methods use specific wavelengths for the light source; this wavelength is closely related to the molecule or radical under analysis to obtain quantitative species concentration measurements. For some other optical methods, the exact value of the wavelength is of little importance. However, this does not mean that mono-chromaticity or coherence in the light is not

needed. Interferometry, holography, LDA and many more methods need coherent light to work, but the actual wavelength of the light can be chosen arbitrarily.

Table 2-1: Summary of non-intrusive combustion diagnostic techniques.

Passive diagnostics (using light or laser sources)	**Active diagnostics** (using flame emission)
• Interferometry • Holography • Tomography • Schlieren • Shadowgraphy • Rayleigh Scattering • Mie Scattering • Laser Doppler Anemometry (LDA) • Particle Image Velocimetry (PIV) • Laser Induced incandescence (LII) • Laser Induced Fluorescence (LIF) • Absorption Spectroscopy • Planar Laser Induced Fluorescence (PLIF) • Raman Spectroscopy • Coherent Anti-stokes Raman Spectroscopy (CARS) • THz Time-domain Spectroscopy (THz-TDS)	• Flame Photography • High Speed Photography • Stereo Digital Imaging • Flame Emission Spectroscopy • Narrow Band Photography

Most combustion engines used for transportation and propulsion, as well as power production, operate at pressures approaching (and sometimes exceeding) 10 MPa. For example, current aviation gas turbines operate under conditions approaching 4 MPa [26]. Therefore it is important to have diagnostic methods that work under these harsh conditions. Sooty flames, especially at high pressures, pose a challenging problem to modern laser based combustion diagnostic techniques. At high pressure the soot particles are so dense that the flame looks solid and electromagnetic waves in the visible or infrared spectrum are not able to penetrate the flame [13].

This study seeks to address the diffusion flame dynamics and instability within the flickering region and the soot temperature profile within the stable flame, utilising the active optical diagnostic method. Thus the main focus of this literature survey relies on non-laser based studies on sooty flames. Since the main parameter under investigation is the pressure effects, a review of the high pressure studies of sooty diffusion flames is initially presented to find a broad knowledge on the existing literature at elevated pressures (section 2.2).

Next the studies on diffusion flames structure, dynamics and instabilities are reviewed based on the effects of three different parameters: fuel type, fuel flow rate, and co-flow. The literature reviewed in section 2.3.1 is used for study of fuel effects on diffusion flames at elevated pressures in Chapter 3. The knowledge on jet fuel velocity (flow rate) effects on flame dynamics is summarised in section 2.3.2 to assist investigation on simultaneous pressure and flow rate dependence of laminar diffusion flames in Chapter 4. Subsequently the literature on the co-flow effects on the flickering behaviour of diffusion flames have been reviewed in section 2.3.3 to help study of the flickering suppression in the non-lifted methane diffusion flames in Chapter 5.

Finally the related literature on two-colour pyrometry method and soot temperature measurements within the stable diffusion flames have been presented in section 2.4 to show the novelty of our approach in the soot temperature measurement in Chapter 5.

2.2 HIGH PRESSURE STUDIES OF SOOTY DIFFUSION FLAMES

Diffusion flames tend to produce more soot; since there may not be sufficient oxidiser for the reaction to go to completion. Soot formation and oxidisation modify the flame dynamics and instabilities in the laminar oscillation flames as well as the flame geometry and temperature field in the stable flames. Two competitive processes govern

the soot emitted from the flame; firstly, the formation and growth of soot particles and secondly, the oxidation of these particles. However, the burn out of soot particles becomes more difficult once they grow larger [27]. Early arrest of their growth is essential for the effective suppression of soot emission. In addition, shortening the fuel residence time in the soot-forming region of the flame is also effective [28]. One of the important parameters in soot formation in combustion process is pressure. Current understanding of the influence of pressure on soot formation and oxidation is very limited, despite the fact that the majority of practical combustion devices operate at elevated pressures [9]. Research efforts related to soot formation in flames at high pressures are limited to few studies. Generally speaking, it is believed that, low pressures reduce carbon formation while high pressures promote it [5].

Schalla and McDonald [18] in 1955 investigated variations of smoke points in diffusion flames by pressure, fuel type, external air flow, oxygen enrichment and fuel temperature. The smoke point is defined as the point of incipient non-fully oxidised soot particles breakthrough the flame tip. This mainly occurs because of an increase in soot formation rate while there is a smaller increase in soot oxidation rate. The results obtained by Glassman [29] indicate that flames emit smoke when the soot temperature in the oxidation zone falls below a certain temperature (e.g. 1300 K for a co-flow diffusion ethene flame). The temperature of the soot decreases as the flow proceeds downstream because of radiation losses. According to the results of Schalla and McDonald [18] the rate at which the fuels can be burned smoke free consistently decreases with increasing pressure. They suggested that, the pressure dependence of soot formation is related to species diffusion process since the diffusion coefficient is inversely proportional to pressure.

In 1972 McArragher and Tanon [30], by reviewing the available high pressure studies, emphasised that there is a surprising lack of information on the effect of

pressure on soot formation and the mechanisms leading to it in diffusion, premixed and explosion flames. One reason is that the study of combustion at high pressures is difficult and dangerous, but it is greatly needed in view of pollution problems in practical combustion devices that work at high-pressure [30]. For a continuous flame the main effect of pressure was found an increase in soot formed proportional to P^n, where n was defined a pressure exponent ($1 \leq n \leq 3$). However, the reverse was found to be true for gaseous explosions, as the soot yield decreases with pressure. This is most probably because the combustion products have a greater chance to approach equilibrium. The view was supported that the diffusion flames show a low pressure limit below which soot does not occur, while for premixed flames the critical fuel/air ratio for soot formation is found to be essentially independent of pressure [30].

In 1977, Miller and Maahs [17] designed and constructed a high-pressure flame system for studying the effect of pressure on nitrogen oxide (NO_x) emission, but also obtained data on soot formation. This burner was tested with a confined laminar methane-air diffusion flame over the pressure range from 1 to 50 atm. The methane was issued from a 3.06 mm diameter port concentrically into a stream of air contained within a 20.5 mm diameter chimney. It is reported that, as the combustion pressure was increased, the flame changed in shape from wide and convex to slender and concave, and there was a marked increase in the amount of luminous carbon. The height of the flame was changed only moderately with pressure. However, the region of stable flame was markedly reduced by pressure. Their results showed that at low pressures carbon formation occurs near the tip of the flame. As the pressure increases the region of carbon formation expands, moving downward into the rest of the flame. The carbon concentration was increased by 3 orders of magnitude in the pressure range of $2.5 \leq P \leq 20$ atm; after 20 atm, little change in carbon concentration was noted. They were also employed the method of two-colour pyrometry (in the visible spectrum) for

soot temperature measurement, with the naturally occurring carbon in the flame as the radiant emitter. Because of the much lower carbon-forming tendency of the small methane flames, no meaningful temperature measurements could be made at pressures below 5 atm and by the time this pressure was reached, the concentration of carbon in the flame had dramatically increased, the reaction zone had become thinner and more condensed, and the separate blue zone was no longer evident. Hence, it might be assumed that no significant separate gaseous reaction zone existed and that all important combustion reactions occurred simultaneously within the visible luminous carbon zone. As the temperature of carbon particles is, in fact, a good indication of the true temperature of the flame gases in the vicinity of the carbon particles [31]. Thus from the temperature graphs appears that the overall flame temperature drops by increasing pressure, most significantly at lower pressures. It shows that, the threshold pressure in change of the flame properties exists and needs to be traced in the obtained data of the present research. The high pressure burners used in the recent high-pressure studies [1, 8, 9, 20] including this study are similar to the design of Miller and Maahs [17].

The effect of elevated pressure (from 1.0 to 2.5 atm) on soot formation was investigated in two-dimensional laminar ethylene-air diffusion flames by Flower and Bowman [32] in 1983. The light-scattering technique was employed to determine the soot volume fraction (soot volume/total volume), particle size, and particle number density. The maximum and integrated soot volume fractions were found to increase approximately as the pressure to a power between 1.5 and 2.0 ($P^{1.5-2}$). The soot yield (mass of soot/mass of fuel) however, increased approximately as the pressure to a power between 0.5 and 1.0. There was no significant effect of pressure found on the size of the soot particles, the increase in the soot volume fraction (f_v) resulted mainly from an increase in the number density of particles.

Three years later (in 1986) Flower and Bowman [19] followed the previous study [32] with an examination of laminar diffusion flames of ethylene-air at a pressure range of 0.1 to 1 MPa (1 to 10 bar). They measured the line-of-sight integrated soot volume fractions and the soot temperatures along the flame centreline. It was conclusively shown a pressure scaling of soot maximum integrated volume fraction with an exponent of 1.2±0.1 from atmospheric to 1 MPa. As the pressure was increased, axial flame diameters decreased. It is also noted that the high conversion to soot is not due only to the fuel type but was contributed by the higher mass-flow rates of ethylene as well [19].

In 1989, Flower [33] published a paper in which soot particle temperatures were determined as a function of axial position in axisymmetric laminar ethylene-air diffusion flames at pressures up to 0.7 MPa (7 bar). The temperature measurement was based on line-of-sight measurements of the emission and absorption of near-infrared radiation by soot particles and thus represented average particle temperatures across the diameter of the flame, weighted by the local soot volume fraction. The experimental apparatus for temperature measurement which was used in Flower study [33] is shown in Figure 2-2. Measurements were made at each location with the shutter open and then with the shutter closed to infer the particle brightness and two-colour temperatures. Flower [33] identified that the visible luminosity from soot, which is an increasing function of soot temperature, decays with increasing height in the flames and as the pressure increases. The decrease in soot luminosity suggests that temperature is affected by the presence of soot as a result of radiant energy transfer from the particles. Temperature, in turn, strongly influences soot-formation and soot-oxidation rates.

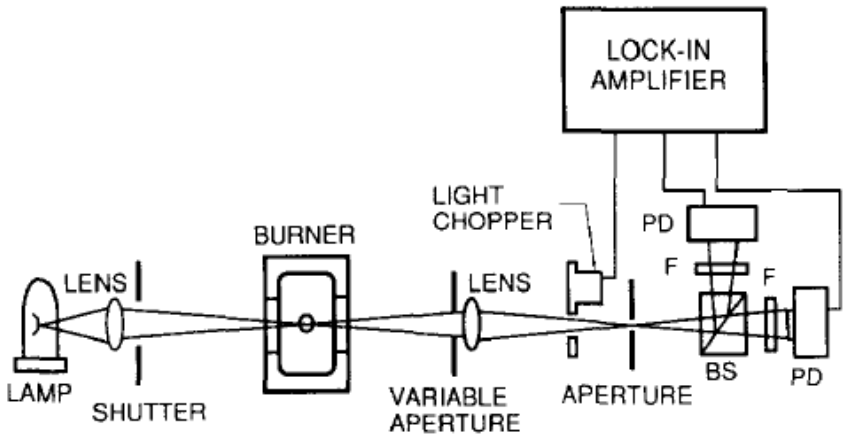

Figure 2-2: Schematic diagram of apparatus used for measuring the temperature of soot particles in a flame by Flower [33] (BS, beam splitter; F, narrow-band interference filter; PD, silicone photodiode).

Lee and Na [34] in 2000, also studied co-flow ethylene-air diffusion flames, performing two-colour pyrometry method in conjunction with an Abel inversion method at pressures up to 0.4 MPa. The soot particle temperature distributions exhibited the reasonable agreement with the flame temperature distributions measured by thermocouples. The measured soot particle temperature showed that the addition of a small amount of air into ethylene did not change the soot particle temperature in soot formation regions. The results indicated a pressure scaling for the maximum integrated soot volume fraction with an exponent of 1.26. The data also imply a square dependence on pressure of maximum local soot volume fraction at a height of 20 mm above the burner rim.

Some of the new high pressure studies [8, 9, 20, 21] reported radially resolved soot concentration and soot temperature measurements in laminar diffusion flames, using soot emission spectroscopy (SSE) and line-of-sight attenuation (LOSA). The schematics of the SSE and LOSA test apparatuses are shown in Figures 2-3-a and b respectively. In brief, in SSE as an active optical soot diagnostic method, line-of-sight radiation emission from soot is measured along chords through the flame. A series of emission

values at a certain height in the flame can be inverted to obtain radially resolved values of emission. When soot optical properties are known or assumed, then temperature and soot volume fraction can be determined [8]. In LOSA, a line-of-sight measurement is made of the intensity of a small light beam (e.g. from an arc lamp) transmitted through a flame. This value when divided by the intensity value of the beam transmitted along the same path without the flame present, the transmissivity of the given chord through the flame can be determined. A series of transmissivity measurements at a given height in the flame can be inverted to obtain radially resolved extinction coefficients from which soot volume fraction can be determined [8]. The LOSA can be considered as a passive optical soot diagnostic method.

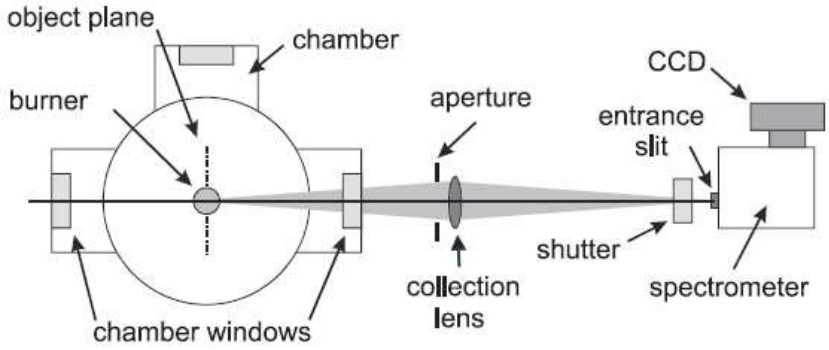

a) Schematic of the spectral soot emission (SSE) diagnostic.

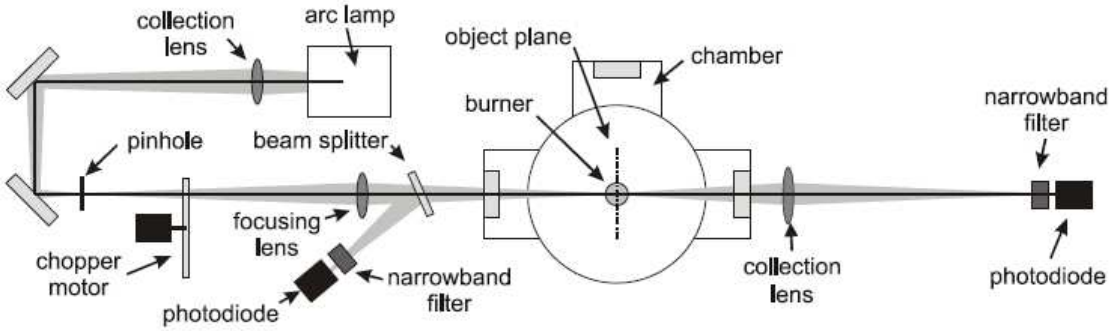

b) Schematic of the line-of-sight attenuation (LOSA) diagnostic.

Figure 2-3: The optical layouts in a) SSE and b) LOSA methods [8].

Thomson et al. [8] in 2005 reported radially resolved soot concentration and soot temperature measurements in laminar diffusion flames of methane at elevated pressures

up to 4 MPa. SSE and LOSA measurements of soot volume fraction were typically agreed within 30% and both methods exhibit similar trends. It was shown that the peak soot concentration varies as P^n, where n = 2 for $0.5 \leq P \leq 2.0$ MPa and n = 1.2 for $2.0 \leq P \leq 4$ MPa. Their measurements of the line-of-sight integrated soot volume fraction are in close agreement with the results obtained by Lee and Na [34] , as well those of as Flower and Bowman [19]. Soot temperature measurements indicate that the overall temperatures decrease with increasing pressure; however, the differences diminish with increasing height in the flame.

McCrain and Roberts [16] in 2005 measured quantitatively the soot volume fraction (f_v) in a laminar diffusion flame, for $0.1 \leq P \leq 2.5$ MPa in methane (CH_4) flames $0.1 \leq P \leq 1.6$ MPa in ethylene (C_2H_4) diffusion flames. The path integrated soot volume fraction, at 65% of the flame height, scales with pressure as $p^{1.0}$ and $p^{1.2}$ for the methane–air and ethylene–air flames respectively. The location of peak soot is observed to move from the edges toward the tip of the flame as the pressure is increased for both fuels. The physical shape of the flame also was found to be very sensitive to pressure. The flame became shorter in height and considerably narrower and the flame structure changed dramatically with increasing pressure. It is reported that the flame was strongly influenced by buoyancy-driven instabilities as pressure was increased.

In 2006 a numerical and experimental study of an axisymmetric co-flow laminar methane-air diffusion flame at pressures range of $5 \leq P \leq 40$ atm was conducted by Liu et al. [20]. Soot volume fraction was experimentally measured using both SSE and LOSA techniques. Numerically, the elliptic governing equations were solved in axisymmetric cylindrical coordinates using the finite volume method. The visible flame diameter was found to decrease with pressure as $P^{-0.5}$. The integrated soot volume fraction was reported to increase with pressure as $P^{1.3}$ for $5 \leq P \leq 20$ atm. The increased

pressure was found to enhance air entrainment into the fuel stream around the burner rim, leading to accelerated fuel pyrolysis. For $20 \leq P \leq 40$ atm both the model and experiment show a diminishing sensitivity of sooting propensity to pressure with a greater decrease in the numerical results than the experimental data.

Bento et al. [9] in 2006 studied the effect of pressure ($0.1 \leq P \leq 0.73$ MPa) on soot formation and structure of the temperature field in co-flow propane–air laminar diffusion flames. The higher pressure limit was set by the fact that propane liquefies above this pressure. The fuel flow rate was selected so that the soot was completely oxidised within the visible flame and the flame was stable at all pressures. Maximum line-of-sight soot concentration along the flame centreline scaled with pressure as $P^{1.4}$ for pressures between 0.2 and 0.73 MPa. Soot temperature measurements indicated that the overall temperatures decreased with increasing pressure; however, the temperature gradients increased with increasing pressure.

Recently (in 2009) Joo and Gulder [21] also examined the effects of pressure on soot formation and structure of the temperature field in a co-flow methane–air laminar diffusion flame. The flame was stable at all pressures and the visible (luminous) flame height, as indicated by soot radiation, remained almost unchanged from 10 to 100 atm. For pressures lower than 10 atm, visible flame heights tended to decrease and the blue flame region near the nozzle exit became more expansive as the pressure neared atmospheric pressure. Peak soot concentrations showed a strong dependence on pressure at relatively lower pressures; but this dependence got weaker as the pressure is increased. Radial temperature gradients within the flame increased with pressure and decreased with flame height above the burner rim.

The results of major reviewed studies on dependence of soot formation by pressure have been summarised in Table 2-2.

Table 2-2: Summary of experimental studies on the pressure dependence of soot in laminar diffusion flames (template from [9]).

Refs.	Pressure range [bar]	Fuel and fuel mass flow rate [mg/s]	Pressure exponent n in $[soot] \propto P^n$		Fraction of fuel's carbon converted to soot
			Path integrated maximum soot	Local maximum soot	
Flower and Bowman [19]	1-10	Ethylene 1.9,2.7, 4.4	1.2±0.1	-	-
Flower and Bowman [32]	1-2.5	Ethylene	1.5~2	1.5~2	$\frac{m_{soot}}{m_{fuel}} \propto P^{0.5–1.0}$
Lee and Na [34]	1-4	Ethylene 3.4	1.26	2 (20 mm above the burner)	-
McCrain and Roberts [16]	1-16	Ethylene 1.3	1.2	1.7	-
	1-25	Methane 1.1	1	1.2	-
Thomson et al. [8]	5-20	Methane 0.55	1.3	2	1
	20-40	Methane 0.55	0.9	1.2	0.1
Bento et al. [9]	2-7.3	Propane 0.49	1.4	1.8	1.1
Liu et al. [20]	5-20	Methane, 0.55	1.3	2	1
Joo and Gulder [21]	10-60	Methane, 0.55 and 0.66	-	-	0.1-0.33

Heavily sooty flames, as found in jet engine combustors for example, are difficult to study using modern laser based combustion diagnostics because of the large number density of carbon particles. At high pressure the soot particles are so dense that the flame looks ‘solid’ and electromagnetic waves in the visible or infrared spectrum are not able to penetrate the flame. Initial results on the penetration of terahertz (10^{12} Hz) waves into heavily sooty flames have been reported by Bassi et al. [13]. It was shown that a beam of terahertz radiation is able to penetrate a heavily sooty flame conditions which are beyond the realm of conventional laser based diagnostics. Ethylene and

methane flames at pressures up to 16 bar in a co-flow high pressure burner were analysed using the new technique of terahertz time-domain spectroscopy (THz-TDS) [1]. Calculations of the theoretical combustion species absorption spectra in the 0.25 THz to 3 THz range have shown that almost all the observable features come from water vapour (H_2O). The technique of terahertz time domain spectroscopy (THz-TDS) is still in its infancy. Attempt on the observation of the absorption lines of other radicals such as OH (1.84 THz and 2.51 THz), CH (2.58 THz), and NH_3 (1.77 THz and 2.95 THz) as well as flame temperature measurement continues.

According to the literature survey presented in this section the majority of the studies on laminar diffusion flames at elevated pressures have been focused on the soot or other species concentrations and temperature profiles within a stable region [8, 9, 16-22]. The effects of pressure, on laminar diffusion flame dynamics and instabilities left almost unattended in literature. The coupling effects of pressure and fuel type and flow rates and also co-flow effects on the flame structure, dynamics, flickering behaviour and instability provide the intact area of interest in sooty flames studies. At atmospheric pressures, the instability of the laminar mixing layer (generally referred to as the Kelvin-Helmholtz instability), and vortices dynamics have been studied extensively [35]. At elevated pressures, however, current understanding of the influence of pressure on dynamics and instability behaviour of laminar diffusion flames is still very limited.

In addition the present doctoral research seeks to investigate the effects of pressure on soot temperature distribution and flame geometry within a stable flame. The two-colour method in NIR region and narrow-band photography are utilised in order to measure the output parameters with a novel and relatively high accurate approach.

2.3 FLAME STRUCTURE AND DYNAMICS

2.3.1 Fuel Effects

Soot spectral emission and line-of-sight integrated soot volume fractions versus pressure have previously been reported [8, 9, 16, 19, 20] to assess the pressure sensitivity of soot formation. These studies also reported that the physical shape of the methane, ethylene and propane diffusion flames are very sensitive to the increase of pressure. The flame changes in height and becomes considerably narrower with the increase of pressure. It is also found that buoyancy-induced instabilities lead to flame flicker at slightly elevated pressures as buoyancy forces scale with pressure [8, 16].

It is well known that the pressure has significant effects on parameters such as temperature, flow velocity, flame structure and thermal diffusivity [36]. Miller and Maahs [17] designed and constructed a high-pressure flame system for studying methane–air diffusion flame in the pressure range of 0.1 – 5 MPa. It is reported that a very marked change occurred in the shape and structure of the methane–air diffusion flame as pressure was increased. Also the region of stable combustion was markedly reduced [17].

The flickering of a laminar diffusion flame is known to be caused by the interaction of the flame and the vortices both inside and surrounding the flame jet. The presence of elementary flame–vortex interactions in diffusion flames was independently observed by Toong et al. [37] and Kimura [38] in propane jet burnt in open air. They suggested that the flickering of a diffusion flame at low frequency, typically ranging from 10 to 20 Hz (first reported by Chamberlin and Rose [39]) could be explained by the formation of buoyancy induced outer toroidal vortices causing the flame front to regularly oscillate or flicker. Recently, the presence of these vortices has been confirmed experimentally and numerically [2, 24, 40-43]. The generation of the outer vortices has been attributed

to a Kelvin–Helmholtz instability driven by a buoyancy induced shear layer surrounding the flame surface [38, 41, 43-45]. For a given Reynolds number, the buoyancy varies with Froude number, which is inversely proportional to the product of gravitational acceleration and square of the ambient pressure.

For diffusion flames with high enough Reynolds number in the transitional regime Chen et al. [40] employed a planar visualisation technique and visualized two distinct vortices; large toroidal vortices outside the luminous flame and small roll-up vortices inside the luminous flame. Methane, ethylene and propane were used as fuels. The frequency of the toroidal vortices was found to correlate with the flame oscillation flicker frequency (*f*). The frequency was in the range 10 to 20 Hz and the vortex convective velocity was approximately 0.8 m/s, over the conditions studied. The flame oscillation frequency showed a weak dependence on burner exit velocity and co-flowing annulus air. The frequency increased as the burner exit velocity or the co-flowing air velocity was increased.

An experimental study of buoyant propane diffusion flames was undertaken by Cetegen and Ahmed [46] to identify the mechanism responsible for the periodic oscillations near the source of these flames. This phenomenon, often referred to as 'puffing' in the literature, exhibits itself as quasi-periodic oscillations of the diffusion flame front near the axisymmetric source of a fire with formation of large scale flaming vortical structures. The puffing frequency shows a definite trend with the burner diameter, *D*, scaling approximately with $D^{-1/2}$. Under normal gravity and atmospheric conditions the puffing frequency for a variety of hydrocarbon fuels can be approximated by the empirical relation, as $f \approx 1.5/D^{1/2}$ [46, 47]. This relation remains valid for small fuel jet velocities (e.g. in buoyant plumes and pool fires) since the jet momentum compared to the buoyancy effect is too weak to notably influence the flickering frequency [23, 40, 43, 45].

Using quantitative rainbow schlieren deflectometry, Albers and Agrawal [24] have shown that the flickering frequency of a hydrogen diffusion flame at sub-atmospheric pressures (0-1 atm) varies linearly with the ambient pressure, i.e., *f=12.5P*. This concurs with a dimensional analysis by Katta and Roquemore [42] relating the vertical velocity of the burnt gases to the characteristic flame height leading to the following relation $f \propto g^{1/2}$. Durox et al. [23] experimentally measure the flickering frequency at sub-atmospheric pressures and reduced gravity levels. They have shown that the relationship between flickering frequency and pressure is given by $f \propto (Pg^2)^{1/3}$ which is valid if the mean width of the flame is greater than the burner nozzle diameter. Otherwise the linear relationship between pressure and frequency holds. At reduced gravity or ambient pressure various researchers have shown that a diffusion flame is wider and longer than their normal gravity flame counterparts [48, 49].

Some experiments have been conducted under increased gravity levels with the flame placed in a centrifuge [50-53]. In the recent work by Sato et al. [53], methane, propane and a mixture of methane-propane were used as the test fuels with artificial gravity levels created up to 14 g. In these investigations increased gravity levels leads to an increase of the flickering frequency but it is hard to distinguish between a 1/2 power or 1/3 power dependency of the gravity due to the coriolis forces present in this type of experiment [51]. It is found that at increased gravity levels the length and surface area of a diffusion flame decreased and the flickering behaviour become more prominent. This was explained by the enhancement of air entrainment which was caused by increased buoyant flow in the flame at higher gravity levels.

Research on laminar diffusion flames at high pressures has been limited to a number of studies focused on the soot and temperature profiles within a stable laminar flame at pressures up to 5.0 MPa [9, 16, 17, 19, 54]. Oscillating methane air diffusion

flame at 10 Hz excitation frequency have been investigated under 2.5 bar pressure by Charwath et al. [15]. The experiments were performed in order to determine soot volume fractions, particle number densities, and mean particle radii. The oscillating flame shows strong instationary effects and increased soot concentrations compared to the steady-state flame of equivalent mean fuel flow. A simple numerical approach is also deduced that explains qualitatively the strong variations of the soot volume fraction in an oscillating flame [15].

There is a lack of knowledge on the influence of elevated pressure on the flame dynamics of a laminar/transitional diffusion flame. To the author's knowledge there has been no quantitative study on the effect of elevated pressures greater than 2.5 bar on the structure and flickering frequency dynamics of a diffusion flame. Most of the non-atmospheric current investigations have been conducted at pressures below atmospheric pressure to reduce the effects of buoyancy. This motivated the study on the change in the geometry of the stable diffusion flames and the instability regions and the dynamics of the flickering jet diffusion flames at elevated pressures up to 16 bar. Three hydrocarbon fuels were also used as the test fuels in order to study the effects of fuel type at elevated pressures. In Chapter 3, a description of the high pressure burner and experimental setup is presented and the results of the study are discussed and concluded.

2.3.2 Fuel Flow Rate Effects

The fuel flow rate effects on flickering behaviour and oscillation of diffusion flames at atmospheric pressure has been studied in different literature [37-40, 55, 56]. According to these studies, laminar diffusion flames are known to oscillate or flicker at a low frequency, typically ranging from 10 to 20Hz, depending upon the operating conditions. Chamberlin and Rose [39] reported that the flicker frequency of about 10 Hz for diffusion free flame was not greatly affected by either the fuel type and flow rate or

the burner size tested. The existence of discrete frequencies in the vicinity of 11 Hz in a range of methane fuel exit velocities (0.9 to 2.6 m/s) were measured by Durao and Whitelaw [56]. Toong et al. [37] studied both free and enclosed flames and the frequency of oscillation of the enclosed flames was found to be a strong function of their surroundings. In the study of Toonge et al. [37] the free-flames again reproduced the 10 Hz behaviour found by Durao and Whitelaw [39].

Hamins et al. [57] analysed experimental data over a wide range of operating conditions and found that the flicker frequency correlated with burner size and fuel jet exit velocity. Kimura [38] revealed that a regular flame oscillation appears, when the fuel-flow rate is increased above a critical value, and it is axially symmetric. The oscillation was found to have no connection with the size of the combustion chamber and the length of the fuel pipe. The frequency of the oscillation for propane diffusion flames was found to be between 10 to15 Hz for the relatively wide change in the fuel flow rate and in the diameter of the port [38].

The flickering of a laminar diffusion flame is known to be caused by the interaction of the flame and the vortices both inside and surrounding the flame jet. An elementary flame–vortex interaction is typically periodic, regular and reproducible in nature and can therefore be easily characterised [24, 39, 58]. Chamberline and Rose [39] ascribed the periodic nature of the phenomenon to alternate increases and decreases in the rate of diffusion of oxygen into the flame. That is to say, when the fuel flow exceeds some critical value an envelope of combustion products is created, which temporarily separates the reactants (quenching of the flame front). There is thus a time interval before the slower moving air can diffuse through this envelope and again create a flame sheet [58]. It can be considered that the flame oscillations occur due to quenching of the flame front in one specific location or region [55].

Generally two distinct vortices have been identified in the jet diffusion flames studies [40, 59, 60]. They are characterised by large toroidal vortices outside the luminous flame and small roll-up vortices inside. Large toroidal vortices in the oxidiser side of the luminous flame convect downstream and interact with the flame to create wrinkles on the flame surface [24]. It was speculated that the vortical structures outside the luminous flame are due to buoyancy-driven instability and are also responsible for the low frequency flame oscillation [40, 59]. Therefore, the frequency of the outer vortices correlated with the flame oscillation frequency [24]. The outer vortices develop because of the Kelvin-Helmholtz type instability in the buoyancy-induced shear layer surrounding the flame surface [42, 44, 59]. The buoyancy effect on the shape and flickering frequency of a diffusion flame has been studied by various researchers in the literature [24, 48, 49, 51, 61, 62]. Buoyancy is directly related to the Froude number, which is inversely proportional to the product of gravitational acceleration and square of the ambient pressure [61, 62].

According to the numerical results of Ghoniem at al. [63], in an axisymmetric vortex sheet of pool fires, the Kelvin–Helmholtz instability is augmented by Rayleigh-Taylor type instability as the roll-up pushes the hot gases outward and the cold air inward with respect to the interface. Also Williams et al. [64] noted the conclusion of several recent studies that buoyant vorticity generation (created by a misalignment of the density gradient and the gravitational vectors) and baroclinic vorticity generation (resulting from a misalignment of the density gradient and the pressure field vectors) are the primary causes of the large-scale toroidal vortices at the periphery of the plumes, which are referred to as “puffing” instability [46, 57].

The phenomenon of flame flickering in diffusion flames is well known and has been extensively studied at atmospheric pressures [24, 37-40, 55, 58, 65, 66] and different gravity levels [50, 51, 53, 67, 68]. It is speculated that the mechanisms

responsible for flame oscillations are highly sensitive to various burner configurations, flame flow conditions and gravitational effects due to buoyancy [55]. It was noted [50, 68] that flicker frequency increases with increasing gravitational level and flicker was dominated by buoyancy. Low-gravity experiments by Bahadori el al. [68] show that the flame flicker frequency is proportional to the square root of the gravitational acceleration.

It was reported by Miller and Maahs [17] that a very marked change occurred in the shape, structure and the region of stable combustion of the methane–air diffusion flame as pressure was increased. It is found [8, 16] that buoyancy-induced instabilities will lead to flame flicker at slightly elevated pressures because the buoyancy forces scale with pressure. Furthermore, experiments by Yuan and Durox [49], reveal that the flame flicker is suppressed at low buoyancy, achieved by reducing the ambient pressure. Still there is a lack of understanding on the influence of elevated pressure on the flame dynamics of a laminar/transitional diffusion flame [10].

Experiments were performed by Albers and Agrawal [24] at sub-atmospheric pressures to scale the effects of buoyancy on flame flicker. The flame flicker frequency was found from Fourier analysis of angular deflection data to vary linearly with operating pressure. In their study [24] different buoyancy levels were achieved by varying the jet exit Froude number, which is inversely proportional to the gravitational acceleration (g) or square of the ambient pressure (p^2) [61, 62]. Flame flickering of jet diffusion flames has been characterised experimentally in terms of pressure and gravitational force by Durox et al. [23]. The measurements show that the relationship between the frequency and the reduced gravity at varying sub-atmospheric pressures is very close to $f \propto (Pg^2)^{1/3}$, when the burners have a sufficiently small outlet diameter. Otherwise the linear relationship between pressure and frequency holds. Most of the current investigations have been conducted at pressures below atmospheric pressure to

reduce the effects of buoyancy. At reduced gravity or ambient pressure, a diffusion flame is wider and longer than their normal gravity flame counterparts [48, 49].

This literature survey shows that the information on the effects of pressure on diffusion flames dynamics is very limited. The objective of this study is to investigate, in detail, the influence of elevated pressures on the flame structure and dynamics of laminar diffusion flames. However, particular attention has been paid to the effect of fuel flow rate. Optical diagnostics (chemiluminescence and high speed imaging) have been used to study the change in flame structure, flickering behaviour and frequencies of the flames oscillations. In Chapter 4, the coupling of fuel flow rate and chamber pressure on the flame dynamics (flickering behaviour) of methane-air diffusion flames is studied over the pressure range of 1 to 10 bar. A wide range of fuel flow rates and pressure are studied in order to gain a better understanding of the influence of these two parameters. It has been observed that the flame properties are sensitive to the fuel flow rate at elevated pressures.

2.3.3 Co-flow Effects

Buoyant laminar jet diffusion flames are known to oscillate at low frequencies, typically within the 10–20 Hz range, depending upon the operating conditions [24, 37-40, 43]. In the study of Davis et al. [2] counter-rotating vortex structures internal and external to the flame surface appear and move upward along with flame sheet bulges. Flickering and tip-cutting (or necking) occur at a frequency of 11–15 Hz. The flickering of a laminar diffusion flame is known to be caused mainly by the interaction of the flame and the vortices. An elementary flame–vortex interaction is typically periodic, regular and reproducible in nature and can therefore be easily characterised [24, 39, 43, 58]. This strong periodicity of structures obviously results from a mutual interaction of

flow structures (determining air entrainment, mixing, flame stretch and compression) and chemical reaction (heat release, buoyancy) [45].

The evolution of vortical flow structures in buoyant jet diffusion flames and their interaction with flame structures have been studied extensively [2, 40, 43, 45, 69]. The axisymmetric, low frequency oscillation of flow and flame structures depends only weakly on the type of fuel, the fuel nozzle size, and the exit velocities of the fuel jet [38, 40, 43, 45, 57]. However, the coherent flow structures in the air co-flow strongly interact with the reaction zone, which ultimately may lead to local flame extinction [40]. These structures, could be observed in the co-flow region, whereas vortical structures inside the flame surface were detected only when contoured fuel nozzles and large jet velocities were employed [40, 43, 45].

In spite of the extensive amount of research work related to the evolution of structures in buoyant jet diffusion flames, a definite and rigorous interpretation of the mechanisms leading to the formation of coherent flow structures is still lacking [43]. The formation of coherent structures is attributed primarily to a modified Kelvin-Helmholtz instability of the flow field [38, 40, 43-45]. However, this mechanism of flow instability cannot explain the evolution of self-excited oscillations, as it takes only the spatial propagation of instability waves into account. Indeed it seems that the closer understanding of diffusion flame instabilities due to formation of outer vortices might be gained by studying the influence of co-flow air on the flame dynamics.

Much work has been reported in the literature relating to the combustion of fuel jets in still air or in parallel co-flowing streams [43, 45, 70-73]. The blow-out limit [72, 74, 75] and the stabilisation mechanism of turbulent [70, 76-78] or laminar [70, 79-83] lifted jet diffusion flame in co-flow of air have been studied extensively. However, the co-flow air effect on the dynamics of laminar non-lifted diffusion flames is left almost unattended in literature.

The blow-out stability limits of co-flowing turbulent jet diffusion flames have been formulated by Dahm and Dibble [74] from a simple description for a physical mechanism by which a turbulent diffusion flame can stabilise itself. Results for co-flowing turbulent jet flames showed a large reduction in the jet blow-out velocity even for relatively small co-flow velocities. They demonstrated that a slower rate of flame spreading occurs when steady flames become more wake-like with increasing co-flow. The strength of an air co-flow can also have a noticeable effect on the flame length in steady turbulent diffusion flames [84]. According to the results of Hermanson et al. [85] the addition of co-flow generally caused an increase in the mean flame length of turbulent ethylene jet diffusion flame puff.

Lee et al. [83] studied characteristics of lifted flames in laminar axisymmetric jets of propane with co-flowing air. They obtained the images of OH* planar laser induced fluorescence (PLIF) and CH* chemiluminescence and the Rayleigh concentration measurement. It has been shown that the positions of maximum luminosity in direct photographs of lifted triple (or tribrachial) flames can reasonably be located along the stoichiometric contour. Note that the base of a laminar lifted flame exhibits a triple structure, consisting of a lean and a rich premixed flame wings and a trailing diffusion flame, all extending from a single location [83, 86]. In study of Lee et al. [83] the stabilisation mechanism of laminar lifted flames has been explained based on the balance of the propagation speed of triple flame and local flow velocity. The lift-off height in co-flow jets was found to increase highly nonlinearly with jet velocity and was sensitive to the co-flow velocity. The blow-out and reattachment velocities decreased linearly with the increase in co-flow velocity.

The numerical simulations of methane-air diffusion flames by Montgomery et al. [73] showed that lift-off height increases with jet exit velocity and with the air co-flow velocity. The flame stabilisation point is located on the stoichiometric surface in the

inner shear layer. It is found that for higher co-flow velocities, the inner-shear-layer vortices begin to form farther downstream, and the jet spreads more slowly(also reported by Dahm and Dibble [74]). The data indicated that the momentum of the co-flowing stream acts in combination with the jet momentum to push the base of the flame farther away. The base of a stable lifted flame, located in the stoichiometric region, propagates continuously into reactants. In the attached flame, however, the stability of the flame base depends upon the maintenance of a local balance between the burning velocity of the premixed mixture and the (mean) velocity of the ongoing flow [87]. Note that unlike the attached flame the lifted flame base does not lose heat to the burner [35].

The effects of co-flow air in the hysteresis regime of turbulent lifted-jet flames were studied using methane and ethylene fuels by Terry and Lyons [77]. The hysteretic region near the nozzle is a region in which a jet flame can be attached or lifted given the same conditions (considering flame is stabilised on an increasing or decreasing path of fuel or air exit velocity). It was observed that the reattachment velocities and lifted flame heights just prior to reattachment vary linearly as for laminar flames in co-flow. Increase in lift-off heights and decrease in reattachment velocities were occurred more quickly as co-flow velocity was increased. The flow regime of the co-flow (i.e., laminar or turbulent) did not appear to affect the behaviour of these flames.

The effect of air velocity on the flame stability limit in turbulent bluff-body stabilised non-premixed flame has also been reported in literature [78, 88]. The bluff body is a basic device to stabilise double concentric jet diffusion flames in industrial burners, for reasons of safety and easy implementation [78]. The bluff-body stabilised non-premixed flame are basically classified into three stable types (recirculation zone flame, central-jet dominated flame and jet like flame) and two unstable types (partially quenching flame and lifted flame). The air to fuel velocity ratio (γ) is the main controlling parameter [78, 88]. It is desirable that the annular air flows entrain part of

the central fuel jet into a low-speed recirculation region in the wake of the bluff body to form a well-stirred combustible mixture for flame stabilisation purpose [89].

The effects of other parameters such as humidity in co-flow air [88], high temperature co-flowing [75] and oxidiser type (air or pure oxygen) [43, 45] on diffusion flame dynamics have also been studied in literature. Gu et al. [88] applied particle image velocimetry (PIV) to study the effect of humidity in co-flow air on the flow field and the flame stability limit in turbulent bluff-body stabilised non-premixed flame. Their results indicate that although generally flame stability shows an increase by air velocity, the addition of steam into air flow causes a reduction in the flame stability. This is due to a decrease in humid air momentum and Damköhler number (*Da=reaction rate/convective mass transport rate*). The decrease of Damköhler number is related to increase in the chemical reactant time due to the diluted oxidiser and the decreased flame temperature.

The stability behaviour of jet diffusion flame developing in a co-flowing high temperature air stream was studied experimentally, using city gas and hydrogen as fuel gases by Takeno and Kotani, [75]. Two distinct types of stability limits were observed; the first was the blow-off of the rim-stabilised flame, and the second was the break-off or extinction of the turbulent portion of the flame at the transition point from laminar to turbulent flow. It is interesting to note that instability in the outer layer has continuous large scale waviness in contrast to the micro-scale turbulence in the un-ignited jet. It has been observed that generally for both hydrogen fuels and city gas, at a constant air stream velocity, the stability region increases by increase in air stream temperature.

The effects of oxidiser type and flow rate on the flow field instability in a methane jet diffusion flame were also studied by Lingens et al. [43, 45], utilising visualisation techniques (PLIF of hydroxyl radicals, OH*, and Mie-scattering) and Laser Doppler Velocimetry (LDV). It was found that the global mode frequency is only marginally

dependent on the fuel flow rate. In contrast, the type of oxidiser and its flow rate have an influence on the frequency of flickering. It is reported [43, 45] that generally a diffusion flame with the co-flow of oxygen oscillate with a lower frequency in comparison with a flame in the co-flow of air at the same flow rates. Their results showed that the oscillation frequency increases first by increase in oxidiser flow rate and then remains almost constant from a certain flow rate onwards. Also the phase velocity of the global mode instability wave grows with increasing air flow rate, but varies only slightly with the fuel flow rate. Lingens et al. [43] concluded that the instability properties of the jet diffusion flame are strongly dependent on the type of oxidiser and its flow rate, but nearly independent of the fuel flow rate. It was further shown by Chen et al. [78] that stabilisation of lifted flames is more sensitive to the co-flow air than the fuel jet velocity at the inception of flame lift-off. The effects of annular air flow on the lift-off heights were found to be lower at higher fuel velocities. The underlying combustion mechanisms, however, depend strongly on the hydrodynamic interactions between the fuel jet and the annular air streams [70].

Thorough interpretations of the instability of non-reacting jet flows were carried out by Huerre and Monkewitz [90, 91]. The character of the instability of a parallel flow is classified as either “absolute” or “convective”. The absolutely unstable flow exhibits a temporally growing instability mode and wave-like disturbances infect the entire flow field and grow everywhere with respect to time [35, 43, 45, 75]. In convectively unstable systems, however, the disturbances are convected downstream from the location of inception faster than it grows so that the flow returns to its undisturbed state [35, 43]. In summary, absolutely unstable systems are oscillators , whereas convectively unstable flows behave like amplifiers of external excitation [43]. The flow density strongly affects the buoyant acceleration of reactive shear layer and may determine the type of instability [10, 43].

The effects of Froude number on stability limits in flames was also investigated in different literature [3, 53, 92]. The Froude number (*Fr*) is a dimensionless number comparing inertia and gravitational forces in the flow. Shu et al. [3] studied the dynamic flame structure and flame-vortex interactions at different Froude numbers (*Fr*), in a fuel-rich premixed (CH_4-air) annular jet sandwiched between a central air jet on the inside and co-flowing air on the outside. They reported that, at high Froude numbers (*Fr=15*, non-buoyant limit), the computed flame exhibits a steady flame structure. For intermediate Fr (*Fr=3*), the buoyant acceleration becomes significant, causing a periodic rollup of toroidal vortices. The flame exhibits steady-state behaviour, despite highly periodic rollup vortices, when the vortices are interacting only in the hot plume of gases above the visible flame. For $Fr < 1.0$, the rollup occurs closer to the burner port; therefore, the flame-vortex interactions create a flickering flame. They reported an increase in the flame flickering frequency by decrease in Froude number. The qualitative nature of flame-vortex dynamics, however, remains fundamentally the same.

Flickering diffusion flames exhibit a wide range of time-dependent, vortex-flame sheet interactions, and thus they provide an important testing ground for evaluating the applicability of chemical models derived from steady flames. For conditions in which flame flicker and tip-cutting occurs, Shaddix and Smyth [93] were found that, the peak soot concentrations in the methane flickering flames are 5.5 to 6 times larger than in a steady flame with the same mean fuel flow rate. The soot enhancement for the flickering propane and ethylene flames is reported only 35 to 60%, independent of the flicker intensity.

The co-flow air was found to be able to modify the soot formation process in diffusion flames as well. The flow field effects on suppression of soot emission (smoke-free flame limits) was studied in literature [18, 27, 28, 94]. Two competitive processes are governed for soot emission from a flame; firstly formation and growth of soot

particles, and secondly their oxidation. However, once the soot particles grow larger the burn out of them become more difficult [27]. By early arrest of their growth and also shortening the fuel residence time in the soot-forming region of the flame, the effective suppression of soot emission can be achieved [28]. It has been noted that at atmospheric pressure, soot limits are controlled by four variables, fuel velocity 'U_f', fuel nozzle diameter 'd_f', air velocity 'U_a' and air exit diameter 'd_a' [28]. It is found that to suppress the soot, by increase of fuel flow rate the air exit velocity needs to be increased with a large slope. However, there exists a soot limiting fuel flow rate above which soot cannot practically be suppressed even by additional increase in air flow rate [18]. It is found also by Katta et al. [95] that in a jet diffusion flame, the magnitude of flame oscillations (flicker) decreases with the amount of soot generated in the flame, however, the frequency of the oscillations does not change. They found experimentally and numerically that soot can influence flame flicker to such an extent that the oscillation is completely suppressed.

The effects of co-flow air on the flickering behaviour of buoyant laminar non-lifted diffusion flames, particularly the observed phenomena of full suppression of the flame flicker and its physical interpretation are left almost unattended in literature. The objective of this study is to investigate, in detail, the co-flow air velocity (flow rate) effects on non-lifted oscillating diffusion flame dynamics and the stabilisation mechanism using experimental approach. Experiments and results in Chapter 5 are focused on the study of the co-flow air effects on steady-state and oscillating laminar methane air diffusion flame. The obtained results present a dataset of flickering flame properties at different air flow velocities.

2.4 SOOT TEMPERATURE MEASUREMENT (TWO-COLOUR METHOD)

Two-colour method is an established optical technique for the temperature measurement of sooting flames. This technique makes use of two narrow band wavelengths in the visible or near infra-red emission. There has been a continuing effort in applying this technique to various situations. Hottel and Broughton [96] initiated application of the two-colour method for measuring the temperature of flame in utility furnaces. Their results indicated that to determine radiation from luminous flames, the two-colour pyrometer may be used with an average error of 5 %. This method has been expanded to measure the temperature of premixed or diffusion open flames [32, 33, 97, 98]. The most broad application of this technique has been found in combustion engines where not only the flame temperature but also the soot concentration in the flame was measured [99]. The values of soot volume fraction measured using two-colour method are coupled to the measured soot temperatures, any errors in measured temperatures will lead to errors in soot volume fractions. Also the wavelengths for two-colour method for two narrow band filters must be selected carefully for accurate temperature measurements [12, 100, 101].

In the last 30 years, the two-colour method has become the most widely used technique for diesel flame temperature and particulate concentration measurements because of its simplicity, low cost and relative ease of application [102]. The multi-colour method has also been developed to achieve higher measurement accuracy [98, 103-105]. These measurements are based on measuring the continuous blackbody radiation emitted by the soot contained in the flame. Therefore no meaningful temperature measurements could be made at the regions of flame that are relatively free of soot concentration. It has been shown in the literature that the temperature difference between the ambient gas temperature and soot-particle temperature is negligible after

the gas and the particles have attained thermal equilibrium [31, 96, 102, 106]. Therefore by measurement of soot temperature the flame gases temperature will be measured indirectly [102].

The sensing elements in non-intrusive pyrometers (e.g. two-colour radiation pyrometer designed by GIBSON [107]) detect only a single-point temperature within a flame. However CCD (Charge-Coupled Device) or CMOS (Complimentary metal-oxide semiconductor) sensors in digital cameras are able to detect two-dimensional intensity distribution of the flames. Since the ratio of the radiated energy in two wavelength bands, received from a sooty flame, is measured therefore two-dimensional soot temperature distribution can be calculated based on two-colour method. Gomes [108] and Kobayashi et al. [109] utilised portraying a flame on film and analysing the image according to the two-colour principle in order to measure temperature distribution of flame. However, their measurements were based on complicated off-line data processing [97].

To study the effect of pressure on flame temperature in 1977 Miller and Maahs [17] employed the two-colour pyrometry in visible spectrum with two disappearing-filament optical pyrometers fitted with interference filters at 500 nm and 650 nm wavelengths. The measured temperature at the tip of the methane diffusion flame in the region of most intense radiation showed a temperature decrease of about 160 K from 1 to 5 atm, while carbon concentration, and hence radiation from the flame, substantially increases. There was a further decrease of about 120K from 5 to 20 atm as carbon concentration continued to increase. From 20 to 50 atm, only a 50 K decrease in temperature took place. In 1989, Flower [33] published a paper in which soot particle temperatures are determined as a function of axial position in axisymmetric laminar ethylene-air diffusion flames at pressures up to 7 bar. The method of temperature measurement was based on line-of-sight measurements of the emission and absorption of near infra-red

radiation by soot particles. This represented average particle temperatures across the diameter of the flame, weighted by the local soot volume fraction. Flower [33] identified that with increasing height in the flames, the visible luminosity from soot decreases as an indicator of soot temperature decrease. As the pressure increased, the decrease in soot luminosity was observed at lower positions in the flame. The decrease in soot luminosity suggests that temperature is affected by the presence of soot as a result of radiant energy transfer from the particles. Temperature, in turn, strongly influences soot-formation and soot-oxidation rates.

Thomson et al. [8] in 2005 reported radially resolved soot concentration and soot temperature measurements at elevated pressures up to 40 bar, in laminar diffusion flames of methane using SSE and LOSA. Soot temperature measurements indicate that the overall temperatures decrease with increasing pressure; however, the differences reduce with increasing height in the flame. In lower parts of the flame, temperatures were about 150 K lower at pressures of 40 bar than those at 5 bar. In the upper half of the flame the differences diminish to 50 K. Bento et al. [9] also used SSE to measure soot temperatures in co-flow propane–air laminar diffusion flames over the pressure range up to 7.3 bar. They reported that the overall temperatures decreased with increasing pressure; however, the temperature gradients increased with increasing pressure.

In Chapter 6 experiments and results are focused on the influence of elevated pressures up to 10 bar on two dimensional soot temperature distribution of ethylene-air laminar co-flow diffusion flame. Two-colour pyrometry technique has been applied in the NIR region by utilising a commercial CMOS digital camera. To the best knowledge of the author, applying two-colour method in the NIR region with a commercial digital camera has been not reported in existing literature. The presented approach is relatively novel and economical in comparison to laser-based methods.

2.5 SUMMARY

A critical review of the literature was presented on three major categories: 1- high pressure studies of sooty diffusion flames, 2- diffusion flames dynamics and instabilities, and 3- soot temperature measurements by two-colour method. The majority of high pressures studies are concerned with the measurements of soot concentration and temperature profiles within a stable region. However, practical combustion devices frequently operate under unsteady conditions at elevated pressures. Laminar oscillating flames provide an opportunity to investigate the phenomena of unsteady combustion while simultaneously taking advantage of the cyclic behaviour of the flame oscillations. There is a lack of knowledge on the influence of elevated pressure on the flame structure and dynamics of a laminar/transitional diffusion flame. To the author's knowledge there has been no quantitative study on the effect of elevated pressures greater than 2.5 bar on the diffusion flames dynamics and instabilities. This has motivated the present study on the change in the geometry of the stable diffusion flames as well as the instability regions and the dynamics of the flickering flames at elevated pressures up to 16 bar.

The coupling effects of pressure and fuel type or flow rate on the flame structure, dynamics and flickering behaviour of laminar buoyant diffusion flames provide an intact area of interest in sooty flames studies. In order to study the fuel effects at high pressure, diffusion flames of three hydrocarbon fuels (methane, ethylene and propane) are investigated in a high pressure co-flow burner facility. The flame oscillation frequency showed a weak dependence on fuel exit velocity at atmospheric pressure studies. It is also known that the pressure has significant effects on parameters such as temperature, flow velocity, flame structure and thermal diffusivity. There is great

interest in studying the coupling between the fuel flow rate and pressure on unstable region and the flickering frequency of laminar diffusion flames.

The combustion community is also interested in studying the effects of co-flow air on the flickering behaviour of buoyant laminar non-lifted diffusion flames, in particular the observed phenomena of full suppression of the flame flicker and its physical interpretation. Consequently, another objective of this research is to carry out a detailed investigation on the co-flow air velocity (flow rate) effects. This part of the research involves study of inception point of the outer toroidal vortices in surrounding co-flow air as well as interaction of these vortices with visible flame and hot plume of gases.

Furthermore, study of temperature distribution plays a significant role in understanding the flame properties at elevated pressures. Accurate and reliable measurements of soot temperature and distribution in the flame by non-intrusive means are also highly desirable to achieve in-depth understanding of combustion and pollutant formation processes. Two-colour measurement of the emission of soot particles in Near Infera-red (NIR) will be utilised to determine the two-dimensional soot temperature distribution in a stable laminar diffusion flame. NIR region is chosen due to less gas molecules/free radical radiation in selected wavelengths in this spectrum. In addition, the present approach is relatively novel and economical in comparison to laser-based methods.

By cross-correlating the obtained data from the present PhD research study, it is expected that a significant understanding of combustion at high pressure and sooty conditions could be gained. This project is directly related to the problems faced in the energy industry and aerospace propulsion systems when elevated pressures and variable fuel and air flow rates lead to combustion instabilities and enhancement of soot formation which are yet to be fully understood.

"The subject of combustion has grown and ramified enormously. Its boundaries with fluid dynamics, chemistry, heat and mass transfer, and variety of other subjects have become increasingly ill-defined, and the useful experimental and theoretical techniques overlap similarly."

F.J. Weinberg (1963)

CHAPTER 3

FUEL EFFECTS ON DIFFUSION FLAMES AT ELEVATED PRESSURES

3.1 ABSTRACT

This study addresses the influence of elevated pressures up to 16 bar on the flame geometry and the flickering behavior of laminar diffusion flames and particular attention has been paid to the effect of fuel variability. It has been observed that the flame properties are very sensitively to the fuel types and pressure. The shape of the flame was observed to change dramatically with pressure. When the pressure increases, the visible flame diameter decreases. The height of a flame increases first with pressure and then reduces with the further increase of pressure. The cross-sectional area of the flame (A_{cs}) shows an average inverse dependence on pressure to the power of n ($A_{cs} \propto P^{-n}$), where $n=0.8\pm0.2$ for ethylene flame, $n=0.5\pm0.1$ for methane flame and $n=0.6\pm0.1$ for propane flame. It was observed that the region of stable combustion was

markedly reduced as pressure was increased. High speed imaging and power spectra of the flame chemiluminescence reveal that an ethylene flame flickers with at least three dominant modes, each with corresponding harmonics at elevated pressures. In contrast methane flames flicker with one dominant frequency and as many as six harmonic modes at elevated pressures.

Keywords: *Diffusion flames; Flame dynamics; Flickering frequency; High-pressure; Fuel variability.*

3.2 INTRODUCTION

The understanding of combustion has been enhanced considerably by studies of laminar flames based on atmospheric and low-pressure conditions. Considerable amount of literature has been published on laminar diffusion flames at atmospheric pressure but many practical combustion devices operate at high pressures to increase thermodynamic efficiency and decrease their physical size [16]. The current understanding of the influence of pressure on thermo-physical properties of sooty flames is very sketchy [8, 9]. It is well known that increased pressure plays a significant role in increasing soot production in spray combustion, premixed and diffusion flames [18, 30, 110-113]. Pressure has also significant effects on parameters such as temperature, flow velocity, flame structure and thermal diffusivity [36].

The phenomenon of flame flickering in diffusion flames is well known and has been extensively studied at atmospheric pressures. However, the exact mechanism of this buoyancy induced instability has not been fully understood. In recent years more focus has been placed on the understanding of more complex turbulent flame structures. In particular in modern combustion systems which typically operate at high pressures exhibiting a wide range of local conditions where flame-vortex interactions are mainly dominant [114]. In such applications, the turbulent combustion zone can be considered

as a collection of elementary flame-vortex interactions of different size and strength. This is coupled to the fundamental aspects of flow, transport and combustion phenomena present in turbulent flames. An elementary flame-vortex interaction is typically periodic and regular in nature and can therefore be easily characterized than is typically the case in direct investigations of turbulent flames. The flickering of a laminar diffusion flame is known to be caused by the interaction of the flame and the vortices both inside and surrounding the flame jet as discussed in session 2.2. Therefore the study of laminar flame dynamics is of great importance to the understanding of not only the laminar diffusion flame itself but also turbulent flames.

The generation of the outer vortices has been attributed to a Kelvin-Helmholtz instability driven by a buoyancy induced shear layer surrounding the flame surface [38, 41, 43-45]. The buoyancy affects the shape and flickering frequency of a diffusion flame [24, 48, 49, 51, 61, 62]. Buoyancy is directly related to the Froude number which is defined as [61, 62]:

$$Fr = \frac{U^2}{gd} = \frac{16m^2}{\pi^2 g d^5 \rho^2} = \frac{C}{gP^2} \qquad 3.1$$

Where ρ is the fuel density, U is the average burner exit velocity, d is the fuel nozzle diameter, m is the fuel mass flow rate, g is the gravitational acceleration and P is the ambient pressure. The density was replaced using the ideal gas law. For a specific burner, the parameter C is defined as, $C = 16m^2R^2T^2/\pi^2 d^5$, where R is the gas constant, which is fixed by fuel temperature (*T)* and mass flow rate (*m)*. Thus, for a given Reynolds number, the buoyancy varies with Froude number, which is inversely proportional to the product of gravitational acceleration and square of the ambient pressure.

The literature related to this part of the study is presented in Chapter 2, session 2.3.1. This review of literature shows a lack of knowledge on the influence of elevated

pressure on the flame dynamics of a laminar/transitional diffusion flame. Most of the non-atmospheric investigations have been conducted at pressures below atmospheric pressure to reduce the effects of buoyancy. In the present research, we investigate the change in the geometry of the stable diffusion flames and the instability regions and dynamics of the flickering jet diffusion flames at elevated pressures up to 16 bar. This study also highlights the fuel type effect on the flame geometry and dynamics of a jet diffusion flame at elevated pressure with a comparison of methane, ethylene and propane fuels. Recent studies at atmospheric and pressurised gas turbine test rigs have shown that changes in fuel composition can cause changes in the combustion instabilities observed [115, 116]. However, there is a lack of quantitative investigations on the fuel variability effect on the flame dynamics of jet diffusion flames, especially at high pressures.

The results presented in this chapter have been published in the Journal of *Fuel* in an article titled, “Fuel Effects on Diffusion Flames at Elevated Pressures” [10].

3.3 EXPERIMENTAL SETUP

The co-flow diffusion flame was studied with the optical diagnostic methods over the pressure range of 1 to 16 bar for methane (CH_4) and ethylene (C_2H_4) and 1 to 7 bar for propane (C_3H_8) diffusion flames. A commercial CCD camera and a visible narrowband filter (516±2.5nm) are used for the measurement of visible flame geometry and height. It is known that a typical CCD camera may be sensitive to infrared radiation. The application of the narrow band filter prevents both the infrared radiation and the saturation of flame during imaging. Also high speed imaging and chemiluminescence measurement have been employed to study the flame dynamics.

The high pressure burner used in this study is designed for working pressures up to 20 bar. This burner is similar to the design of Miller and Maahs [17]. The chamber,

which has an internal height of 600 mm and an internal diameter of 120 mm, is shown schematically in Figure 3-1. A classic over ventilated Burke-Schumann [117] laminar diffusion flame is produced which is stabilised on a nozzle with an exit diameter of 4.5 mm. The tip of nozzle is tapered to reduce recirculation and the formation of turbulent eddies in the air and fuel flow. Methane, ethylene and propane were the selected fuels supplied from a compressed gas cylinder, regulated by a needle valve, and measured by a calibrated mass flow meter with 1% full scale accuracy.

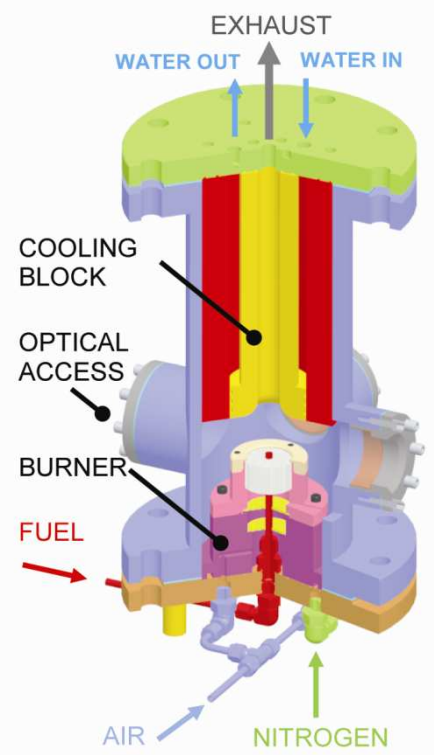

Figure 3-1: Cross-section of the high-pressure burner.

For the first set of experiments the mass flow rates for methane, 0.12 slpm (standard litres per minute), ethylene, 0.1 slpm and propane, 0.06 slpm were kept constant for all pressures for the same global heat release rate. Also for the unstable flame dynamics measurement, both methane and ethylene flow rates were kept constant for all pressures at 0.21 slpm. Co-flow air is supplied from a compressed air bottle into the burner and is diffused using a layer of glass beads and is followed by a honeycomb structure with 1.5 mm diameter holes which straightens the flow. Co-flow air was controlled by a

needle valve to produce a constant mass flow rate of 15 slpm for all the diffusion flames. Table 3-1 shows the physical properties of fuel and air streams for the experiments.

To pressurise the chamber, nitrogen flow was introduced through the base of the burner using a ring of 1.5 mm diameter holes. The nitrogen flow also keeps the chamber walls cool and the window ports free of condensation and soot. Increasing the pressure within the vessel was achieved by increasing the flow rate of nitrogen and simultaneously decreasing the flow rate of the exhaust by adjusting the back-pressure regulating valve which can maintain the chamber pressure anywhere between 1 and 16 bar. Optical access to the burner is provided by four windows which have a diameter of 50 mm and a thickness of 20 mm; two are made from fused silica (quartz) and two from high-resistivity float-zone silicon (HRFZ-Si). The fused quartz windows provide optical access in the visible band whilst the HRFZ-Si windows provide access in the far infrared up to 1000 µm, which were used for a different study based on terahertz-time domain spectroscopy [13, 118].

Table 3-1: Fuels and air parameters in fuel type experiments.

Gas Type	Volume Flow Rate		Mass Flow Rate [mg/s]	Velocity [m/s]	Re No.	Fr No.
	slpm [L/min]	[m^3/s]				
Methane (CH_4)	0.12	2.00E-06	1.36	0.138	36.61	0.450
	0.21	3.50E-06	2.38	0.241	64.07	1.377
Ethylene (C_2H_4)	0.1	1.67E-06	1.96	0.115	61.13	0.312
	0.21	3.50E-06	4.12	0.241	128.37	1.377
Propane (C_3H_8)	0.06	1.00E-06	1.91	0.069	74.43	0.112
Air	15	2.50E-04	301	0.230	513.82	0.171

The optical system used for the real-time measurement of flame light emissions is shown schematically in Figure 3-2. With optical access through one of the fused-silica lens, the total flame surface area is focussed using a spherical lens onto a 5 mm

diameter bundle of fine fibre optical cable. The bundle of fine fibres is bifurcated randomly into two equal subdivisions to produce two channels of light signals of the same intensity from the same imaged volume. Each channel is then guided to two individual photomultiplier tubes (ORIEL model 70704). At the end of each channel a CH* and C_2* interference filter at wavelengths of 430±5 nm and 516±2.5 nm were used respectively. Obviously, what is measured are the summation of the soot light and chemiluminescence of CH* and C_2* at the two chosen wavelengths for a diffusion jet flame. Nevertheless the availability of two wavelengths may provide qualitative information on flame chemistry. The intensity of the filtered light is converted into voltage signals which is captured by an analogue to digital data acquisition card (National Instruments PCI-MIO-16E-1) at 5000 samples per second averaged over a duration of 4 seconds. Real-time signal processing was performed by using a LabVIEW 8.5 virtual instrument (VI) to obtain the flame flickering frequency spectrum of the flame light emission. Optical access gained through the second fused-quartz window is used to capture the evolution of the structure of the flame using a high speed camera (Hi-Dcam) capable of capturing a maximum of 500 frames per second.

For the flame geometry measurements within the stable regions, the high speed camera was replaced by a commercial CCD (charge-coupled device) digital camera (Olympus- E-100RS) to capture the colour flame photographs and also the narrow band (516 nm) photos of the flame.

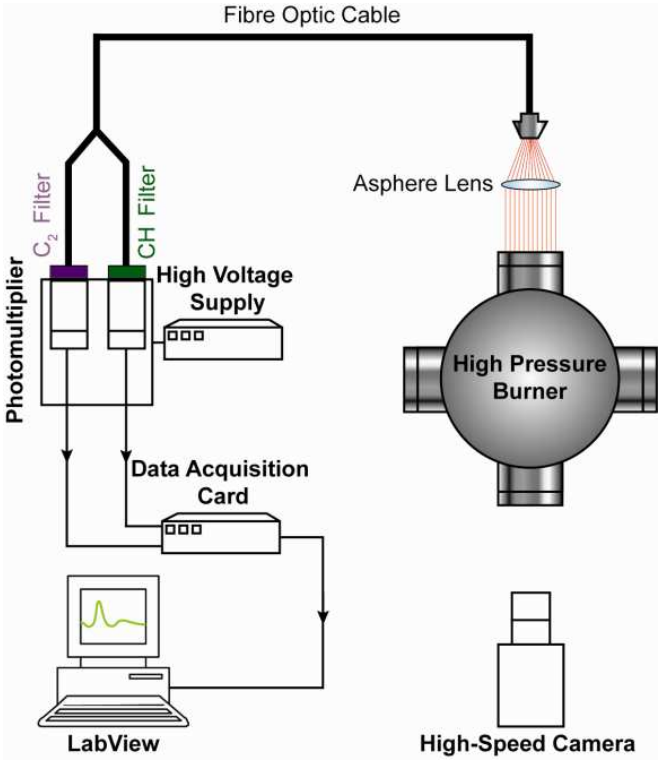

Figure 3-2: Schematic of the experimental setup

3.4 RESULTS AND DISCUSSION

The stable operating range for the burner is shown in Table 2. The onset of flame flickering occurs in methane flames from the flame tip at 8 bar and became visually unstable (the instability was extended towards the burner nozzle) at 12 bar for a flow rate of 0.12 slpm. However, for a lower flow rate of 0.05 slpm the burner has a stable flame in the entire operating regime of the burner. In contrast a propane diffusion flame was far more stable than a methane flame. The main reason for this stability may be attributed to the stronger soot formation tendency of propane in comparison with methane and the impact of soot on reduction of flame flicker [119]. It is worth mentioning here that the maximum operating range for propane is 7.3 bar since propane liquefies above this pressure at a room temperature (21 ºC). A propane flame is stable in all the stated flow rates in Table 3-2. The ethylene flame becomes visually unstable at a pressure of 6 bar with a flow rate of 0.21 slpm.

Table 3-2: Stable operating flow regimes of the high-pressure burner.

Fuel	**Fuel flow rate (slpm)**		
	0.05	0.12	0.21
Methane	Stable	12 bar	2 bar
Ethylene	Stable	Stable	6 bar
Propane	Stable	Stable	Stable

In all flames at atmospheric pressure, the flame had a bulbous appearance and is wider than the burner nozzle exit diameter. By increasing pressure it was observed that the flame narrows and it's width at all heights within the flame decreased. At elevated pressures, due to the increased presence of soot which acts as a reaction intermediary, the reaction processes are different from those acting at atmospheric pressure [17]. This may explain the significant change in flame shape with the increase of pressure. Soot particles are higher in density than other combustion products, and cannot diffuse away from the primary flame region as easily a gaseous product might. Combustion must therefore be maintained by oxygen diffusing inward to the primary flame region, resulting in a narrowing flame structure [17]. As pressure increases, the density will increase as well. By keeping the fuel mass flow rate constant ($\rho U A_{cs} = const.$) at all pressures, the mass conservation equation leads to the narrower flame cross section area at elevated pressures. It has been described by Liu et al. [20] that the physical effect of pressure affects the flame and soot formation through the pressure dependence of the mixture density ($\rho \propto P$), the binary diffusion coefficient ($D_{ij} \propto P^{-1}$), and the potential change in residence time due to change in the flame shape and possibly the processes of particle coagulation and agglomeration.

As the pressure was increased, axial flame diameters decreased, giving an overall stretched appearance to the flame as noted by Flower and Bowman [19] and Thomson et al. [8]. This effect increases the flame height up to a specific pressure with further

increases in pressure causing a decrease in flame height. Despite the flame being over-ventilated with co-flow air, for the ethylene and propane flames an extended line of soot at the flame tip appears at a pressure of 4 bar which increases with intensity and the black coloured soot spreads downward toward the base of the flame with the further increase of pressure (See Figure 3-3).

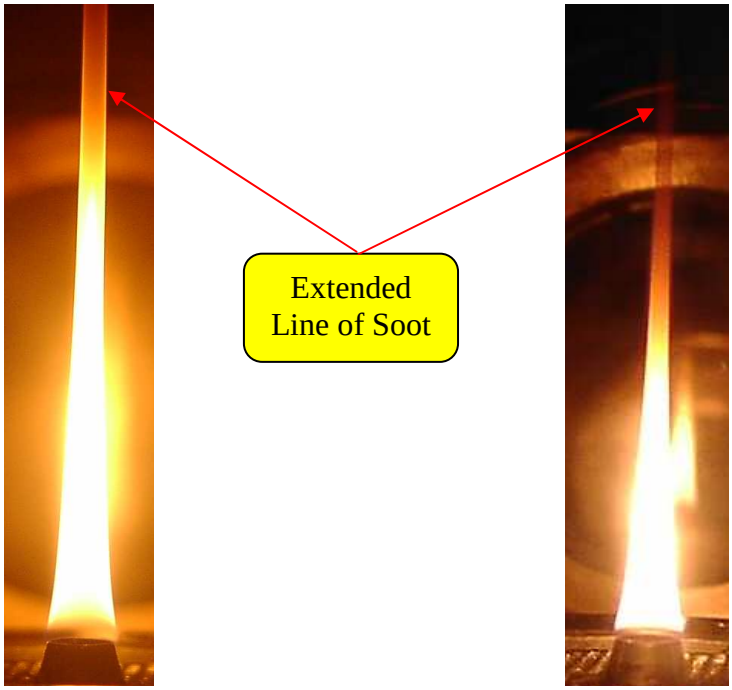

(a) Propane (0.06 slpm) – air (15 slpm) (b) Ethylene(0.1 slpm) – air (15 slpm)

Figure 3-3: Appearance of the extended line of soot (smoke) at the tip of (a) propane and (b) ethylene diffusion flames at 4 bar. The smaller visible flame in the background was a reflection of the flame itself on one of the windows.

Figure 3-4 shows the narrow band images (by applying C_2^* filter) of propane-air co-flow diffusion flame at different pressures at 1/80 sec camera exposure time. Due to the clear boundaries of the visible flames in these narrow band photos the measurement of the flame geometry (height and width) can be achieved with a greater accuracy.

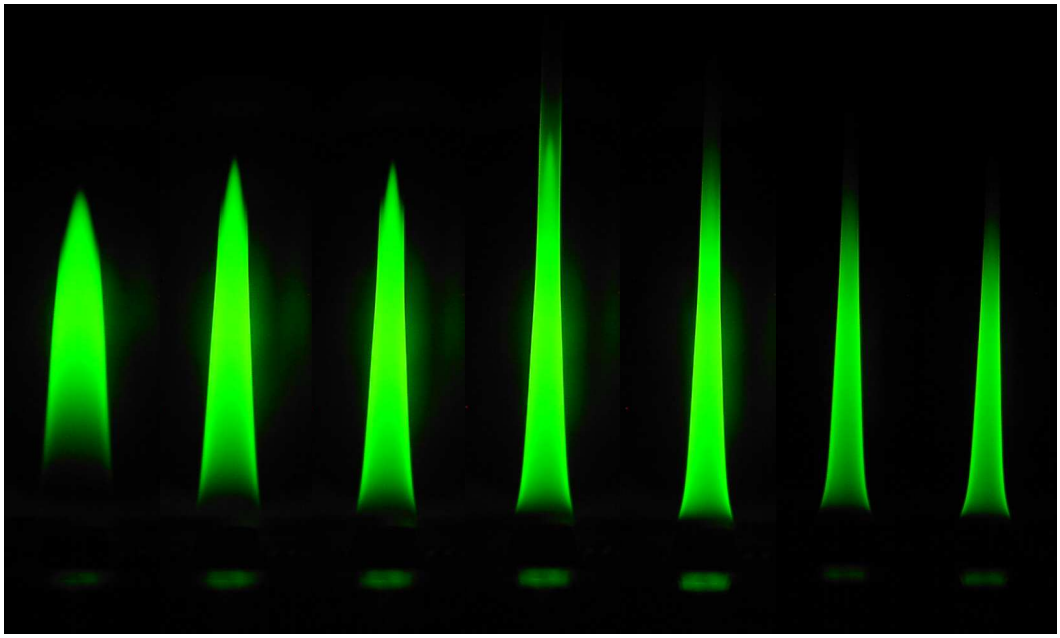

1 bar 2 bar 3 bar 4 bar 5 bar 6 bar 7 bar

Figure 3-4: Photos of propane (0.06 slpm)-air (15 slpm) diffusion flame by applying C_2* filter (Camera exposure time 1/80 sec)

The comparison of ethylene (0.1 slpm), methane (0.12 slpm) and propane (0.06 slpm) flame heights at different pressures are presented in Figure 3-5. The visible flame heights were measured from the tip of the fuel nozzle to the tip of the flame in the photos captured by applying a narrow band filter (516 nm) in the visible spectrum. The peak flame heights were observed to occur at a pressure of around 4 bar for ethylene and propane flames and at around 6 bar for methane flame. This flame height decrease at higher pressures is due to the increase in soot production. The soot zone was observed to extend down toward to the burner nozzle as pressure increases. The increase in the ethylene and propane flame heights between 1 and 4 bar are approximately 28% and 21% respectively with a decrease of 35% and 14% above 4 bar to their lowest values at 16 and 7 bar for ethylene and propane flames respectively. This trend is consistent for methane flames with 18% increases from 1 to 6 bar and an average decrease of 27% between 6 and 16 bar. Furthermore, the onset of flickering with a methane flame occurs at 8 bar with a rms of about 1 mm and the flickering amplitude increased with pressure

to its maximum amplitude, approximately 3.5 mm, at 16 bar (as shown in Figure 3-5 by vertical error bars).

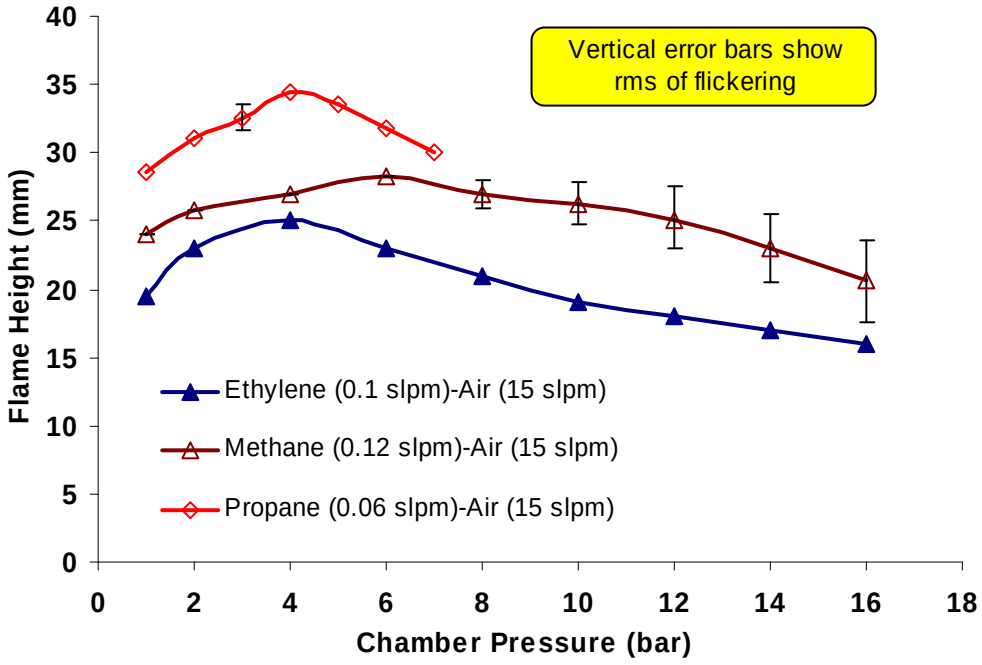

Figure 3-5**:** Co-flow laminar diffusion flame heights at different pressures.

When the pressure was increased, the axial flame diameters were observed to decrease, giving an overall stretched appearance to the flame as noted in previous works [8, 9, 16, 19, 36]. The cross-sectional area of the flame (measured from the radius defined by the outer edges of the sooting region at each height) shows an average inverse dependence on pressure to the power of 0.8±0.2 ($1/P^{0.8\pm0.2}$) for ethylene flames, 0.5±0.1 ($1/P^{0.5\pm0.1}$) for methane flames and 0.6±0.1 ($1/P^{0.6\pm0.1}$) for propane flames. As an example the cross-sectional area of the ethylene-air co-flow diffusion flame at different heights and pressures is presented in Figure 3-6.

According to the results of this study the flame cross-sectional area decreases with pressure according to the fuel type as $P^{-0.5 \text{ to } -1}$. Through scaling reasoning, Glassman [36] concluded that the flame cross-sectional area should decrease with pressure as $P^{-0.5}$. McCrain and Roberts [16] observed that this area scaled with pressure as about $P^{-0.9}$ for

methane-air flames and $P^{-1.1}$ for ethylene-air flames. However, the recent studies by Thomson et al. [8], Liu et al. [20] and Bento et al. [9] in a similar burner show that the visible flame cross-sectional area decreases with pressure as P^{-1}. The variation of flame cross-sectional area scaling with pressure may be attributed to differences in burner configuration, co-flow air or fuel velocities and the nozzle diameter. The effects of these parameters are worthwhile for further investigation.

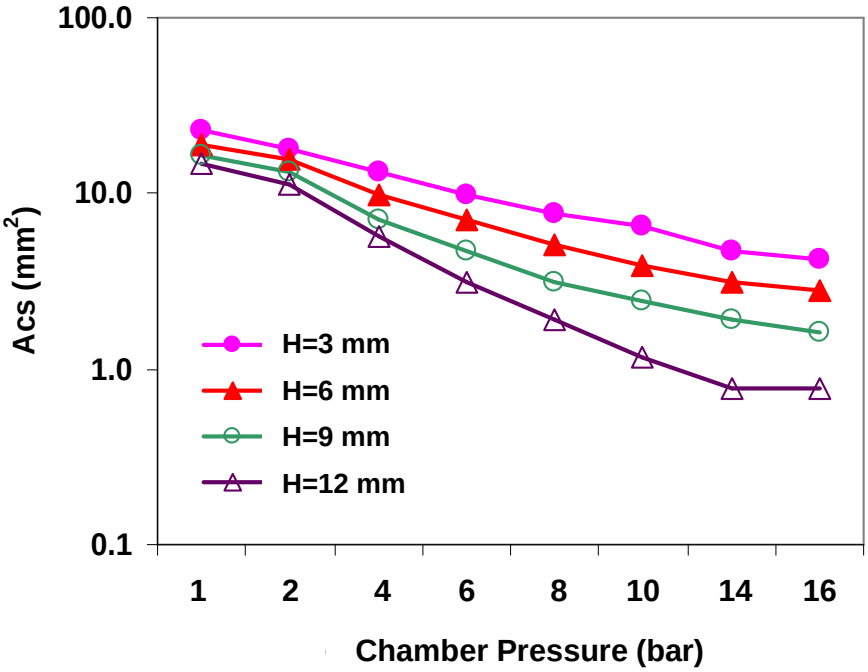

Figure 3-6: Cross-sectional area (A_{cs}) of the ethylene (0.1 slpm)-air (15 slpm) flame at different pressures and heights.

The ethylene flame exhibited good stability at all pressures up to 16 bar. In the propane flame at 3 bar a small amount of local flicking occurs at the tip of the flame (see Figure 3-5). However, the flickering disappears at pressures greater than 4 bar due to the appearance of a long line of the soot (see Figure 3-3). This phenomena is in agreement with the very recent finding of Katta et al. [65] that soot can influence flame flicker to such an extent that the oscillation is completely suppressed. In the methane flame, the flame dramatically changed to an unstable flame beyond 12 bar. The flickering at the tip of flame with rms of about 3.5 mm was observed at 16 bar and this

instability moves down towards the burner nozzle. These results are in agreement with the observations of other literature [8, 9, 16, 17, 19, 22, 120]

The effect of elevated pressures on the flickering behaviour of diffusion flames can be clearly observed in the unstable regime of methane and ethylene flames; a chosen flow rate of 0.21 slpm was used for flame dynamic measurements for both methane and ethylene. Images of the methane and ethylene diffusion flames are presented in Figures 3-7-A-a and B-a respectively. At atmospheric pressure, the flame shape is convex and its maximum width is wider than the burner nozzle exit diameter. Soot formation is more dominant at the tip of the flame. At higher pressures the flame luminosity dramatically increases.

The soot formation increases and the flame narrows with a concave shape. Previous high pressure studies of diffusion flames have been focused on soot studies of stable flames at lower flow rates. For higher flow rates obvious flame necking starts to occur. The necking of the flame can be explained by the presence of local buoyancy induced toroidal vortices which are formed at the flame surface bringing in fresh air to mix with the fuel at the flame front. The higher fuel flow rate means that the fuel jet is able to induce stronger vortex which would then produce better fuel and air mixing. As a result, the fuel could be burnt faster near the vortex which causes the necking to occur. The effect of increased buoyancy at higher pressures is clearly highlighted in the high-speed images shown in Figures 3-7-A-b and A-c for methane flame and Figures 3-7-B-b and B-c for ethylene flame with a periodic necking of both methane and ethylene flames. At higher pressures, a larger surface area of the flame tip is detached and burned out (see Figures 3-7-A-c and B-c). This may be explained by the scaling of buoyancy with pressure (see Equation-3.1) which will increase the convective velocity at the flame surface, causing an increase in the acceleration of toroidal vortices which correlate with the flame surface oscillations at the same frequency [40]. The vortices bring in more

fresh air to the flame surface, therefore a stronger local fuel-air diffusion occurs, resulting in local necking of the flame and larger break-up of the flame tip at elevated pressures.

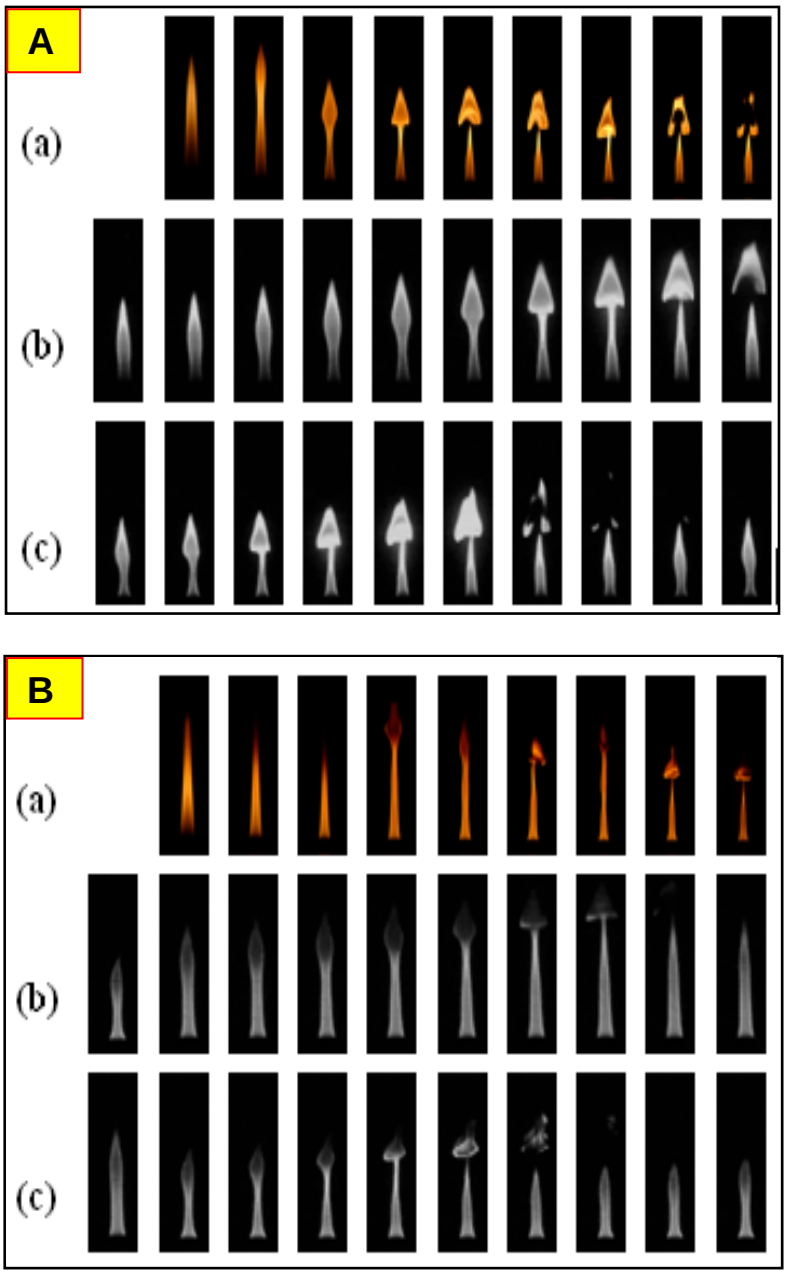

Figure 3-7: (A) Methane and (B) Ethylene diffusion flame pictures, (a) normal images taken by a digital camera at exposure time of 1/2000 sec for pressures 1, 2, 4, 6, 8, 10, 12, 14 and 16 bar (from left to right respectively). (b) and (c) are high speed images at pressures of 8 bar and 16 bar respectively. The framing rate is 500 fps and the time interval between two consecutive images is 2 ms.

The difference between the ethylene and methane flames at elevated pressures is very pronounced as can be seen in the high-speed images, the break-up of the methane flame at 16 bar is very uniform with a pair of equal size pockets of flame highlighting the structure of the outer toroidal vortex at the base of flame bulge with further separation at the tip of the breakaway flame as it is burning out. Whilst the flame tip of the ethylene flame at the same pressure is burnt out in a more turbulent manner, with a wrinkled flame surface consisting of small roll up vortices of varying amplitude. The smoking tendency in ethylene-air diffusion flame was observed to be relatively higher than methane-air flame which was modified the flickering behaviour of this flame.

The power spectra of the chemiluminescence from the flame are shown in Figure 3-8, which shows that atmospheric flames of ethylene have a peak frequency of 12.75 Hz which is half of the peak frequency of methane shown in Figure 3-8-a. Two other noticeable peak frequencies at 6.75 Hz and 13.75 Hz are observed for the power spectra of ethylene flame shown in Figure 3-8-d. This concurs with the spectra obtained of an ethylene diffusion flame by Chen et al. [40] at a downstream location of an 11 mm burner tube diameters. They suggested that the sub-harmonic frequency (6.75 Hz) results from vortex pairing; where the convective velocity of the vortex slows down as it moves up and outward allowing the next vortex formed at the burner exit to catch up producing a sub-harmonic frequency. Under elevated pressure the methane flame exhibits frequency spectra with as many as six harmonics of the peak flickering frequency (see Figures 3-8-b and c.). These observed harmonics indicate that the flame has a clearly defined coherent structure which can be confirmed from observing flame images in Figure 3-7-A. In contrast, the power spectra in Figures 3-8-e and f show that the ethylene flame has a far more complex spectrum. The dominant flickering frequency is found to match the methane flicker frequency. However, there exists other discrete peak frequencies are observed, each with their corresponding harmonics. The frequency

spectra reflect the more complicated flame dynamics of the ethylene flame discussed earlier as shown in Figure 3-7-B.

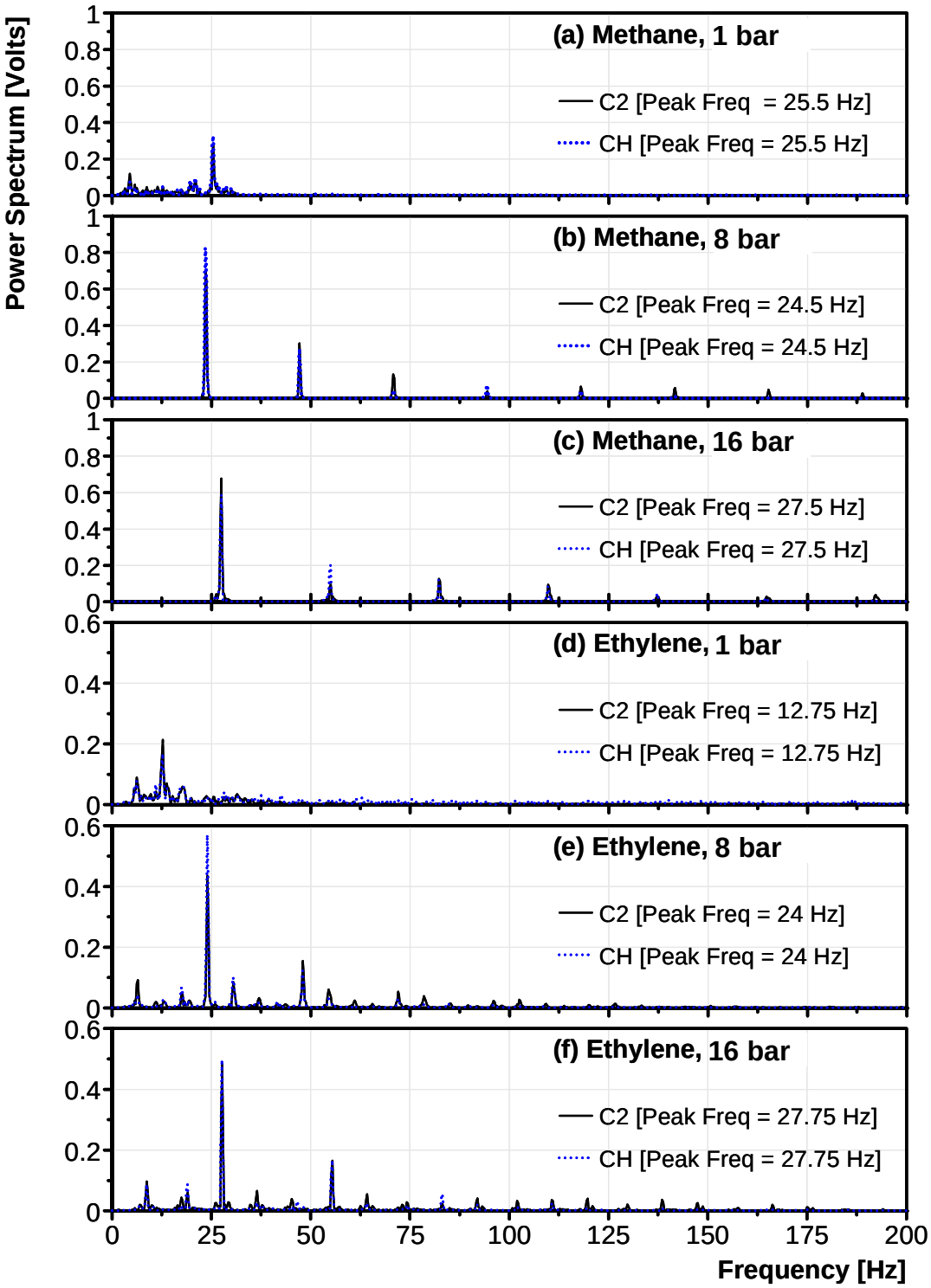

Figure 3-8: Frequency spectra for ethylene and methane diffusion flames at elevated pressures. (a) Methane at 1 bar (b) Methane at 8 bar (c) Methane at 16 bar (d) Ethylene at 1 bar (e) Ethylene at 8 bar. (f) Ethylene at 16 bar.

The influence of pressure on the flickering frequency of ethylene and methane is shown in Figure 3-9. For both fuels the dominant flickering frequency is very similar (21.5 Hz at 2 bar) and varies linearly with pressure from 2 bar onwards, which is in agreement with previous works [23, 24]. The power spectrum of the ethylene flame may appear complex at first glance, but the linear variance of the alternate frequency modes with pressure as shown in Figure 3-9. The second and third dominant peaks indicate that the flame consists of a collection of elementary flame-vortex interactions which varies in of different size and strengths.

The experimental results clearly demonstrate that fuel types have a strong effect on flame dynamics. From published data and our experience it is known that the Reynolds number has little effect on flame flickering frequency in the laminar flame regime and at atmospheric condition. The pressure is observed to have effect on the flame flickering frequency. The pure fluids effect caused by pressure change must be small if the mass flow rate is the same. The recent work of Katta et al. [42] may be of importance. They reported that the strong radiation heat loss from the soot was able to modify the flame stability significantly. This is one of the areas worth of further investigation. It is known that the pressure would affect the soot production significantly. The different reaction mechanisms of each fuel may also play an important role. A manifestation of this is the clearly observable different soot number density for burning each fuel.

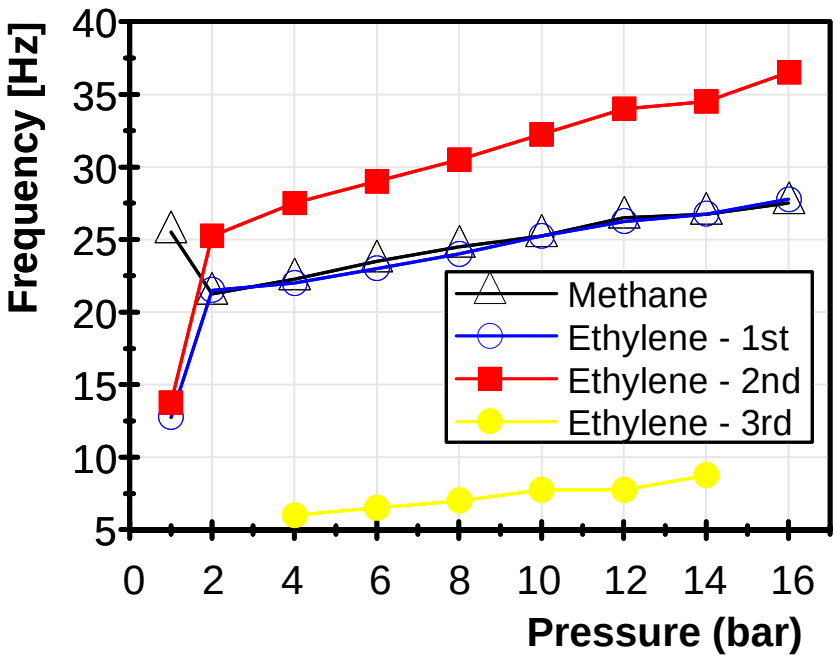

Figure 3-9: Changes in peak frequencies with pressure for methane and ethylene diffusion flames (three most dominant peaks for ethylene).

3.5 CONCLUSION

Experiments were conducted in a high-pressure burner on the influence of elevated pressure on flame shape and buoyancy induced instabilities with ethylene, methane and propane fuels. The results show that the flame dynamics is dependent on the fuel used. It was observed that flame properties are very sensitive to elevated pressures. The shape of the flame changes dramatically with increasing pressure. When the pressure increases, the axial flame height increases initially and then starts to decrease with further increases in pressure. The average cross-sectional area of the flame (A_{cs}) shows an inverse dependence on pressure to the power of n ($A_{cs} \propto P^{-n}$), where $n=0.8\pm0.2$ for ethylene flames, $n=0.5\pm0.1$ for methane flames and $n=0.6\pm0.1$ for propane flames.

It was observed that the region of stable combustion was markedly reduced as pressure was increased. The experiments confirm that a linear dependency between the dominant flickering frequency of the flame and pressure exists. Harmonic frequencies were observed for both methane and ethylene at elevated pressures. In particular, for the

ethylene flame a complex power spectrum was observed consisting of at least three peak frequency modes with their corresponding harmonics. High-speed images illustrate that the break-up of the methane flame at elevated pressures is uniform with a pair of vortex rings at the base of flame bulge which breaking away a bulk of the flame tip with further split in this bulk, as it is burning out. In contrast, the ethylene flame consists of a vortex ring which breaks away in a more turbulent manner which can be split into at least three dominant coherent structures. Each has its own harmonics that are most likely formed as the vortices break up towards the tip of the flame as confirmed in the power spectra.

To date, there is a lack of in-depth investigation on the formation of these harmonics and further investigations are required, especially on the fuel and co-flow velocities effects on the diffusion flame dynamics and instabilities, where vortex dynamics play a crucial role in the formation of different flickering modes in fuels such as methane.

"Never is a body of flame, like that which you just saw rising from the ball of the shape it appears to you. It consists of a multitude of different shapes, succeeding each other so fast that the eye is only able to take cognisance of them at all once."

M. Faraday (1791-1867)

CHAPTER 4

FUEL FLOW RATE EFFECTS ON FLAME DYNAMICS AT ELEVATED PRESSURES

4.1 ABSTRACT

The chamber pressure and fuel flow rate effects on the flickering behaviour of methane-air diffusion flames was studied over the pressure range of 1 to 10 bar. Photomultipliers and high speed imaging techniques have been used to study the frequency and magnitude of the flame oscillation and the change in global flame shape. The instability behaviour of the flame was observed to be sensitive to both the fuel flow rate and pressure. Particularly, it has been observed that the flame responds to the change of pressure more when the pressure is relatively low. High-speed imaging has shown that the periodical break-up of the methane flame at higher flow rates is almost symmetric. However, the methane flames at lower flow rates oscillate in a more waving manner due to the alternating lateral nature of the outer vortices. The average flame

luminosity was observed to increase with pressure up to 6 bar then it starts to decrease with the further increase of pressure. The flame oscillation magnitude (L_f) and oscillation wavelength (λ) were obtained from the high speed imaging database. It has been observed that the trends of these parameters correlate well with the standard deviation (σ) of mean pixel intensity (MPI), measured from the flame high speed images. The increase in fuel flow rate was observed to increase the magnitude of oscillation. The dominant flickering frequency of a methane diffusion flame varies with the chamber pressure as a function of P^n ($f=15.7P^{0.17}$).

Keywords: *Diffusion flames; Flame dynamics; Flickering frequency; High-pressure.*

4.2 INTRODUCTION

Detailed knowledge on the simultaneous pressure and flow rate dependence of thermo-physical properties of laminar diffusion flames are of significant relevance to the understanding of combustion process and instability. Many systems operate at high pressures, such as diesel engines and gas turbine combustors. Research on laminar diffusion flames at high pressures has been limited to a number of studies focused on the soot and temperature profiles within a stable laminar flame [8, 9, 16-22]. However, only a few experimental studies have been carried out on diffusion flame dynamics at sub-atmospheric [23, 24] and at elevated pressures [10]. The current understanding of the coupling effects of pressure and fuel flow rate on thermo-physical properties of sooty flames is still weak. It is well known that increased pressure plays a significant role in increasing soot concentration, leading to an overall decreasing soot temperature in diffusion flames [8, 9, 33]. Pressure also has significant effects on parameters such as flow velocity, flame structure, flickering behaviour and thermal diffusivity [10, 36].

Fuel flow rate also modifies the flame geometry and oscillation of the diffusion flames. Roper [121] proposed that the height of a buoyancy-dominated laminar co-flow

diffusion flame, established on a circular fuel nozzle, scales with fuel flow rate and inversely proportional to the coefficient of diffusion. Hottel and Hawthorne [122] investigated laminar flames of city gas burning in free air. In the laminar regime, the flame height increased with velocity to a maximum, when a flickering was first noted at the flame tip. On further increasing the velocity, the flame height decreased and the flame became turbulent. The oscillation starts when the fuel flow exceeds some critical value which is mainly attributed to the buoyancy induced instabilities and formation of outer toroidal vortices. However, the exact mechanism of this buoyancy induced instability has not been fully understood. Elevated pressure also enhances the formation and growth of these kinds of vortices as discussed in the last chapter. The simultaneous study of fuel flow rate and pressure was found to be of much interest for combustion community due to practical application of the study.

In last chapter we investigated the influence of elevated pressures up to 16 bar on the flame structure of laminar diffusion flames whereas particular attention has been paid to the fuel type effects [10]. It has been observed that the flame properties are very sensitive to the fuel type at elevated pressures. The geometry of the stable flame and the instability region of the flame were observed to change dramatically with pressure according to the fuel type. In this study, the coupling of fuel flow rate and chamber pressure on the flame dynamics (flickering behaviour) of methane-air diffusion flames is studied over the pressure range of 1 to 10 bar. Optical diagnostics (chemiluminescence and high speed imaging) have been used to study the change in flame geometry, frequency and the magnitude of flame oscillations. A wide range of fuel flow rates and pressure were studied in order to gain a better understanding of the influence of these two parameters.

The literature and the technical issues, related to this part of the study are presented in chapter 2, session 2.3.2. The presented results in this chapter have been published in

the Journal of *Combustion Science and Technology*, in a paper titled, "Methane Diffusion Flame Dynamics at Elevated Pressures" [123].

4.3 EXPERIMENTAL SETUP

The most promising burner design for high-pressure studies of sooted flames is the co-flow burner. It consists of two concentric tubes: an inner fuel tube and an outer air tube. The burner is thus annular, and can be run in either premixed or non-premixed mode. For the non-premixed flame, the inner tube contains only fuel and the outer co-flow tube contains the oxidiser. The flame attaches itself to the rim of the burner, where its heat loss is maximised [1]. The ground-breaking work in this area was performed by Miller and Maahs [17], who developed a co-flow, non-premixed flame burner and tested its stability limits under pressures between 0.1 to 5.0 MPa. The high pressure burner used in this study (see Figure 3-1) is similar to the burner applied with them [17]. The chamber has an internal height of 600 mm and an internal diameter of 120 mm. A classic over ventilated Burke–Schumann [117] laminar diffusion flame is produced which is stabilised on a fuel nozzle with an exit diameter of d_f=4.5 mm.

Gaseous methane (CH_4) fuel was supplied from a compressed gas cylinder regulated by a needle valve and measured by a calibrated mass flow meter with 1% full scale accuracy. The calibration of mass flow meters are performed by manufacturer at the standard conditions for temperature and pressure (STP) which are 70 ºF (21.1 ºC) and 14.7 psia (1.01 bar) respectively, using dry nitrogen gas. The calibration can then be corrected to the appropriate gas desired based on relative correction gas factors. The flow ranges of methane and air mass flow meters are 0-0.6 slpm and 0-50 slpm respectively, with the maximum working pressure of 500 psia (34.47 bar). During each set of the experiments, the methane mass flow rates of 0.1, 0.15, 0.2, 0.25 slpm (standard litres per minute) were kept constant at all pressures. Co-flow air is supplied

from a compressed air bottle into the burner and is diffused using a layer of glass beads, after which a honeycomb structure with 1.5 mm diameter holes is used to straighten the flow. Co-flow air was controlled by a needle valve to produce a constant mass flow rate of 15 slpm through a coaxial air nozzle with an equivalent exit diameter of d_a=37.2 mm, for all the diffusion flames. A schematic of the flow delivery and chamber exhaust systems is depicted in Figure 4-1.

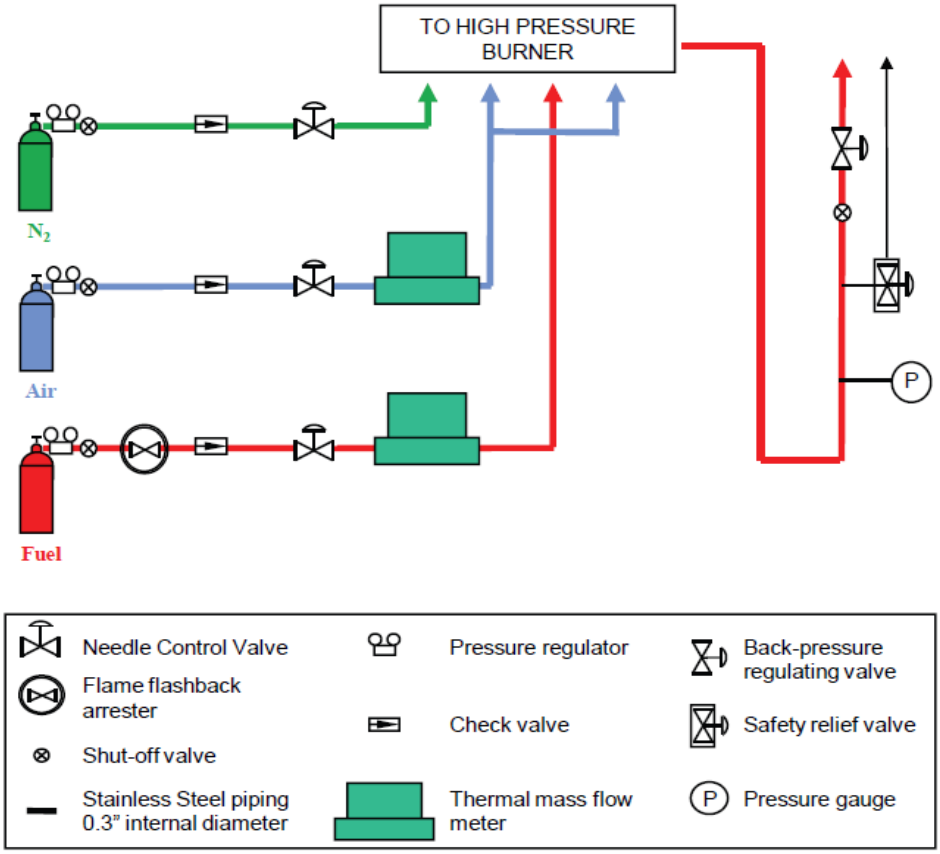

Figure 4-1: Schematic of the flow and exhaust control system for the high pressure burner [1].

To pressurise the chamber, nitrogen flow is introduced through the base of the burner using a ring of 1.5 mm diameter holes. Increasing the pressure within the vessel is achieved by increasing the flow rate of nitrogen (in the range of 0-15 slpm) and simultaneously decreasing the flow rate of the exhaust by adjusting the back-pressure regulating valve. This maintains the chamber pressure between 1 and 20 bar.

Table 4-1 shows the physical parameters of fuel and air streams for experiments. The fuel nozzle jet exit Reynolds numbers (*Re*) of the methane flow rates of 0.1, 0.15, 0.2 and 0.25 slpm were 31, 46, 61 and 76, respectively. The Reynolds number of the co-flow air through the air exit nozzle was about 514. The Reynolds number was calculated under the assumption that the flow had properties at atmospheric temperature and pressure. Increasing the pressure for a constant mass flow rate (m) does not significantly change the Reynolds number (Re) because viscosity (μ) only weakly depends on pressure [124]. One may then conclude that all flows were laminar.

Table 4-1: Fuel and air parameters in fuel flow rate experiments.

Gas Type	Volume Flow Rate		Mass Flow Rate [mg/s]	Velocity [m/s]	Re No.	Fr No.
	Slpm [L/min]	[m^3/s]				
Methane (CH4)	0.1	1.67E-06	1.13	0.115	30.51	0.312
	0.15	2.50E-06	1.7	0.172	45.76	0.703
	0.2	3.33E-06	2.27	0.230	61.02	1.249
	0.25	4.17E-06	2.83	0.287	76.27	1.952
Air	15	2.50E-04	301	0.230	513.82	0.171

The experimental setup and the optical system used for the real-time measurement of flame light emissions are shown in Figure 4-2. Two fused-quartz windows provide optical access to the burner in the visible band. The global flame light emission is focussed onto a 5 mm diameter bundle of fine fibre optical cable using a spherical lens. The bundle of fine fibres is bifurcated randomly into two equal subdivisions to produce two channels of the same signal intensity from the same imaged volume. Each channel is then guided to a photomultiplier tube ORIEL model 70704). At the end of each channel OH* and CH* interference filters at wavelengths of 308±2.5 nm and 430±5 nm are used respectively. The summation of the soot light and chemiluminescence of OH* and CH* at the two chosen wavelengths are measured. The availability of two

wavelengths may provide qualitative information on the flame chemistry. The intensity of the filtered light is converted into voltage signals which are captured by an analogue to digital data acquisition card (National Instruments PCI-MIO-16E-1) at 5000 samples per second averaged over a duration of 4 s. Real-time signal processing was performed by using a LabVIEW 8.5 virtual instrument (VI) to obtain the flame flickering frequency spectrum of the flame light emission. Optical access gained through the second fused-silica window is used to capture the evolution of the structure of the flame using a digital monochrome high speed camera. The camera uses a mega pixel resolution CMOS sensor and provides full resolution images (1024 x 1024) at frame rates up to 3,000 fps (frames per second). It has been found that a framing rate of 3,000 fps with a camera shutter speed of 1/3000 s is optimum to capture the full details of the flame flickering and to avoid image saturation.

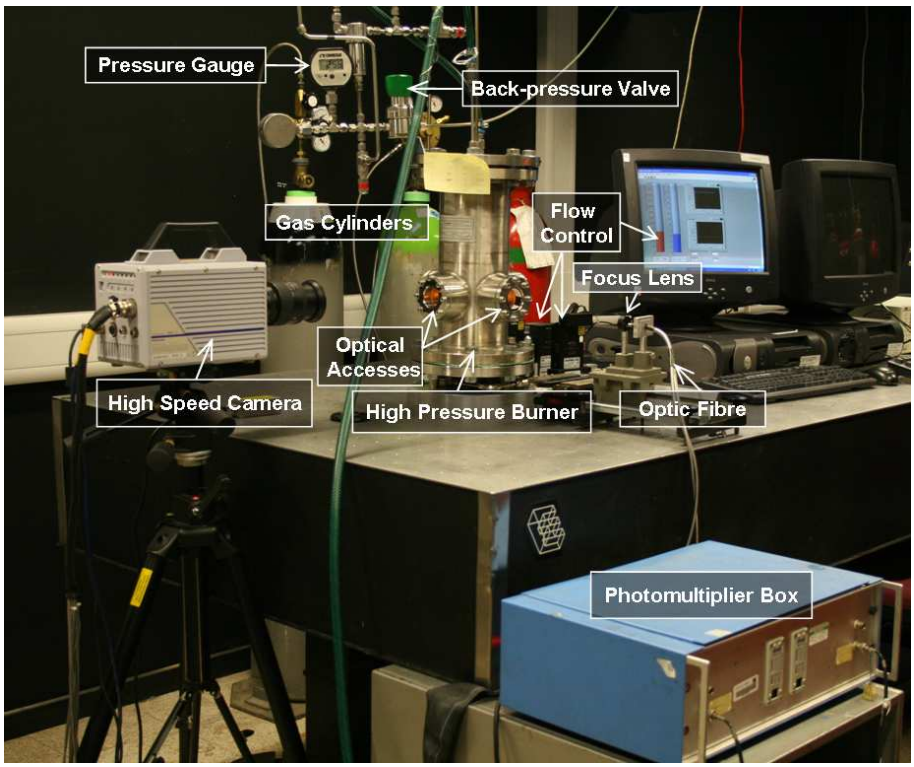

Figure 4-2: Experimental setup for flame dynamics measurements.

4.4 RESULTS AND DISCUSSION

The stable operating range for the burner is dependent on the fuel type, flow rate and the chamber pressure [10]. The effect of elevated pressure on the flickering phenomena of diffusion flames can be clearly observed in the unstable regime of methane flames for the chosen flow rates of 0.1, 0.15, 0.2 and 0.25 slpm. At atmospheric pressure, the flame shape is convex and its maximum width is wider than the burner nozzle exit diameter. The soot formation is dominant at the tip of the flame [9]. At higher pressures the soot formation dramatically increases because pressure affects the mechanism of soot formation. The flame narrows with a concave shape due to increase in fuel and air densities, while maintaining a constant mass flow rate, according to the law of conservation of mass [10, 20]. Pressure enhances the outer vortices to induce stronger flame oscillations. At atmospheric pressures, the flames appear stable at all test fuel flow rates. However, by increasing the pressure a very marked change occurred in the shape, structure and region of stable combustion. It has been observed that stronger changes of the flame geometry, temperature distribution and flickering behaviours occur at the early stages of the pressure increase.

The oscillation (flickering) of a laminar diffusion flame is known to be caused by the interaction of the flame and the vortices both inside and surrounding the flame jet. Change in both flow rate and pressure can cause vital changes in the interaction of the flame and the outer flame vortices. It is well known that the outer vortex is due to buoyancy-driven Kelvin-Helmholtz type instability and the frequencies of these vortices are well correlated with the flame bulge and the flame oscillation frequency [40, 42, 44, 59]. Although a prediction was made and later confirmed by experiments, the influence of fuel flow rate on the flickering frequency is not significant over the range of flow rates used but it has a significant effect on the magnitude of oscillation at different

tested pressures. The magnitude of oscillation (L_f) in a flickering flame is defined by the distance between the flame lowest (H_f-*min*) and highest (H_f-*max*) heights; where H_f-*ave* is the average of the oscillating flame heights. The flame height is identified as a distance from the exit of fuel nozzle to the tip of visible flame. The oscillation wavelength (λ) is defined by the length of the separated part of the flame at the moment of separation. In a stabilised (stable) flame, the flame height and the maximum flame width are characterised by 'H_f' and '*b*' respectively. The definitions of flame scale parameters and general location of the outer vortices are presented in Figure 4-3.

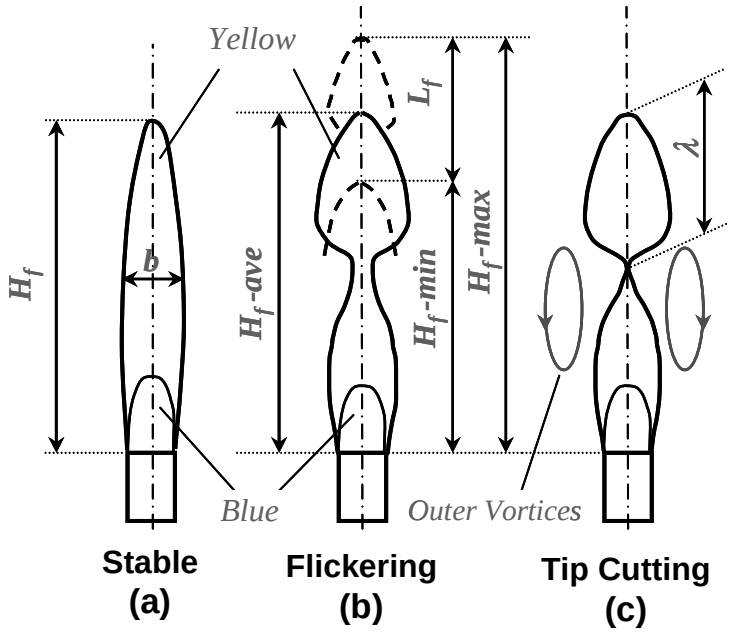

Figure 4-3: Definitions of flame scale parameters in (a) Stable (Stabilised), (b) Tip flickering, and (c) Tip cutting flames, as well as the location of the outer vortices.

It is observed that a regular flame oscillation appears when the fuel flow rate is increased above a critical value. At a higher fuel mass flow rate, the threshold pressure for a flame to become unstable is lower. At a flow rate of 0.15 slpm, the onset of observable flame flickering occurs in the flame tip at a chamber pressure of 2 bar and a small flame is periodically detached from the main flame at 4 bar. However, for a lower fuel flow rate of 0.1 slpm, the burner appears to produce a stable flame until 6 bar. Although during the entire operating regime of the burner it is shown via subtraction of

two consecutive high speed images that even a stable flame has always a very small flickering at the tip. At larger flow rates (0.2 and 0.25 slpm) and at atmospheric pressure, flames are visually stable. However, above a chamber pressure of 2 bar, very large oscillations were recorded. At a flow rate of 0.2 slpm a large flame separation was found at 4 bar. In contrast, flame separation started at 2 bar for a flow rate of 0.25 slpm. The size of the oscillation wavelength has been observed to increase initially with both fuel flow rate and pressure and then decreases with a further increase of pressure. For methane flame at lower flow rates (0.1 and 0.15 slpm) the maximum oscillation wavelength has been found to occur at 8 bar. However at higher flow rates (0.2 and 0.25 slpm) this length was a maximum at 4 bar (see Figure 4-4).

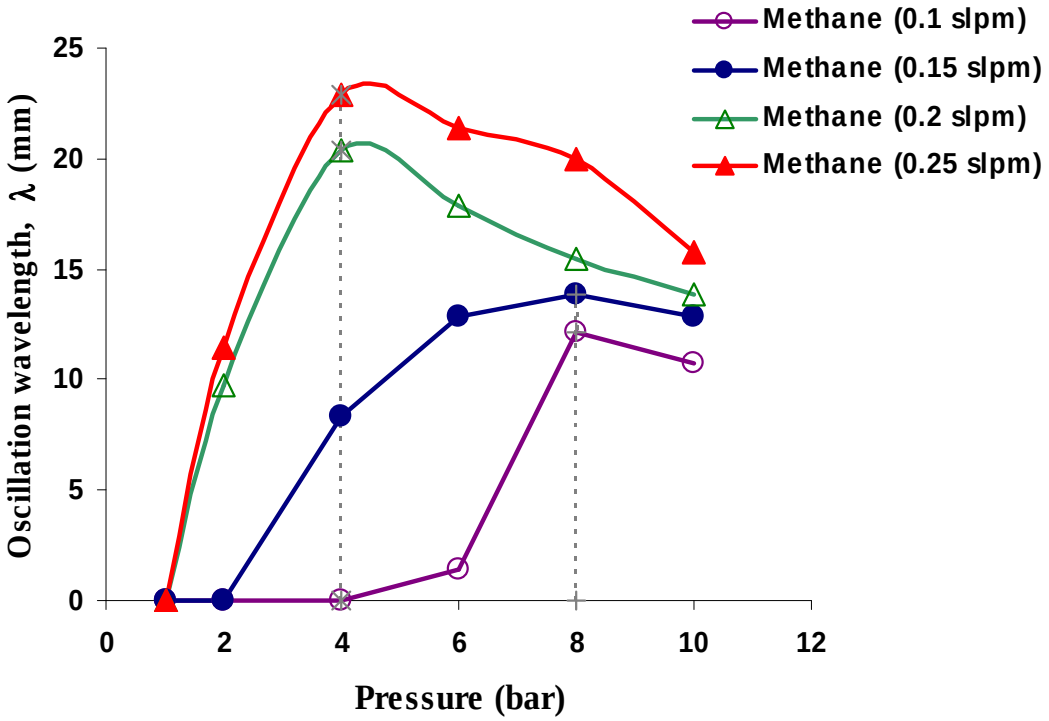

Figure 4-4: Oscillation wavelength (λ) for the methane flame at different flow rates at elevated pressures.

The oscillation magnitude generally was increased with fuel flow rate. However, the maximum oscillation magnitude has been observed to occur again at 4 bar and 8 bar for higher and lower methane flow rates respectively. The trends are consistent with the

trends of oscillation wavelength for both the higher and lower methane flow rates (see Figure 4-4). The initial increase in the flame oscillation magnitude can be explained by the dominant effect of pressure on enhancement of Kelvin–Helmholtz type of instabilities. After which, at a certain pressure soot generation effects become more dominant. It is found by [65] that in a jet diffusion flame, the magnitude of flame oscillations (flicker) decreases with the amount of soot generated in the flame, however, the frequency of the oscillations does not change. The maximum oscillation magnitude of methane at flow rates of 0.2 and 0.25 slpm was measured to be 24 and 26 mm respectively. This length was 15.7 and 18 mm at its maximum for 0.1 and 0.15 slpm methane flow rates respectively.

A sequence of high speed images of methane-air diffusion flames at 0.15 and 0.25 slpm fuel flow rates and at three different pressures of 2, 6 and 10 bar (labelled a, b and c) are shown in Figure 4-5 and Figure 4-6 respectively. The time interval between two consecutive images is 3.3ms. The lower part of each row (a, b and c) contains the resultant images obtained by subtraction of two consecutive images of the flame with a 1.6 ms time interval. The high-speed images illustrate the structure of the outer toroidal vortices outside the luminance flame and the subtraction of images show how the luminance boundaries of the flame is growing in the base and tip of the flame. Therefore, in a sequence of the flame oscillation, the image subtraction technique is able to highlight the flame surface change at certain time interval. For a methane flow rate of 0.15 slpm and at 2 bar, the flame appears stable to the naked eye (see Figure 4-5-a), however, through the subtraction results of the images (see images below row (a) in Figure 4-5) the oscillating nature of the flame is visualised from the flame moving boundaries. The rate of the flame's boundary changes increase and then decrease in a complete cycle of flame oscillation.

At higher pressures, the flame luminosity dramatically rises due to the increased formation of soot. The flame narrows and changes to concave shape, leading to flame bulge, necking and separation. The flame bulge is believed to be formed due to the rotational flow inside the outer vortices. The mechanism is speculated to be that the toroidal vortex below the flame bulge moves the flame surface radially outward while the one above the bulge drags the flame surface inward [40]. The outer vortices enhance the fuel-air mixing at some instant; as a result, the local burning rate increases leading to necking and quenching of a portion of the flame tip.

By increasing the chamber pressure, the formation and growth of outer toroidal vortices become more evident and regular flame necking is observable (see Figure 4-5-b). It is also interesting to note that this flame changes more dramatically at the flame tip and the lower part while the necking part has a slower pace of change. From Figure 4-5-b it appears that the flame oscillation is not symmetric at this flow rate and the outer vortices make the flame oscillate side by side. This phenomenon becomes more dominant at higher chamber pressures. The flame images at 10 bar (see Figure 4-5-c) and the resultant images of consecutive image subtraction clearly show the waving structure of oscillation.

The periodic nature of the flame necking and separation is due to alternate vortex shedding. The flame is then seen in its original state, as there is a time interval before the slower moving air can diffuse through this envelope and again form an envelope of flame that will extinguish later [39]. The flickering behaviour of methane diffusion flames at lower flow rates (0.1 and 0.15 slpm with the fuel mean jet exit velocity of U_f=0.12 and 0.17 m/s respectively) appears to be consistent with the planar visualised methane diffusion flame of Chen el al. [40] with Re=110 (U_f=0.19 m/s). They did not mention the waving oscillation behaviour of low jet exit velocity flames, however it is evident from the images they have presented (Fig 3-b in reference [40]).

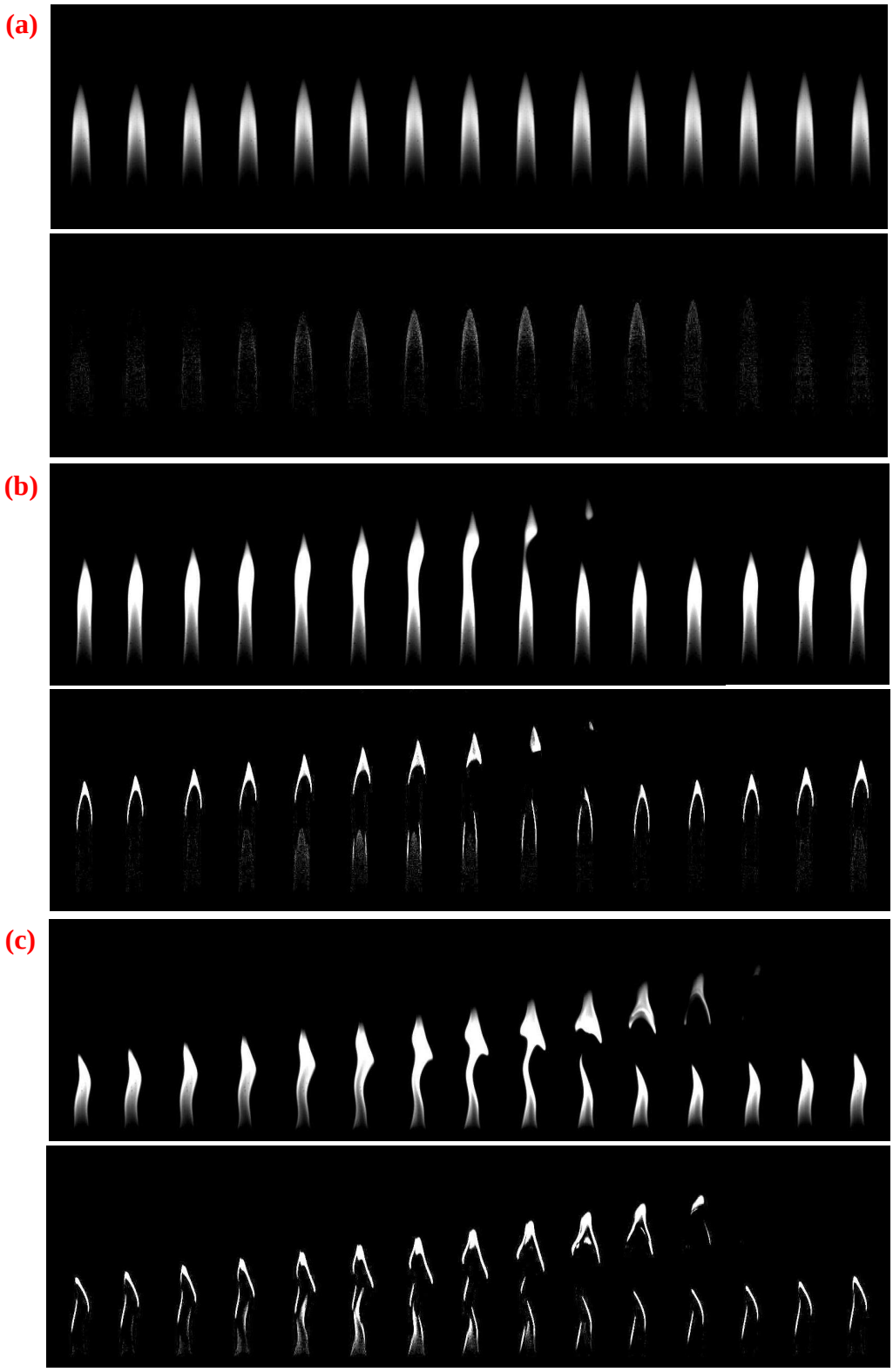

Figure 4-5: Methane (0.15 slpm)-air (15 slpm) diffusion flame pictures, taken by a digital high speed camera (FASTCAM-Ultima APX) at shutter speed of 1/3000 s at pressures (a) 2 bar (b) 6 bar (c) 10 bar. The framing rate is 3000 fps and the time interval between two consecutive images is 3.3 ms. The lower part of each row (a, b and c) belongs to the subtraction of two consecutive images of the flame at that pressure with 1.6 ms time interval.

It is worth noting that in the study of Chen el al. [40] the inner roll up vortices did not appear at the lower flow rates (Re=110 and 410), but the well defined roll-up vortices inside the luminance flame appeared at a flame height of 20 mm at Re=2390 where the size of the vortices grew rapidly upstream.

For higher flow rates, obvious flame bulge and necking starts to occur at lower pressures. A higher fuel flow rate means that the fuel jet is able to induce a stronger vortex, which would then produce better fuel and air mixing. As a result, the fuel could be burnt faster near the vortex, which causes the necking and separation to occur faster. The effect of increased buoyancy at higher flow rates is clearly highlighted in the high speed images shown in Figure 4-6 for a methane flame with a flow rate of 0.25 slpm. The flame appears to be almost stable at 1 bar, but strong oscillation at a low frequency which results in flame necking and separation was observed at 2 bar. The images of this flame at 2 bar have been presented in Figure 4-6-a. These images highlight the presence of large outer toroidal vortices outside the luminance flame. The subtracted images of Figure 4-6-a (below the original images) show how the luminance boundaries of the flame is growing in the base and tip of the flame during flame oscillation. The increase in oscillation magnitude and wavelength due to formation of the bigger outer vortices are clear from comparison of these images (Figure 4-6) with methane flame images at the same pressure but lower flow rate (Figure 4-5). According to the subtraction of images, presented in Figure 4-5 and Figure 4-6, at lower pressures and flow rates oscillations mainly occur at the flame tip. However, change of luminance flame boundaries at higher pressures and flow rates show that oscillation is dominant at both flame tip and base. It has been observed that the luminance boundaries of flame tip are growing almost twice as fast as the flame base boundaries.

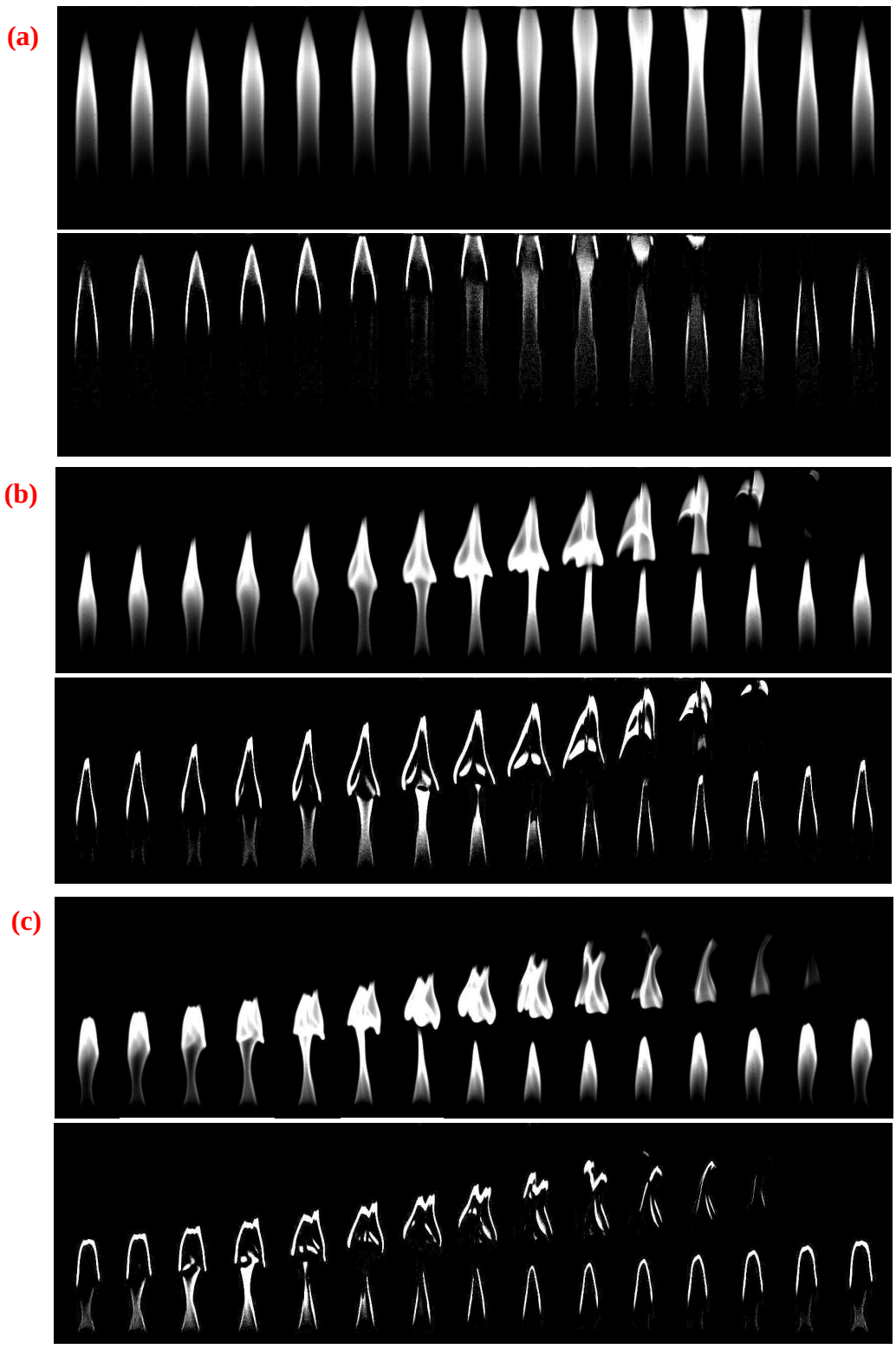

Figure 4-6: Methane (0.25 slpm)-air (15 slpm) diffusion flame pictures, taken by a digital high speed camera (FASTCAM-Ultima APX) at shutter speed of 1/3000s at pressures (a) 2 bar (b) 6 bar (c) 10 bar. The framing rate is 3000 fps and the time interval between two consecutive images is 3.3 ms. The lower part of each row belongs to the subtraction of two consecutive images of the flame at that pressure with 1.6 ms time interval.

At higher pressures, a larger chunk of the flame tip is periodically detached and burned out (see Figures 4-6-b and c, at 6 and 10 bar respectively). This may be explained by the scaling of buoyancy with pressure which will increase the convective velocity at the flame surface. This causes an increase in the acceleration of toroidal vortices, which correlates with the flame surface oscillations at the same frequency [40]. The vortices bring in more fresh air to the flame surface, therefore, a stronger local fuel-air mixing occurs, resulting in local necking of the flame and larger break-up of the flame tip at elevated pressures. Images in Figures 4-6-b and c show that the break-up of the methane flame at higher flow rates is almost symmetric with a pair of equal size pockets of flame highlighting the structure of the outer toroidal vortex at the base of flame bulge with further splitting of the breakaway flame. Conversely, the methane flames at lower flow rates oscillate in a more waving manner with a lower oscillation magnitude and wavelength and smaller detached flame tip (see Figures 4-5– b and c).

Figure 4-7 shows the typical flame/vortex interaction in a jet co-flow diffusion flame at pressures of 6 and 10 bar at methane flow rates of 0.15 and 0.25 slpm (all at the same instant sequence of 1.65 ms in a complete flickering cycle). This is according to the typical flame/vortex interaction presented by Renard et al. [114] and Katta et al. [65]. The side by side formation and growth of outer vortices at lower methane flow rates is evident in Figures 4-7-a and c, however, these vortices are almost symmetric at higher flow rates of methane (see Figures 4-7-b and d). The first identifiable outer vortex, at a flow rate of 0.25 slpm and pressure of 6 bar (at a particular instant presented in Figure 4-7-b) is located at 7 to 24 mm above the burner nozzle. An obvious flame bulge is seen after the "dislocated saddle" point A, which is located at a height of 25 mm above the burner nozzle (see Figure 4-7-b). The different positions of the outer vortices at 0.15 and 0.25 slpm methane flow rates are clearer at higher pressures (Figures 4-7-c and d respectively). The identifiable outer vortices at a flow rate of

0.15 slpm and the pressure of 10 bar is located at approximately 3 to 13 mm followed by a second vortex at 14 to 24 mm at one side above the burner. However, at the other side, the first vortex is located at 6 to 18 mm followed by a vortex located at above 19 mm (Figure 4-7-c). The first outer vortices of flame with 0.25 slpm methane at 10 bar pressure are located symmetrically at 5 to 21 mm either side of the flame at this sequence (Figure 4-7-d). As the evolution of a large scale structure is governed by Kelvin–Helmholtz instabilities, the frequency, mutual interaction and energy distribution among various length-scales are controlled by the initial conditions of the flow. Combustion processes strongly modify the instability mechanisms but coherent structures similar to those observed in non-reacting flows may be generated in an annular jet diffusion flame by forcing it at a preferred mode frequency [114].

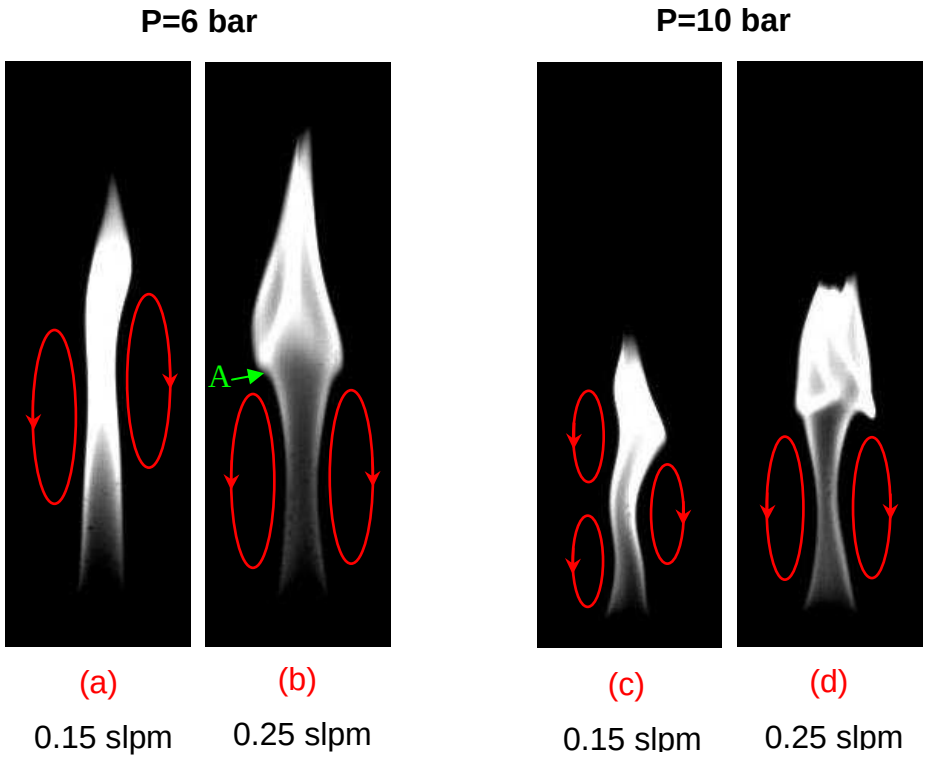

Figure 4-7: Typical flame/vortex interaction in a jet co-flow diffusion flame at pressures 6 and 10 bar for methane flow rates of 0.15 and 0.25 slpm (all at the same instant sequence of 1.65 ms in a complete flickering cycle).

The graphs of mean pixel intensity (MPI) of the flame high speed images versus time, at methane flow rate of 0.25 slpm at 6 bar, and the Fast Fourier Transform (FFT) analysis of the data for peak frequency measurement have been shown in Figures 4-8-a and b respectively. The MPI as an arbitrary unit (a.u.) was measured by image processing using MATLAB®. The maximum points of the cyclic MPI graph correspond to the maximum emission of flame; similarly the minimums refer to the minimum flame emission after burning out of the detached part periodically.

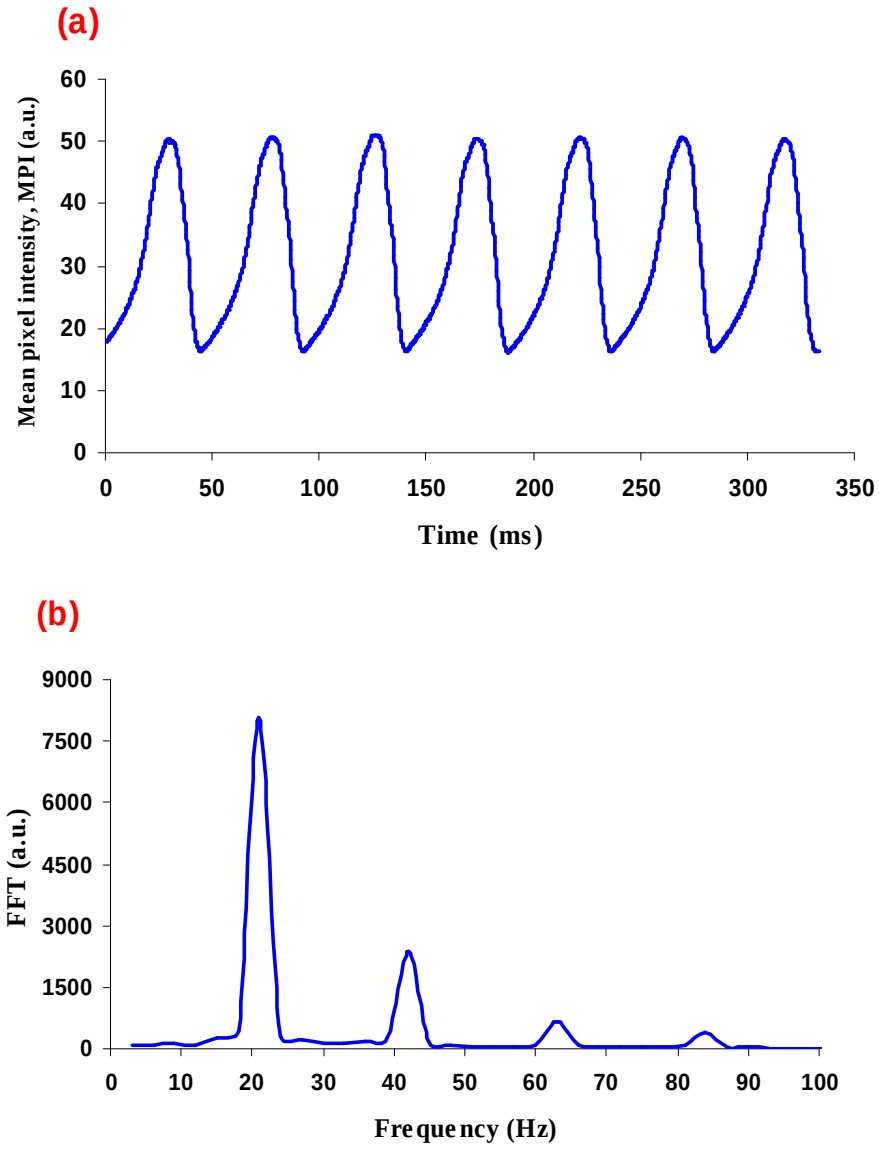

Figure 4-8: Methane (0.25 slpm)-air (15 slpm) diffusion flame at 6 bar (a) Mean pixel intensity (MPI) of flame high speed images (b) FFT analysis of MPI for peak frequency measurement.

The average of MPI values for a full data-range of high speed images at different pressures have been presented in Figure 4-9. The average flame luminosity at 0.25 slpm is almost 1.6 times that of the flame at 0.15 slpm. These intensities have been observed to increase until a certain pressure, then decrease with the further pressure increase. According to these results, the maximum intensities occur at 6 bar for all flow rates tested (see Figure 4-9).

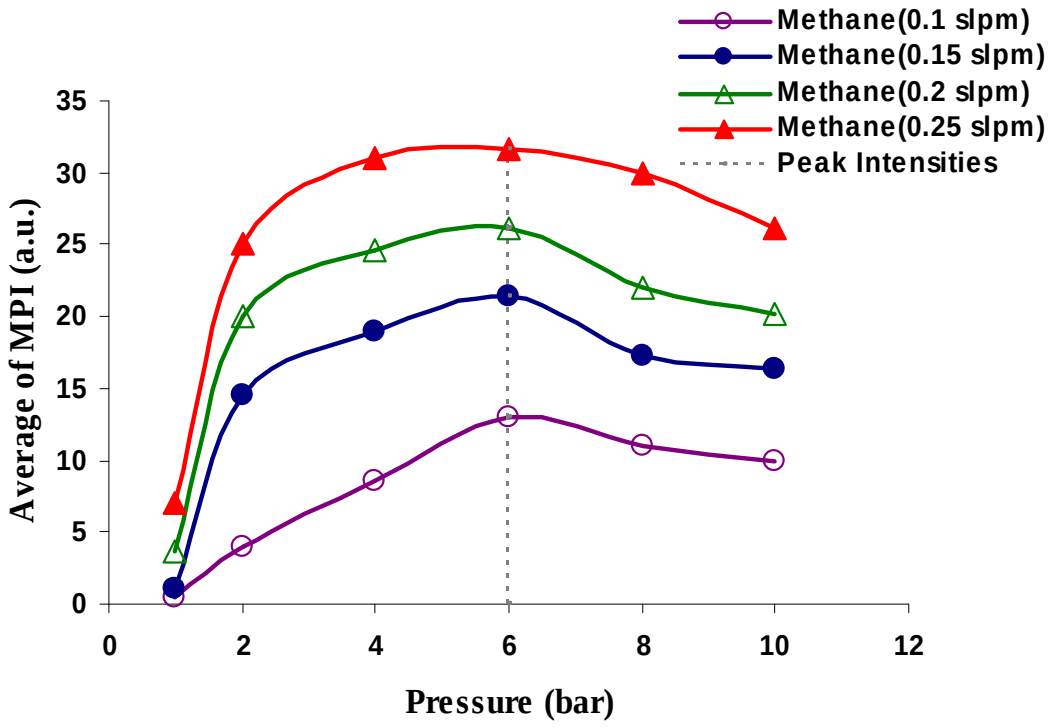

Figure 4-9: Average of mean pixel intensity (MPI) values for the methane flames at different fuel flow rates and pressures.

The trend of these results is consistent with the previous results, in which the maximum height of a stable laminar methane diffusion flame occurred at 6 bar [10]. In addition, the standard deviation (σ) of MPI, measured from the flame high speed images show that the higher flow rate generally results in more flame fluctuation and intensity variation in comparison with lower fuel flow rates (see Figure 4-10). The maximum standard deviation of MPI for 0.2 and 0.25 slpm of methane flow rates were observed at 4 bar. This maximum occurred at 8 bar for a methane flow rate of 0.1 and 0.15 slpm.

The higher value of this intensity fluctuation refers to giving off a larger portion of the detached flame (indicated by oscillation wavelength) during the flame oscillation. These results are also consistent with the trend of maximum oscillation magnitude observed for these flames (see Figure 4-4). It appears that the standard deviation of MPI can be a general indicator of the flame oscillation wavelength and magnitude trends.

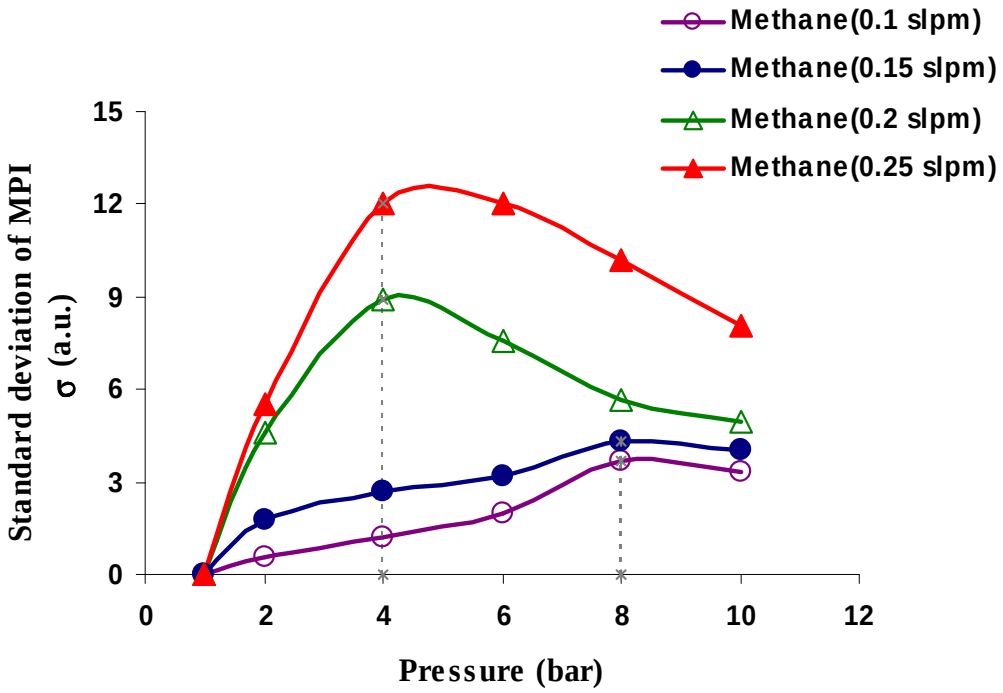

Figure 4-10: Standard deviation (σ) of mean pixel intensity (MPI) from high speed images of the methane diffusion flames at different fuel flow rates.

The power spectra of the flame emissions, by collecting the radiation spectrum at OH* and CH* emission bands using the interference filter, are shown in Figure 4-11. The frequency spectra of methane flame at 0.15 slpm (see Figure 4-11-a) shows that at atmospheric pressure, the flame has a dominant (peak) frequency of 16 Hz and three other noticeable peak frequencies at 5.75, 11.75 and 12.75 Hz, each with lower amplitude than the dominant frequency. Under elevated pressure, the methane flame at 0.15 slpm clearly exhibits frequency spectra with the peak frequencies of 21.25 Hz and 23.25 Hz at 6 and 10 bar respectively, each with as many as six harmonics of the peak

flickering frequency (see Figures 4-11-b and c). These observed harmonics indicate that the flame has a clearly defined coherent structure which can be confirmed from the flame images in Figure 4-5.

The influence of pressure on the flickering frequency of methane at a higher flow rate (0.25 slpm) is shown from comparison of power spectrums at 1 bar (see Figure 4-11-d) with 6 and 10 bar (see Figures 4-11-e and f respectively). At atmospheric pressure, methane at 0.25 slpm flickers with the dominant frequency of 16.5 Hz and three other noticeable peak frequencies of 4.75, 11.75 and 14.5 Hz. This flame under elevated pressure oscillates with the peak frequencies of 21 Hz and 23.25 Hz at 6 and 10 bar respectively. The corresponding harmonics are also observable at these pressures. For both fuel flow rates the dominant flickering frequency are very close to each other at a certain pressure.

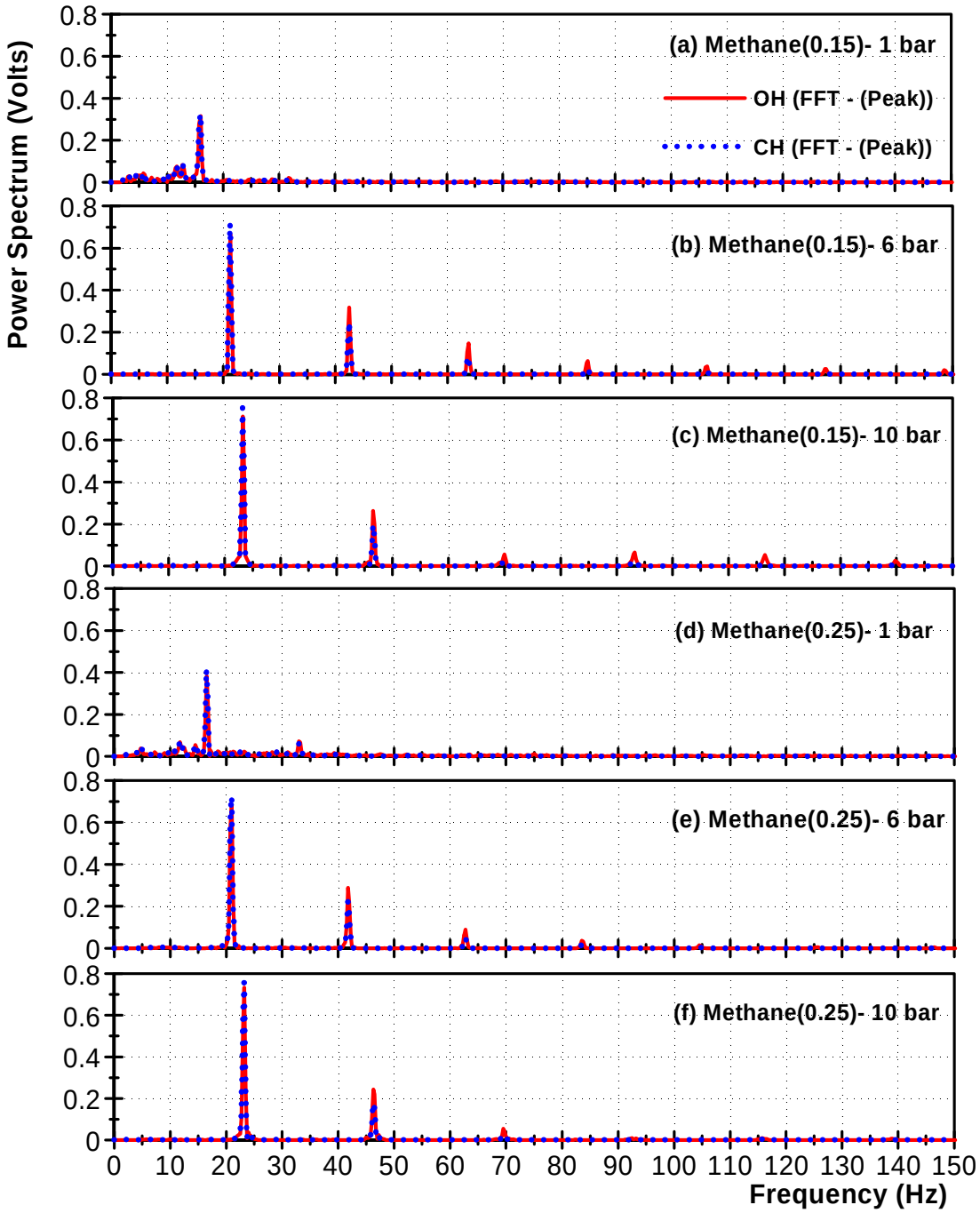

Figure 4-11: Frequency spectra for methane diffusion flames at elevated pressures. (a), (b) and (c), Methane (0.15 slpm) at 1 bar, 6 bar and 10 bar respectively and (d), (e) and (f) Methane (0.25 slpm) at 1 bar, 6 bar and 10 bar respectively.

The flickering frequency results of methane flame at different flow rates (0.1, 0.15, 0.2, 0.25 slpm) and elevated pressures up to 14 bar are presented in Figure 4-12. It has been observed that the influence of fuel flow rate on the flickering frequency is not significant over the range of flow rates used, although it has a quite significant effect on the flame oscillation magnitude and wavelength. This confirms that the weak influence

of fuel flow rate (jent momentum) on dominant frequency is valid not only at atmospheric pressure but also at elevated pressures. However, pressure has a significant effect on the dominant frequency enhancement. This confirms the hypothesis previously made on the weak influence of the jet momentum compared to the buoyancy effects [23]. It has been observed that methane flames at different fuel flow rates flicker with one dominant frequency and as many as six harmonic modes at elevated pressures. The dominant flickering frequency of a methane diffusion flame varies locally in a linear manner with the chamber pressure. However, globally the trends suggest a curve fit of $f \propto P^n$. The pressure exponent (n) was found to be about 0.17 at different flow rates. The power-law fashion indicates a decreasing dependence of flickering frequency on pressure above 10 bar. Figure 4-12 shows the dominant flickering frequency of a methane diffusion flame at different fuel flow rates with the curve of best fit on the trend of dominant frequency change by pressure ($f=15.7P^{0.17}$).

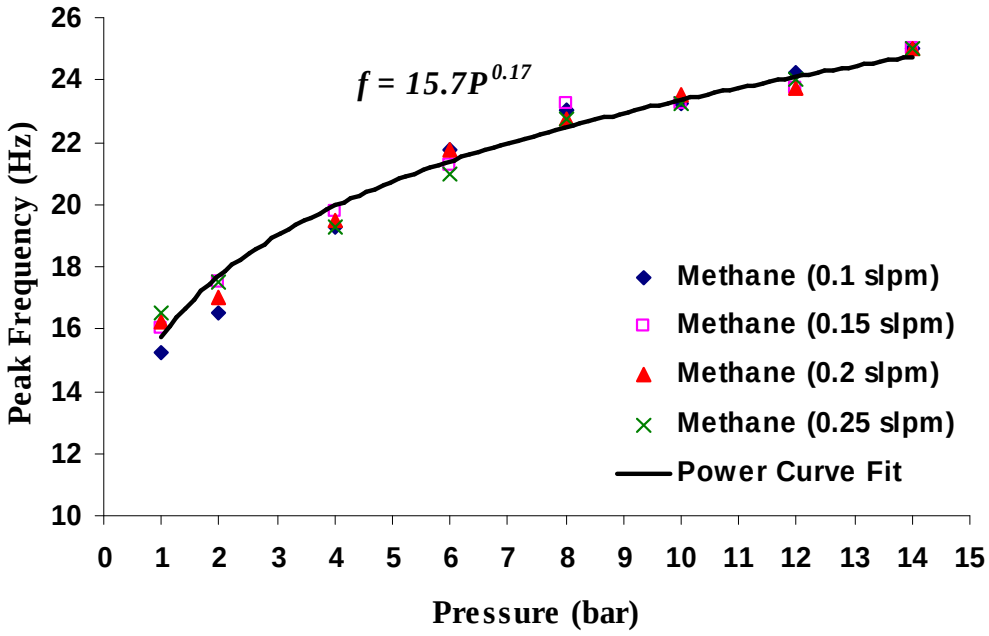

Figure 4-12: Peak oscillation frequencies of the methane air diffusion flame at different fuel flow rates at elevated pressures and the curve of the best fit.

It is worth highlighting that diffusion flames at elevated pressures are very sooty, the power spectra collected by the photomultipliers represent the summation of soot particles emission and the OH* and CH* spectra at wavelengths of 308±2.5 nm and 430±5 nm respectively. It has also been observed that in all the cases of flame chemiluminescence at elevated pressures (unstable flame) power spectra at CH* and OH* emission band are superimposed but the CH* band radiation (power spectrum) is higher than the OH* band radiation at the dominant frequency. However, at higher frequency harmonics, the relative position of each peak swap position (see Figures 4-11-b, c, e and f). At atmospheric pressure (stable flame) both spectra are completely superimposed with the same magnitude of power spectra (see Figures 4-11-a and c). At lower pressures, the blue zone at the centre of the flame envelope and next to the nozzle exit is quite clear (this part of the flame, mostly contains CH* radicals). The images by Clemens et al. [125] reveal OH* zones that appear as thin filaments connected by a diffuse region; also Leo et al. [126] suggested that the OH* concentration strongly increases with the oxygen content in the oxidiser stream. At higher pressures, the yellow region of diffusion flame will be more dominant and the stronger outer vortices bring more oxygen to the plane mixing layer of flame. Thus the emission of OH* radicals will be more dominant at a flickering flame tip and detached part of the flame tongue.

A steeper change in the thermo-physical properties of methane diffusion flame were observed at the early stage of the chamber pressure increase. The average intensity of the flame high speed images was observed to increase by an order of about 3.5 times at fuel flow rates of 0.15 slpm and 0.25 slpm from 1 bar to 2 bar. However, the maximum change in the average pixels intensity at higher pressures was of the order of 1.3 for both previously mentioned fuel flow rates (see Figure 4-9). The change of flame flickering frequencies from 1 to 2 bar is also very pronounced. At 1 bar, only the dominant frequency was clearly observable (see Figures 4-11-a and d) while there were

as many as six corresponding harmonics at 2 bar for both flow rates. With further increase in chamber pressure, the change of peak frequency follows the trend presented in Figure 4-12.

The main reason for these steeper changes of flame properties at initial steps of pressure increase can be attributed to the quick change in the flame shape from convex to concave through the pressure dependence of the mixture density ($\rho \propto P$) and the binary diffusion coefficient ($D_{ij} \propto P^{-1}$). At elevated pressures, due to the increased presence of soot (which acts as a reaction intermediary), the reaction processes are also different from those acting at atmospheric pressure. The temperature decreases due to more formation and illumination of the soot particles. [127] indicated a decreasing dependence of soot yield on pressure above 10 bar. Also the results of the present study show a decreasing dependence of flickering frequency on pressure above 10 bar. It means after a certain pressure the gradient of changes in flame properties will decrease.

4.5 CONCLUSION

Experiments were conducted in a high-pressure burner to investigate the effects of fuel flow rate and chamber pressure on the flickering behaviour of methane-air diffusion flames. Global flame emission dynamics and high speed imaging have been applied to study the methane diffusion flame dynamics at different flow rates across a pressure range of 1 to 10 bar.

The experimental results clearly demonstrate that both pressure and fuel flow rate have a strong effect on the diffusion flame dynamics. The pressure is observed to change the flame shape, structure, flickering magnitude and frequency due to enhancement in the formation and growth of outer toroidal vortices. The mass flow rate effects on oscillation magnitude and structure of vortices emerge from high speed

images. The flickering frequency, however, remains almost constant at each pressure despite increase in fuel flow rate.

High-speed images have shown that the periodic break-up of the methane flame at higher flow rates (0.2 and 0.25 slpm) and elevated pressures is almost symmetric, with a pair of equal size pockets of flame highlighting the structure of the outer toroidal vortices with further separation at the tip of the breakaway flame part and it then splits into at least two wrinkled coherent flame structures .However, the methane flames at lower flow rates (0.1 and 0.15 slpm) oscillate in a more waving manner and the flame tip is burnt out consisting of one portion of flame tongue. A steeper change was also observed on the flame structure, temperature field and dynamics of methane diffusion flame at early stages of the increase in chamber pressure.

The average of mean pixel intensity (MPI) values in a full sequence of flame images (proportional to the flame emission intensity) at all methane flow rates has been found to increase with pressure up to 6 bar then it starts to decrease with the further increase of pressure. For methane flame at lower flow rates the maximum oscillation wavelength (λ) and maximum standard deviation (σ) of MPI have been observed to occur at 8 bar. However at higher flow rates these parameters were maximum at 4 bar. The increase in fuel flow rate increases the magnitude of oscillation (L_f). The flickering frequency, however, remains almost constant at each pressure. It has been observed that methane flames flicker with one dominant frequency and as many as six harmonic modes at elevated pressures. The peak flickering frequency of a methane diffusion flame generally varies with the chamber pressure as a function of P^n ($f=15.7P^{0.17}$).

"Vortex interactions with flames play a key role in many practical combustion applications. Such interactions drive a large class of combustion instabilities and control to a great extent the structure of flames. "

P. H. Renard (2000)

CHAPTER 5

CO-FLOW AIR EFFECTS ON DIFFUSION FLAME DYNAMICS

5.1 ABSTRACT

This chapter describes experimental investigation of co-flow air velocity effects on the flickering behaviour of laminar methane diffusion flames. In this study, chemiluminescence, schlieren, and high speed photography along with digital image processing techniques have been used to study the change in global flame shape, the instability initiation point, the frequency and magnitude of the flame oscillation. Four cases of methane flow rates at different co-flow air velocities are investigated. It has been observed that the flame dynamics and stability of co-flow diffusion flame are strongly affected by the co-flow air velocity. When the co-flow velocity has reached at certain value the buoyancy driven flame oscillation was completely suppressed. The schlieren imaging has revealed that the co-flow of air is able to push the initiation point of outer toroidal vortices beyond the visible flame to create a very steady laminar flow

region in the reaction zone. Then the buoyancy driven instability is only effective in the plume of hot gases above the visible flame. It is observed that a higher co-flow rate is needed in order to suppress the flame flickering at a higher fuel flow rate. Therefore the ratio of the air velocity to the fuel velocity, γ, is a stability controlling parameter. The velocity ratio, γ, was found to be 0.72 for the range of tested flow rates. The oscillation frequency was observed to increase linearly with the co-flow rate, a, as; $f=0.33a+11$. The frequency amplitudes, however, were observed to continuously decrease as the co-flow air was increasing. The oscillation magnitude (L_f) and the oscillation wavelength (λ) were observed to decrease towards zero as the co-flow air was increasing. Whereas the average oscillating flame height behaviour was observed to be bimodal. It was initially enhanced by the co-flow air then starts to decrease towards the stabilised level. This height was observed to remain almost constant after stabilisation, despite further increase at air flow rate.

Keywords: *Diffusion flames; Co-flow air; Flame dynamics; Flickering Suppression.*

5.2 INTRODUCTION

Diffusion flames are desirable from the consideration of safety in practical systems, they generally have inferior pollutant emission characteristics due to the stoichiometric combustion and long residence times involved [3]. The knowledge about steady-state laminar diffusion flames has progressed rapidly over the last few years. This includes the modelling and measurement of different aspects, like soot concentration and temperature distribution. Practical combustion devices, however, often operate under unsteady conditions. Laminar oscillating flames provide an opportunity to take advantage of the repeatability of the oscillations from cycle to cycle in investigating the phenomena of unsteady combustion [15]. Furthermore, laminar oscillating flames keep their rotational symmetry, which simplifies data evaluation and reduces the expenditure

of time of computational work [15]. However the study of combustion processes is still difficult because of the complex interactions between the fluid dynamics and the chemistry [2].

It is well known that the mechanism behind oscillation of laminar diffusion flames is attributed to the interactions between flame and vortices both inside and surrounding the luminance flame. The generation of the outer toroidal vortices has been attributed to a Kelvin–Helmholtz instability driven by a buoyancy induced shear layer surrounding the flame surface [38, 41, 43-45]. Therefore buoyancy affects on the shape and flickering frequency of diffusion flames. It is speculated that the frequency of the outer vortices correlated with the flame oscillation frequency [24].

Buoyancy is directly related to the Froude number (*Fr*), which is a dimensionless number comparing inertia and gravitational forces. In fluid dynamics *Fr* can be viewed as the ratio between the stream velocity and the velocity of the fastest surface wave ($Fr = U/(gd)^{1/2}$), where U is the fluid mean velocity and '*g*' the gravitational acceleration and '*d*' is the characteristic length (for example fuel nozzle or air exit diameter). An alternate definition used in combustion studies is ($Fr = U^2/(gd)$) where each of the terms on the right have been squared. This form is the reciprocal of the Richardson number that expresses the ratio of potential to kinetic energy. Consequently it can be conducted that the Froude number of the fuel jet is controlled by gravity level, diameter of the nozzle, fuel properties, and fuel flow rate [53]. In addition the Strouhal (*St*) number is a dimensionless number describing oscillating flow mechanisms. The *St* is often given as, $St = fd/U$, where *f* is the frequency of vortex shedding. According to the normal-gravity experiment reported by Hamins et al. [57] the flickering frequency of non-premixed flames burning methane was characterised by the Strouhal number (*St*)

as a function of the Froude number (*Fr*). They concluded that the relation between *St* and *Fr* follows, $St \propto Fr^{-0.57}$.

Change in combustion flow field by varying fuel or air flow rates result in change of different aspects of flame properties, i.e., flame geometry, flickering behaviour, combustion stability and temperature field. The coherent flow structures in the air co-flow strongly interact with the reaction zone, which ultimately may lead to local flame extinction [40]. The formation of coherent structures is attributed primarily to a modified Kelvin-Helmholtz instability of the flow field [38, 40, 43-45]. These structures, could be observed in the co-flow region, whereas vortical structures inside the flame surface were detected only when contoured fuel nozzles and large jet velocities were employed [40, 43, 45]. In spite of the extensive amount of research work related to the evolution of structures in buoyant jet diffusion flames, a definite and rigorous interpretation of the mechanisms leading to the formation of coherent flow structures is still lacking [43].

Interestingly, during the experiments on diffusion flame dynamics the effects of change in co-flow air on oscillation behaviour of methane diffusion flame was found to be very pronounced. Co-flow air was observed to modify dynamics of a flickering methane diffusion flame to such an extent that the flame oscillations were suppressed (stabilised). The results tend to be more interesting when it was noticed that the co-flow air increases the flame flickering frequencies while decreasing the oscillation magnitude until the flame instability suppression mode. Indeed it seems that the closer understanding of diffusion flame instabilities due to formation of outer vortices might be gained by studying the influence of co-flow air on the flame dynamics. The co-flow air effect on the dynamics of laminar non-lifted diffusion flames is left almost unattended in literature. The objective of this study is to investigate in detail, the co-

flow air flow rate (velocity) effects on non-lifted methane diffusion flame dynamics using experimental approach.

The literatures related to this part of the study are presented in Chapter 2, session 2.3.3. Part of the presented results in this chapter has been submitted to the journal of *Energy Conversion and Management (ECM)* in a paper titled, "Impact of Co-flow Air on Buoyant Diffusion Flames Flicker", which is under review [128].

5.3 EXPERIMENTAL SETUP

The atmospheric co-flow burner used in this study which is able to produce a classic over ventilated Burke–Schumann [117] laminar diffusion flame is shown in Figure 5-1. The flame is stabilised on a fuel nozzle with an exit diameter of d_f=4.5 mm. During each set of the experiments, the gaseous methane (CH_4) mass flow rates of 0.2, 0.25, 0.3, 0.35 slpm (standard litres per minute) were kept constant at all air flow rates. Co-flow air is supplied from a compressed air bottle into the burner and is diffused using a layer of glass beads, after which a honeycomb structure with 1.5 mm diameter holes is used to straighten the flow. Co-flow air was controlled by a needle valve to produce a range of mass flow rates from 1 to 20 slpm through a coaxial air exit nozzle with a shroud diameter of 37.8 mm.

Table 5-1 shows the physical parameters of fuel and air streams for experiments. The fuel (methane) jet exit velocities are in a range between 0.23 to 0.4 m/s (23 to 40 cm/s) and the Reynolds numbers (*Re*) of 61 to 107. However the air exit velocities are in a region of 0.05 to 0.31 m/s (5 to 31 cm/s) with the *Re* in the range of 102 to 685. One may then conclude that all flows were in laminar mode during all sets of experiments. The buoyant acceleration of hot gases outside the diffusion flame surface can cause shear-layer rollup, leading to the formation of toroidal vortex rings, which then interact with the flame surface or the separated plume region depending upon the

value of the Froude and Reynolds number [3]. From Table 5-1 it appears that Froude number, which is directly proportional to the square of mean fluid velocity increases by increase at fuel or air flow rates. The maximum *Fr* of the fuel stream was about 3.8 at 0.35 slpm of methane flow rate and the maximum *Fr* of the co-flow air is calculated to be about 0.3 at 20 slpm of air flow rate. The *Re* and the *Fr* of the air streams have been calculated base on the hydraulic diameter of annulus air port (D_H= Do-Di=31.5 mm).

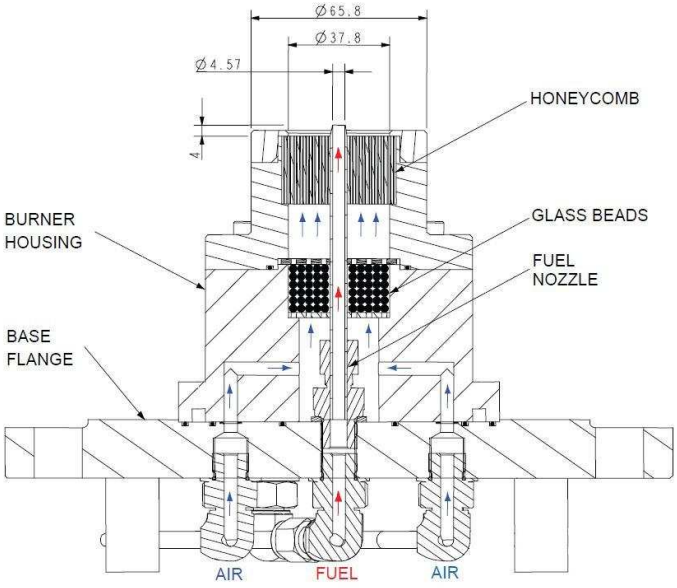

Figure 5-1: Cross-section of the co-flow diffusion flame burner.

Table 5-1**:** Fuel and air parameters in co-flow air experiments.

Gas Type	Volume Flow Rate		Mass Flow Rate [mg/s]	Velocity [m/s]	Re No.	Fr No.
	Slpm [L/min]	[m^3/s]				
Methane (CH_4)	0.2	3.33E-06	2.27	0.230	61.02	1.249
	0.25	4.17E-06	2.83	0.287	76.27	1.952
	0.3	5.00E-06	3.40	0.344	91.52	2.810
	0.35	5.83E-06	3.97	0.402	106.78	3.825
Air	3	5.00E-05	601	0.046	102.76	0.007
	5	8.33E-05	100	0.077	171.27	0.019
	7	1.17E-04	140	0.107	239.78	0.037
	10	1.67E-04	200	0.153	342.55	0.076
	13	2.17E-04	260	0.199	445.31	0.129
	15	2.50E-04	301	0.230	513.82	0.171
	20	3.33E-04	401	0.307	685.09	0.304

The optical system used for the real-time measurement of flame light emissions is shown schematically in Figure 5-2. The chemiluminescence (photomultipliers) setup has been explained in details in the previous chapter (section 4.3). The summation of the soot light and chemiluminescence of OH* and CH* at the two chosen wavelengths are measured. Thus, the availability of two wavelengths may provide qualitative information on the flame chemistry. The intensity of the filtered light is converted into voltage signals which is captured by an analogue to digital data acquisition card (National Instruments PCI-MIO-16E-1) at 5000 samples per second averaged over a duration of 4 s. Real-time signal processing was performed by using a LabVIEW 8.5 virtual instrument (VI) to obtain the flame flickering frequency spectrum of the flame light emission.

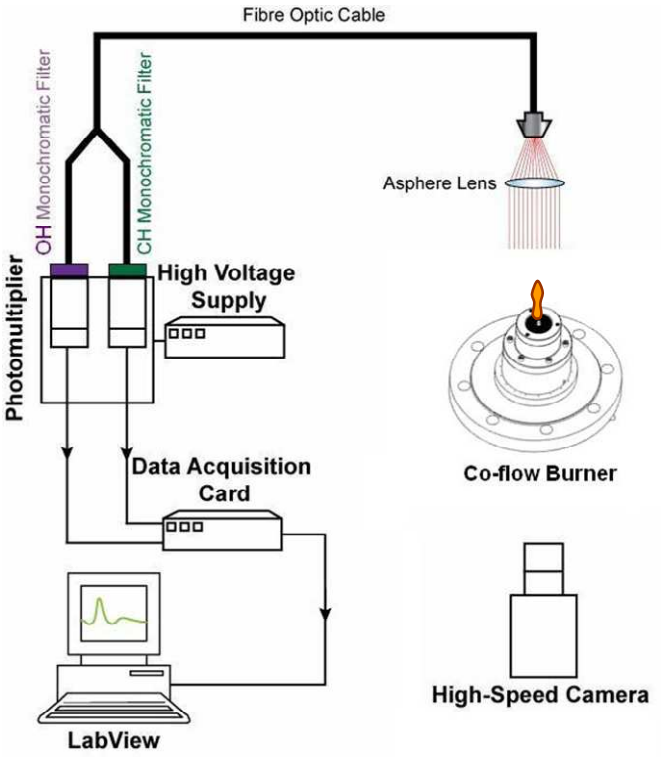

Figure 5-2: Schematic of the experimental setup.

To capture the evolution of the structure of the flame a digital monochrome high speed camera (Photron FASTCAM SA-3) has been used which can record up to 120,000 fps (frames per second). The camera uses a mega pixel resolution CMOS

sensor and provides full resolution images (1024 x 1024) at frame rates up to 2,000 fps. It has been found that a framing rate of 2,000 fps with a camera shutter speed of 1/5,000 s is optimum to capture the full details of the flame flickering and to avoid image saturation. Also in the all tested cases, the evolutions of hot gases and their interaction with the co-flow air were captured by a Z-type high speed schlieren imaging system, utilising the same framing rate (2,000 fps) and 1/200,000 s shutter speed.

5.4 RESULTS AND DISCUSSION

In buoyant co-flow diffusion flames the stable (non-flickering) operating range for the burner is dependent on the fuel and co-flow types and flow rates, also nozzle exit diameters and the ambient pressure [10]. The stable methane diffusion flame is convex in shape (has a bulbous is appearance) and its maximum width is wider than the burner nozzle exit diameter. In an unstable flame the acceleration of hot reaction zone leads to an axisymmetric flow field, which exhibits at least tree inflation points on either side of the symmetry axis [45]. It has to be noted that in laminar methane diffusion flame at atmospheric pressure the soot formation is mainly dominant at the tip of the flame, however the base of flame was observed to be mainly bluish and relatively free of soot particles [9, 10]. According to the generic shape of a laminar annular diffusion flame (LADF) issuing from a standard co-flow burner, the flame front reaction zone, or flame surface, is defined as the surface on which the equivalence ratio (φ) is equal to one. In the other word, the flame front can be described as a locus of point at which air and fuel meet in proportions equivalent to those observed under stoichiometric conditions [1]. It should be noted the visible luminous flame boundaries by the naked eye do not exactly correspond to this surface [129].

The following results are obtained from the experimental study on the effect of co-flow air on the flickering behaviour of laminar diffusion flames which is not reported in

existing literature. Change in co-flow rate cause vital changes in the interaction of the flame and the outer flame vortices. It is well known that the outer vortex is due to buoyancy-driven Kelvin-Helmholtz type instability and the frequencies of these vortices are well correlated with the flame bulge and the flame oscillation frequency [40, 42, 44, 59]. The fuel flow rate does not have a significant effect on oscillation (flicker) frequency of diffusion flame [37-40, 55, 56]. The co-flow air, however, is found to strongly modify not only the oscillation frequency but also the oscillation magnitude (L_f) and the oscillation wavelength (λ) of the flame. The definitions of flame scale parameters and the outer vortices position are presented in Chapter 4, Figure 4-3. The flame height is defined as a distance from the exit nozzle to the tip of flame. In a stabilised (stable) flame, the flame height and the maximum flame width are characterised by 'H_f' and 'b' respectively.

It is observed that in a methane flame with zero co-flow, a regular self-exited flame oscillation (flicker) appears when the fuel flow rate is increased above a critical value (0.1 slpm). These oscillations are thus attributed to instability in laminar buoyant fuel jet and the flow field which may develop a sinusoidal oscillation and form periodic vortices. Self-excited and axisymmetric wave-like structures, propagate up-and downstream of the burner rim [43, 45]. These cause the flame to flicker and when strong may result in tongues of flame periodically breaking off from the main flame [4]. It has to be noted that the buoyant diffusion flame instabilities are associated with buoyancy induced and shear layer force sources. The Froude Number (Fr) is representative of the buoyancy induced type of instability however shear forces between non reacting flow fuel jet and the surrounding air layer cause the hydrodynamic (Kelvin–Helmholtz) type of instability. The Kelvin–Helmholtz instability can occur when velocity shear is present within a continuous fluid or, when there is sufficient velocity difference across the interface between two fluids.

In this study, four cases of methane flow rates at different co-flow air velocities are examined. A full cyclic sequence of high speed images of methane-air diffusion flames at 0.3 slpm fuel flow rate (nozzle mean velocity of 34 cm/s) and without co-flow air (zero co-flow) is shown in Figure 5-3-a. The time interval between two consecutive images is 5 ms. The lower part of this row contains the resultant images obtained by subtraction of two consecutive images of the flame with a 2.5 ms time interval. The high-speed images illustrate the structure of the outer toroidal vortices outside the luminance flame and the subtraction of images show how the luminance boundaries of the flame is growing in the base and tip of the flame. Therefore, in a sequence of the flame oscillation, the image subtraction technique is able to highlight the flame surface change at certain time interval. A regular and reproducible oscillation was observed in this flame due to periodic interaction of flame/vortices in flame and surrounding air. The rate of the flame's boundary changes increase and then decrease in a complete cycle of flame oscillation. Initially the main pack of change is belonged to the flame tip and then it is observed at both tip and neck of the flame, after which necking separates the bulged section of the flame. The flame bulge is believed to be formed due to the rotational flow inside the outer vortices. The mechanism is speculated to be that the toroidal vortex below the flame bulge moves the flame surface radially outward while the one above the bulge drags the flame surface inward [40]. The outer vortices enhance the fuel-air mixing at some instant and consequently the local burning rate increases leading to necking and quenching of a portion of the flame tip. At zero co-flow flame the separated part of the flame presents almost a rounded bubble shape.

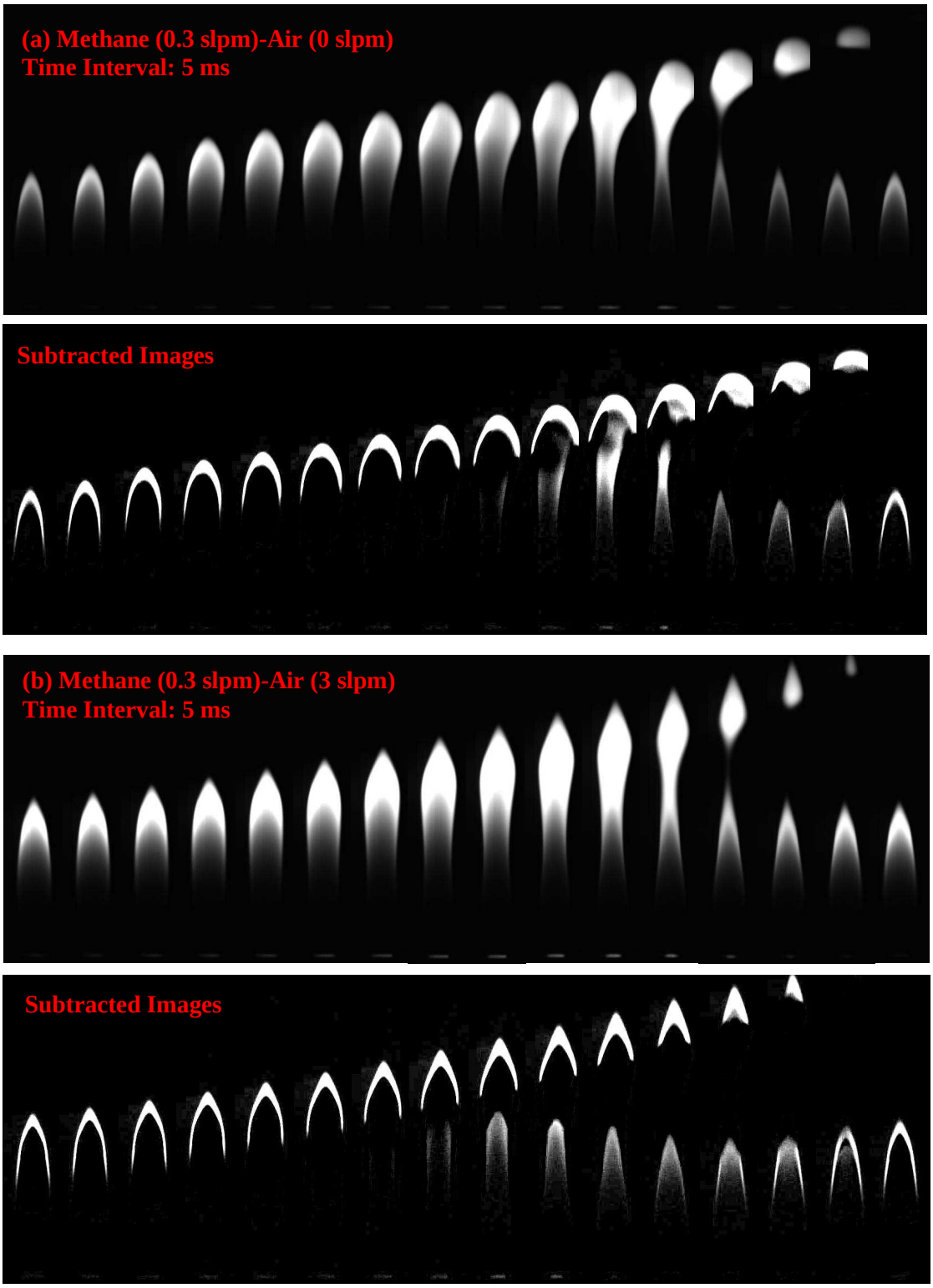

Figure 5-3: Methane (0.3 slpm)-air ((a) 0 slpm & (b) 3 slpm) diffusion flame pictures, taken by a digital high speed camera (FASTCAM-SA-3) at shutter speed of 1/5,000 s. The framing rate is 2,000 fps and the time interval between two consecutive images is 5 ms. The lower part of each row belongs to the subtraction of two consecutive images of the flame with 2.5 ms time interval.

By start of blowing the co-flow air and increasing the flow rate (and as a result the exit velocity) of air to 3 slpm (4.6 cm/s), the formation and growth of outer toroidal vortices become more evident. It was observed that the regular flame necking and separation is happening faster by increase in co-flow air. The flame shows a small stretch in the direction of blowing co-flow with a decrease in the size of the separated tongue of flame. Also the geometry of this part was changed to almost a lozenge shape (see Figure 5-3-b). The subtracted images of this flame (lower part of Figure 5-3-b) clarify a continue change in the flame tip boundaries which are generally sharper than the flame boundaries with zero co-flow (Figure 5-3-a). It is also interesting to note that this flame changes more dramatically at the flame tip and base while the necking part has a slower pace of change. The periodic nature of the flame necking and separation is due to alternate vortex shedding. The flame is then seen in its original state, as there is a time interval before the slower moving air can diffuse through this envelope and again form a flame envelope that will burn-out later [39]. A stronger outer vortex would then produce better fuel and air mixing. As a result, the mixture could be burnt faster near the vortex, which causes the necking and separation to occur faster. In other words, the extinction occurs when the induced field of the vortex is sufficiently strong to cause a localised flow reversal within the fuel stream, the reaction zone then being drawn outwards into the vortex [35]. This happens naturally in small diffusion flames where the flicker involves complete separation of the flame tip [40].

For larger flow rates of co-flow air at 5 slpm (7.7 cm/s), obvious flame bulge and necking starts to occur at higher heights of the flame. As a result a smaller chunk of flame is detaching from the main body (see Figure 5-4-a). A higher co-flow air flow rate means that the air jet is able to push the vortices outside the luminous flame farther downstream of visible flame. There was a significant decrease observed in the oscillation magnitude (L_f) and wavelength (λ) by co-flow air increase. The flame tip of

the methane flame at 7 slpm (10.7 cm/s) air was observed to flickering with about 1.5 mm rms without any separation from the flame tip (see Figure 5-4-b). In this case the flame appears almost stable to the naked eye, however, through the subtraction of consecutive images the oscillating nature of the flame is revealed by the flame moving boundaries (see images below Figure 5-4-b). A co-flow air flow rate of 7 slpm may be defined as an intermittency transient mode between strongly flickering and suppressed (stabilised) flames at air flow rates of 5 slpm and 10 slpm respectively. The most striking result to emerge from the data is that, when the co-flow air flow rate (velocity) is increased to 10 slpm (15.3 cm/s), the flame oscillation is completely suppressed (stabilised). The decrease in Kelvin-Helmholtz and buoyancy driven instabilities and also change in the initiation point of the toroidal vortices (instability initiation point) by the increase of co-flow air can be the main physical explanation behind this interesting phenomenon.

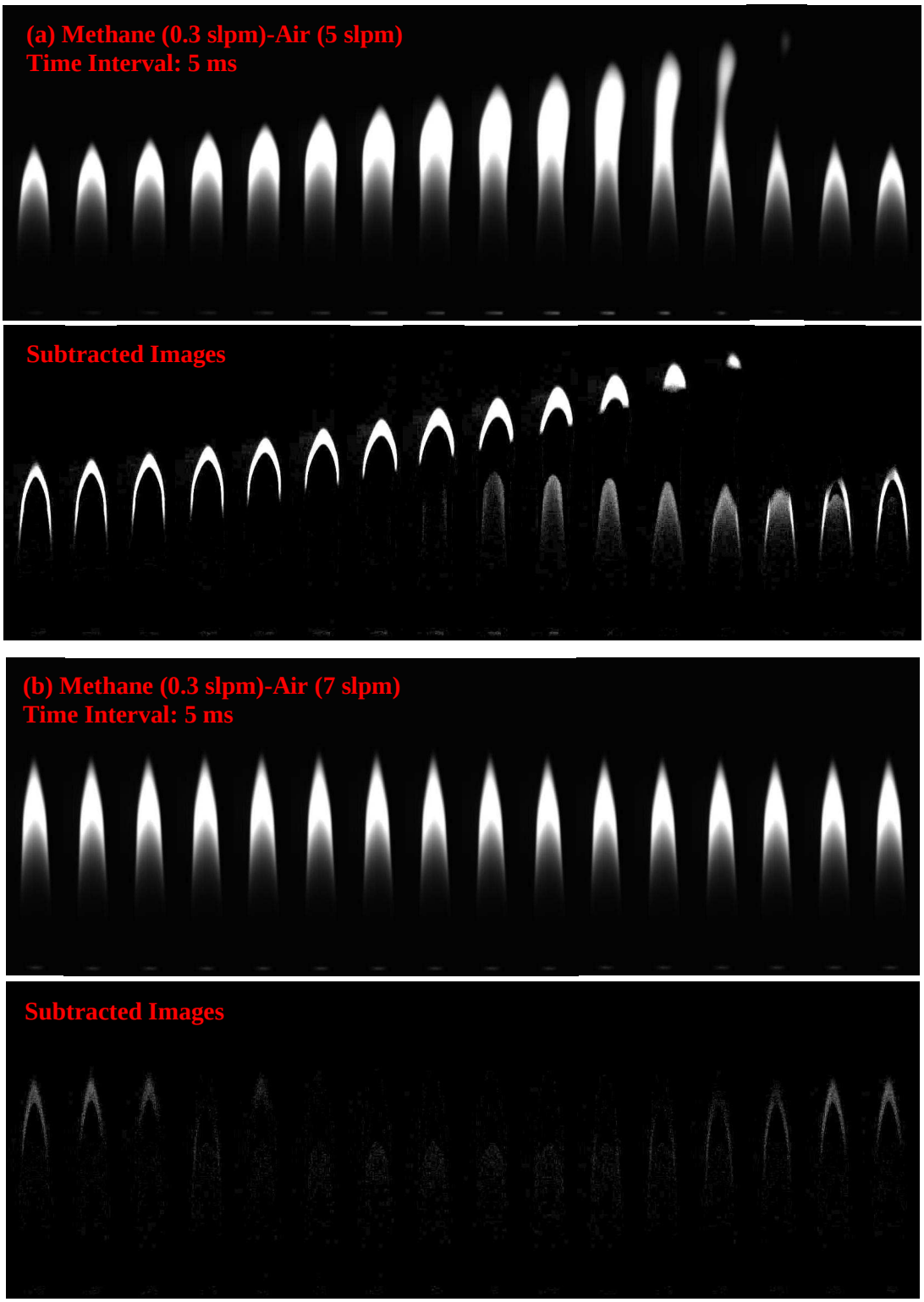

Figure 5-4: Methane (0.3 slpm)-air ((a) 5 slpm & (b) 7 slpm) diffusion flame pictures, taken by a digital high speed camera (FASTCAM-SA-3) at shutter speed of 1/5,000 s. The framing rate is 2,000 fps and the time interval between two consecutive images is 5 ms. The lower part of each row belongs to the subtraction of two consecutive images of the flame with 2.5 ms time interval. Methane flame at 7 slpm air flow rate is flickering slightly at the tip with a peak frequency of low amplitude. This flame is in intermittency mode from tip flickering to a stabilised flame at 10 slpm of co-flow air.

In the event that the flow leaving a nozzle the shear and inertial forces produced periodically follow-up eddies [14]. This is reported by Gaydon and Wolfhard [4], from schlieren images, when a gas or liquid is suddenly set in motion through a nozzle, it does not at first emerge as a coherent jet, but tends to creep initially round the edge of the burner, a potential flow pattern being established to begin with. Later the momentum of issuing gas will cause it to form a coherent jet.

In Figure 5-5-a, a coherent jet flow pattern, visualised by schlieren photography, of methane gas (none burning cold flow) continuously emerging from the fuel nozzle to atmosphere at flow rate of 0.3 slpm is presented. The vortices have convected downstream due to jet momentum of fuel stream. After flame ignition, generally, fuel gas will flow outwards in all directions according to a potential flow pattern and the direction of flame propagation will always be directly opposed to the flow of the gas, particularly when the Reynolds number is very small [4]. Since the flame is supported by injecting a fuel jet in an annular co-flowing ring, oxygen is consumed inside the annular ring thus a diffusion flame is established. The temperature rise in the reaction zone causes buoyant convection around the flame. Subsequently, the buoyant acceleration of hot gases outside the diffusion flame surface can cause shear-layer rollup, leading to the formation of toroidal vortex rings, which then interact with the flame surface or the hot plume downstream of the flame, depending upon the value of the Froude and Reynolds number. The convected vortices squeeze the flame at certain locations and bulge at others, which leads to flame pinch off and flicker.

Figure 5-5-b shows a sequence of Schlieren images of the methane diffusion flame at a fuel flow rate of 0.3 slpm. From the left to the right, the air co-flow rate is at 0, 3, 5, 7, 10, 15 and 20 slpm respectively. When there is no co-flow the inception of instabilities starts almost from the nozzle tip and convents down stream. At least two inflection (saddle) points flowed by hot gases bulges can be seen in this picture after

which the shedding vortices street is visualised. Increasing the co-flow rate to 3 and 5 slpm was observed to shift the location of these points to farther downstream of flame. At co-flow of 7 slpm the saddle points are almost waived and the vortex street starts at 146 mm above the burner nozzle. It means co-flow air is able to shift the initiation point of the outer toroidal vortices to downstream of the visible flame height. Obviously, the visible flame will become stable if the instability initiation point is well downstream of the visible flame position. By increasing the co-flow air flow rate to 10 slpm the vortices are shift to a height of 209 mm above burner nozzle which is quite far from the visible flame height (60 mm). Since the outer vortices are interacting just with hot plume gases beyond the diffusion flame a stabilised flame is produced. By increasing more co-flow rate to 15 and 20 slpm the instability initiation point was observed to move from 214 to 270 mm above the burner nozzle.

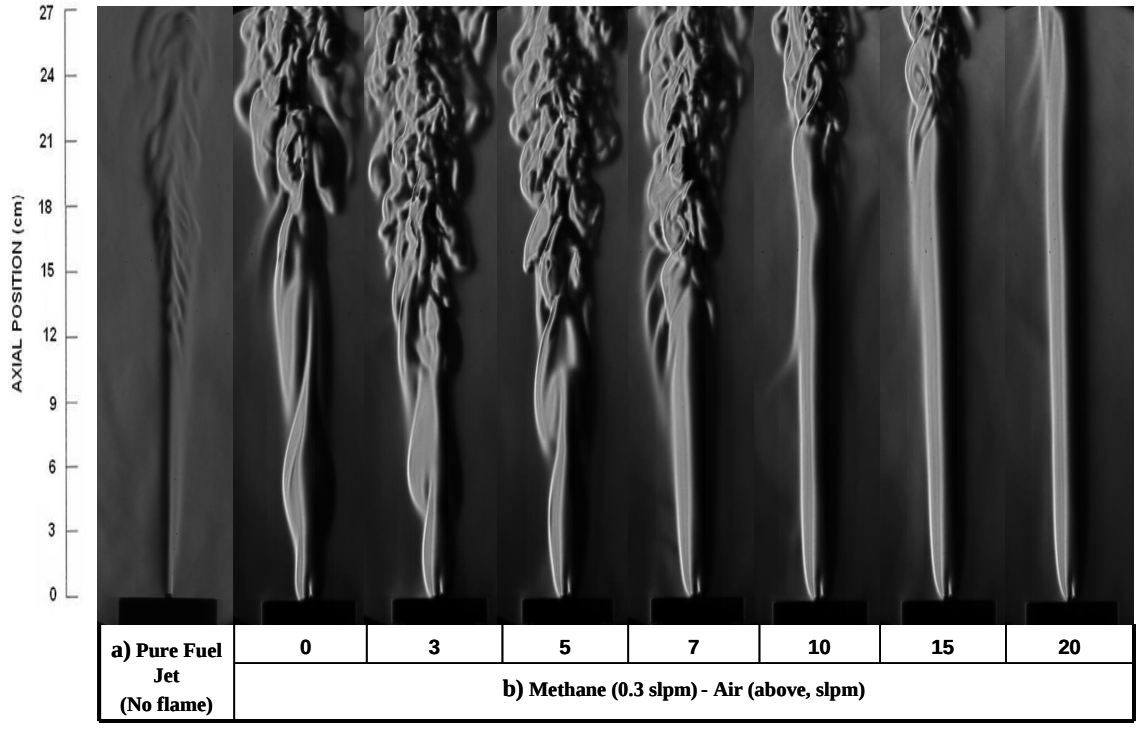

Figure 5-5: Schlieren photographs of: a) The emergence of a pure methane jet into the still air (atmosphere), and b) Methane-air diffusion flames at different co-flow rates. In all the cases, the methane flow rate was kept at 0.3 slpm. The images are taken at 1/200,000 s shutter speed (captured by Q. Wang).

Interestingly, the height of stabilised flame (H_f), after suppression, was observed to remain almost constant despite further increase at air flow rate. Figure 5-6 shows the stabilised methane flame heights at different methane flow rates of 0.2, 0.25, 0.3 and 0.35 slpm at three co-flow rates from suppression flow rate and onwards. The stabilised flame heights at 0.2, 0.25, 0.3 and 0.35 slpm were measured to be 39, 50, 60, 71 mm respectively. This is however, the schlieren pictures (see Figure 5-5-b) show that the additional co-flow air results moving the instability initiation point gradually towards farther downstream of visible flame region.

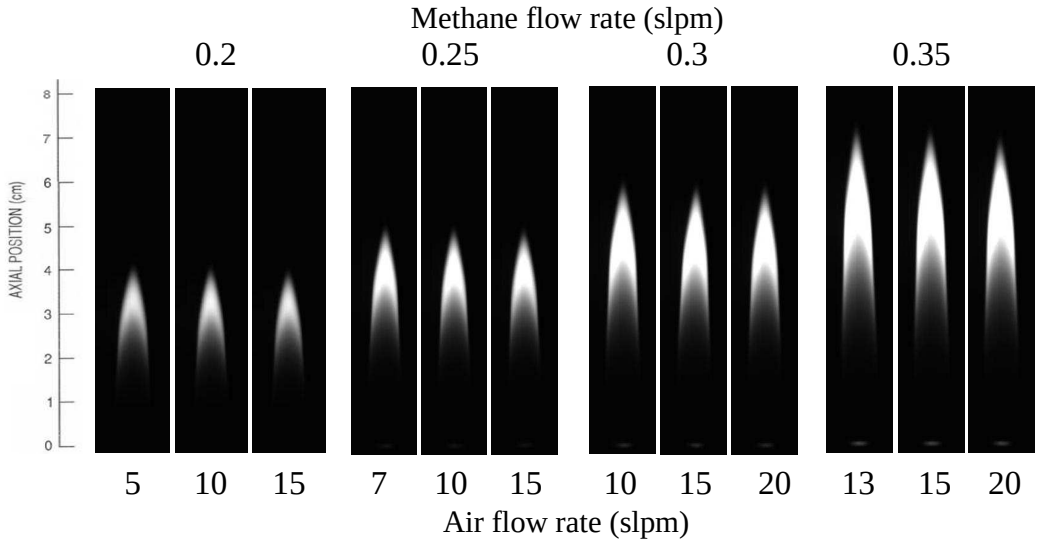

Figure 5-6: Stabilised (suppressed) methane-air diffusion flame height (H_f) at different fuel and air flow rates. The height of flame remains almost constant at each fuel flow rate despite increase in co-flow air flow rate.

It is found that the higher flow rates of co-flow air are needed to suppress flickering of the flames at higher fuel flow rates. Therefore the ratio of the air velocity to the fuel velocity, γ, is a stability controlling parameter. The suppression flow rates of co-flow air for methane flames at fuel flow rates of 0.2, 0.25, 0.3 and 0.35 slpm were measured to be 5, 7, 10 and 13 slpm respectively. It has to be noted that a flame with a flame tip rms flicker less than 1% in the flame height has been considered as a stable (stabilised) flame [8]. Figure 5-7 shows that almost a linear trend exists for corresponding co-flow

air velocity required for the fully suppression of the flickering methane flame. The velocity ratio, γ, of co-flow methane flame as a stability controlling parameter was found to be 0.72 for the range of tested flow rates.

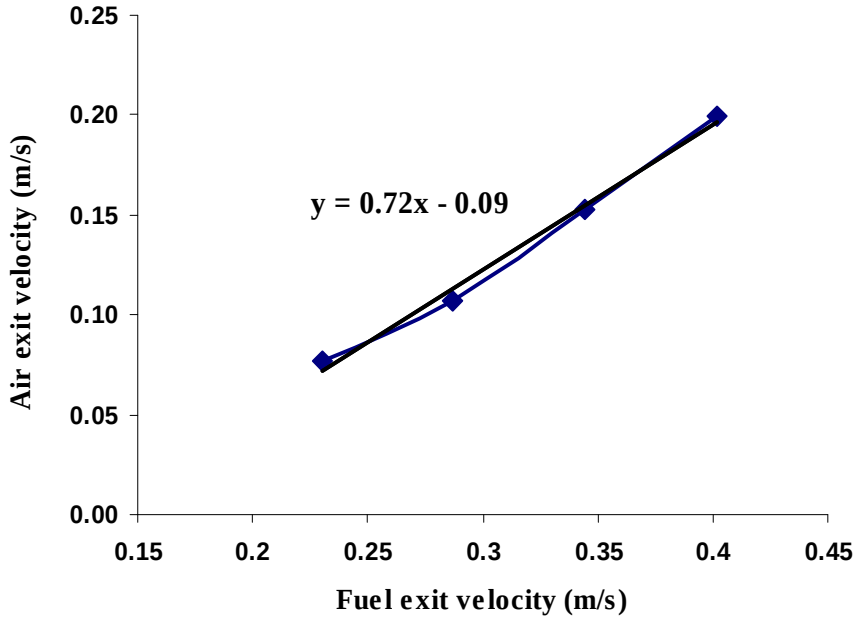

Figure 5-7: Corresponding co-flow air velocity required for fully suppression of flame flickering at different fuel (methane) exit velocities.

Figure 5-8 presents the maximum oscillating flame height (H_f-*max*) of methane flame at different fuel and air flow rates, measured from the flame high speed images. At lower flow rates of methane (0.2 and 0.25 slpm) H_f-*max* was observed to decrease by adding and increasing the rate of co-flow air from zero to the suppression (stabilised) flow rate. After which the visible flame heights, were observed to remain almost constant by adding more co-flow air to the flame. At higher flow rates of methane (0.3 and 0.35 slpm), H_f-*max* was found to increase with co-flow until the air flow rates of 5 and 7 slpm respectively (see Figure 5-8). In contrast the minimum oscillation flame height (H_f-*min*) was observed to increase continuously from its minimum (in the flame without co-flow) to its maximum (in the flame at stabilisation flow rate) for all the methane flow rates (see Figure 5-9). In other word, the co-flow air is able to decrease the oscillation magnitude of flame.

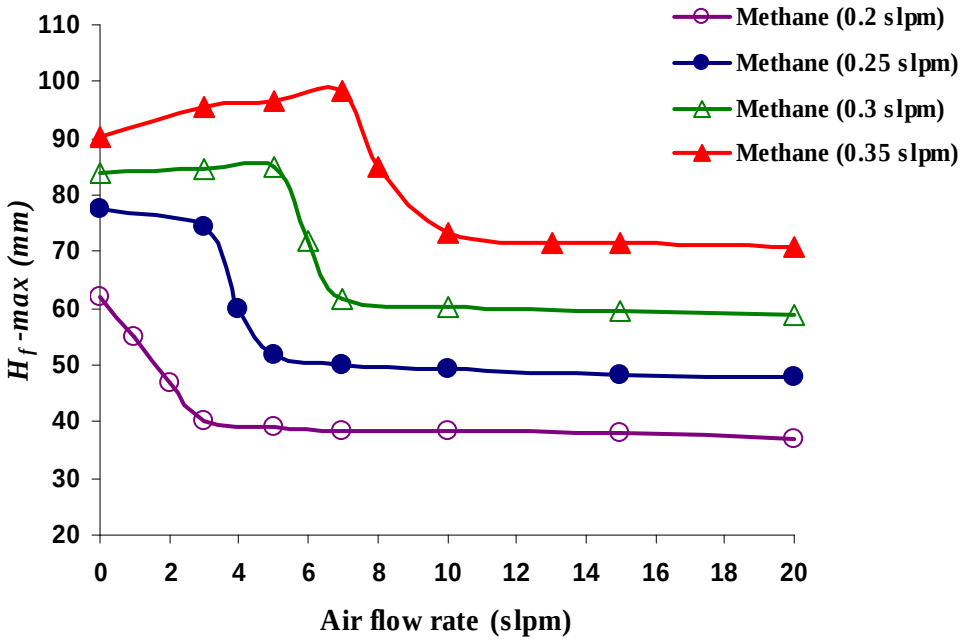

Figure 5-8: Maximum oscillating flame height (H_f-*max*) changes by air flow rate until suppression occurs, after which the height of flame remains almost constant.

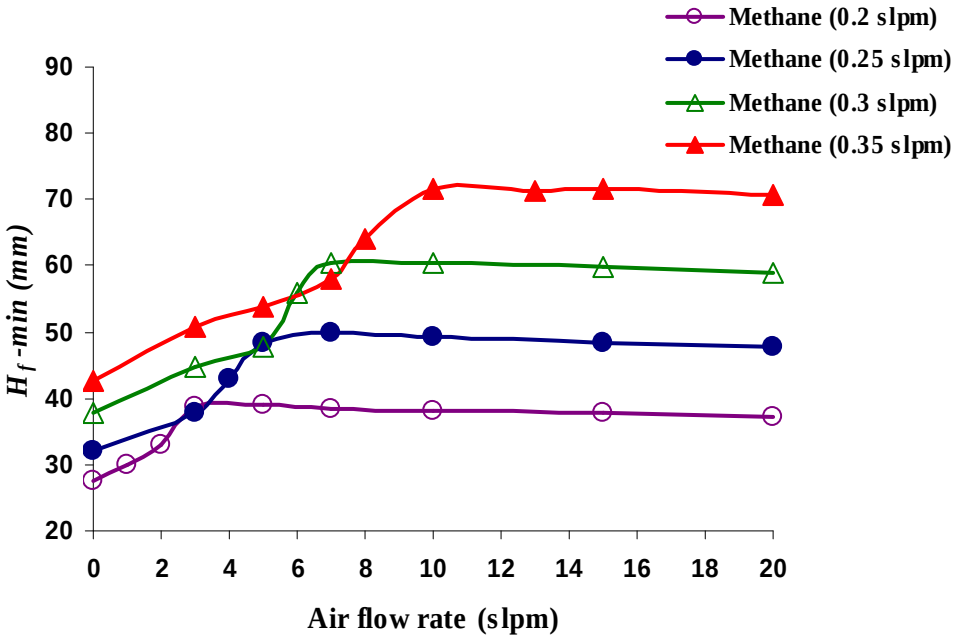

Figure 5-9: Minimum oscillating flame height (H_f-*min*) changes by air flow rate until suppression occurs, after which the height of flame remains almost constant.

The average flame height (H_f-*ave*), however, shows an initial stretch in the flame height by increasing co-flow rate from zero after which at a certain flow rate the average flame height starts to be decreasing to its stabilised level, H_f (see Figure 5-10).

At higher methane flow rates, the maximum of 'H_f-*ave*' was observed to occur at higher flow rates of air as well. The maximum of 'H_f-*ave*' was measured for methane flames at 0.2, 0.25, 0.3, 0.35 slpm at 1, 3, 5 and 7 slpm of co-flow air respectively. The initial stretch of flame by co-flow air can be attributed to the increase in shear layer momentum between co-flow flux and the visible flame outer boundaries. By adding more co-flow air, due to decrease in the flame oscillations, H_f-*ave* was observed to decrease towards its stabilised level (H_f). The initial 'H_f-*ave*' at zero co-flow was observed to be larger than H_f at lower methane flow rates (0.2 and 0.25 slpm), However at higher flow rates of methane (0.3 and 0.35 slpm), H_f-*ave*, initially was found to be larger than H_f, then by co-flow it reached to it's maximum, followed by decreasing to the stabilised level (H_f). It has to be noted that the density of air is almost twice (1.8) more than the density of methane and the air viscosity is almost 1.5 times more. As a result buoyancy induced and shear layer forces may grow faster by increase in co-flow flux in comparison with change in methane jet exit velocity. In combustion fluids are containing very large density variations and the buoyancy forces associate with density differences. Therefore, they can give rise to hydrodynamic instability. In fires and jet flames, these forces can enhance hydrodynamic instability indirectly by producing unstable convection currents [35].

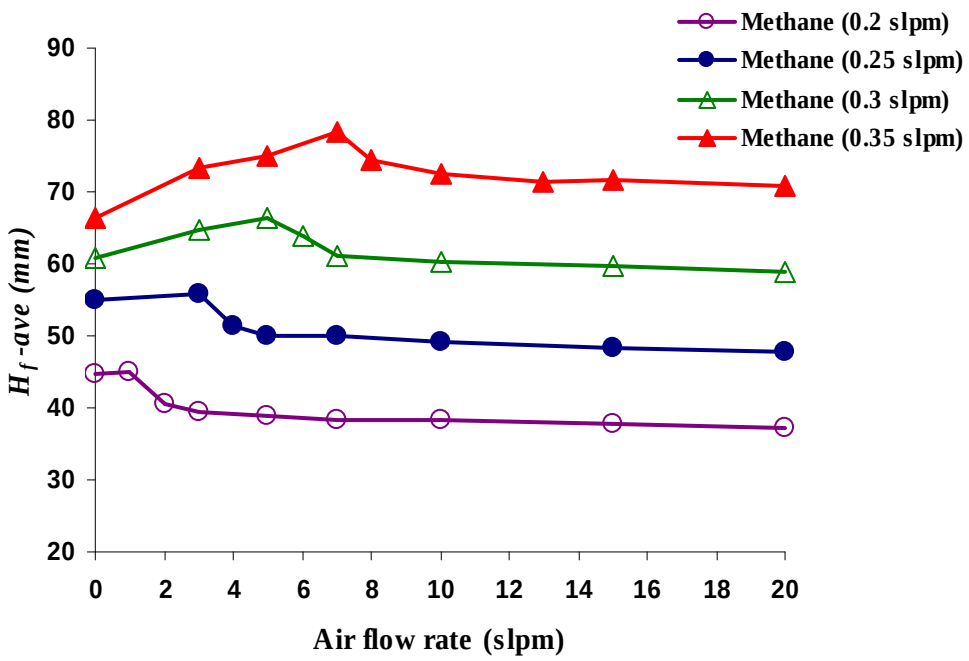

Figure 5-10: Average oscillating flame height (H_f-*ave*) stretches initially then decreases to the stable flame height level, and then remains almost constant with the further increase of air flow rate.

It is apparent from the previous discussion on the change of oscillation flame heights by co-flow air that the oscillation magnitude (L_f) tends to decrease by increase at co-flow air up to the suppression flow rate. As noted earlier, L_f in a flickering flame is defined by the distance between the flame lowest (H_f-*min*) and highest (H_f-*max*) heights. As shown in Figure 5-11, the flame oscillation magnitude (L_f) at all fuel flow rates are gradually decreasing towards zero by increasing the co-flow air. The rates of decrease show a steeper gradient at co-flow rates close to the suppression flow rate. The results obtained from the analysis of flame high speed images also show that co-flow air is able to push the inception points of instabilities farther downstream and as a result the necking part of the flame, towards the flame tip.

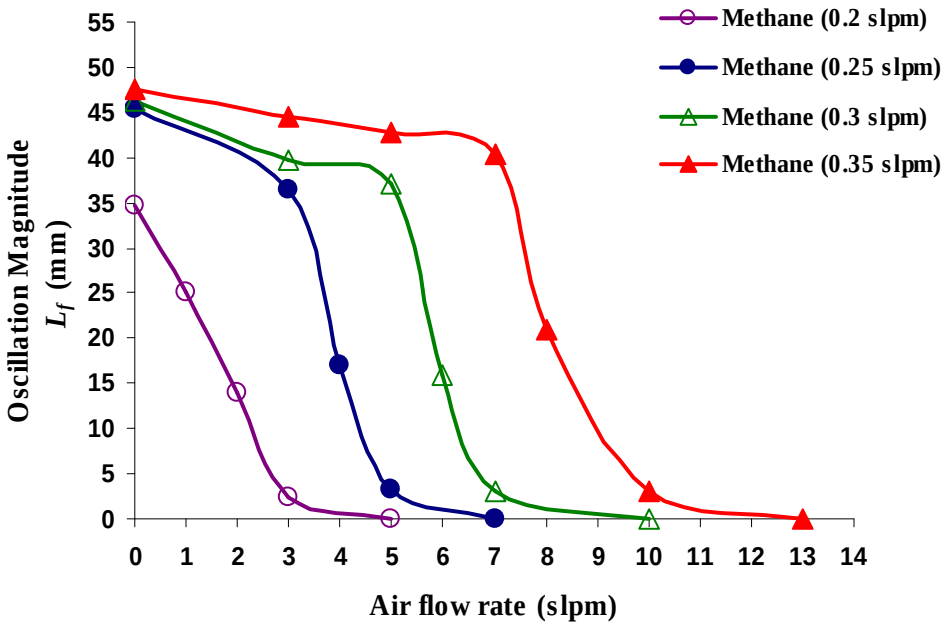

Figure 5-11: Flame oscillating magnitude (L_f) generally decreases by increase in co-flow air flow rate. At suppression flow rates this parameter is almost zero.

The oscillation wavelength (λ) also demonstrates a quick decrease from its maximum at no co-flow to zero at 3, 5, 7 and 10 slpm of air for methane flames at 0.2, 0.25, 0.3 and 0.35 slpm fuel flow rates respectively (see Figure 5-12). The decrease in the length of the separated part of the flame at the moment of separation (λ) is also obvious from the high speed images of methane flame at increasing co-flow rate (see Figure 5-3 and Figure 5-4). The observation to emerge from the comparison between the trends of L_f and λ (Figure 5-11 and Figure 5-12 respectively) is that after a certain air flow rate, the tip cutting of flame was completely stopped but flame tip flickering still existed. More co-flow of air is needed to fully stop the flame tip flickering to achieve a fully suppressed (stabilised) flame.

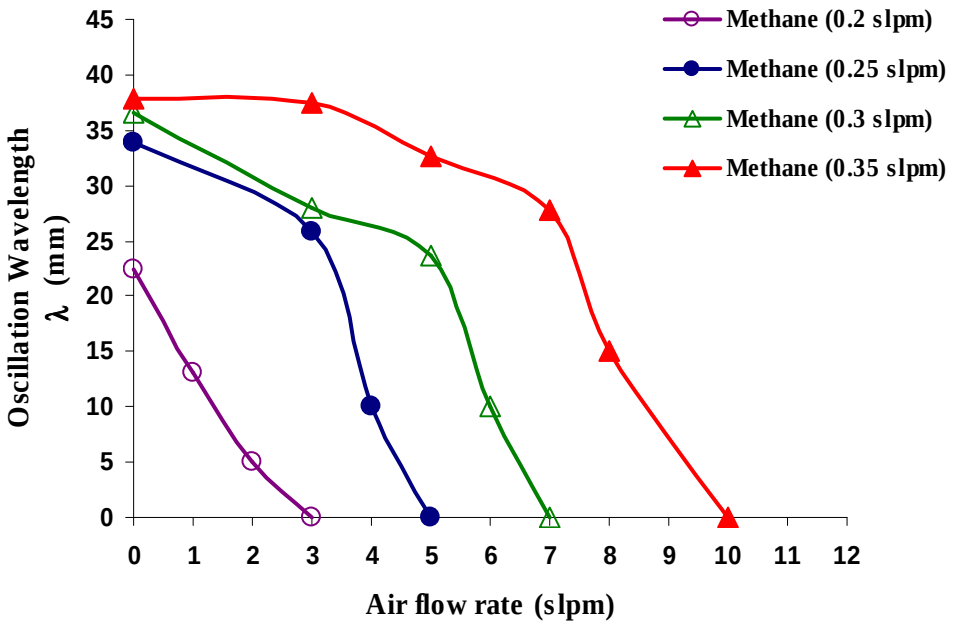

Figure 5-12: Flame oscillating wavelength (λ) generally decreases by increase in co-flow air but it reaches to zero before the suppression air flow rate.

It is clear that, the outer vortices tend to move along the flame centreline symmetrically. At low air flow rates (exit velocities), the Froude number is decreased, the buoyant acceleration becomes increasingly significant, and toroidal vortices roll up periodically due to the Kelvin-Helmholtz instability. Subsequently, a larger chunk of the flame tip is periodically detached and burned out (bulk flickering flame [53]). This may be explained by the scaling of buoyancy with Froude number as the rollup vortices occur closer to the burner port. This increases the convective velocity at the base of the flame surface. The vortices then convect downstream and interact with hot plume downstream of the flame as well. By increase at the air flow rate (moderate Fr) the vortices convect downstream, they interact at higher heights of visible flame and also with hot plume downstream of the flame. As a result a smaller chunk of flame are detaching by vortices. Nevertheless, the rollup process is highly periodic and the flickering frequency obtained from the Fast Fourier Transform (FFT) of chemiluminescence history and also from the instantaneous flame high speed images

shows a noticeable increase in peak flickering frequencies. By further increase at flow rate of air the outer vortices pushed farther downstream by co-flow resulting in lower interaction of flame vortices. It was observed from a certain air flow rate, no more flame tip cutting was occurred and only a tip flickering flame existed [53]. The flickering was periodic and the flickering frequency is increased as well. Beyond a certain co-flow rate, it was observed that there is no significant flame-vortex interaction and the flame flickering is fully suppressed; the flame exhibited a totally steady (stabilised) behaviour. This is attributed to the fact that the rollup occurs far downstream of the visible flame region. The vortex structures are also relatively weak and interact only with the hot plume of gases.

The stabilised methane diffusion flame is convex in shape (has a bulbous in appearance) and its maximum width is wider than the burner nozzle exit diameter. Whilst adding more co-flow air to the stabilised flame, it was observed that the maximum width of the flame (*b*) at all fuel flow rates show a gradually decrease with linear trends (see Figure 5-13). The slopes of the linear trends of '*b*' show smaller decrease rates at the higher fuel flow rates. The decrease in flame width by co-flow can be attributed to the effects of shear layer forces in the plane mixing layer between two parallel uniform streams of fuel and air. The higher air velocity at the flame boundary brings more fresh air to the flame surface, resulting in more air diffusion to the reaction zone which generally increases the burning rate as well. For small laminar diffusion flame, the burning rate of the combustion process depends on the rate of inter-diffusion between fuel and oxidant. This is to achieve the necessary proportion for reaction to occur along the reaction boundary. Turbulence plays a major role, for large scale diffusion flame, where the additional entrenchment of air due to flame movement would have further impact on the rate of combustion.

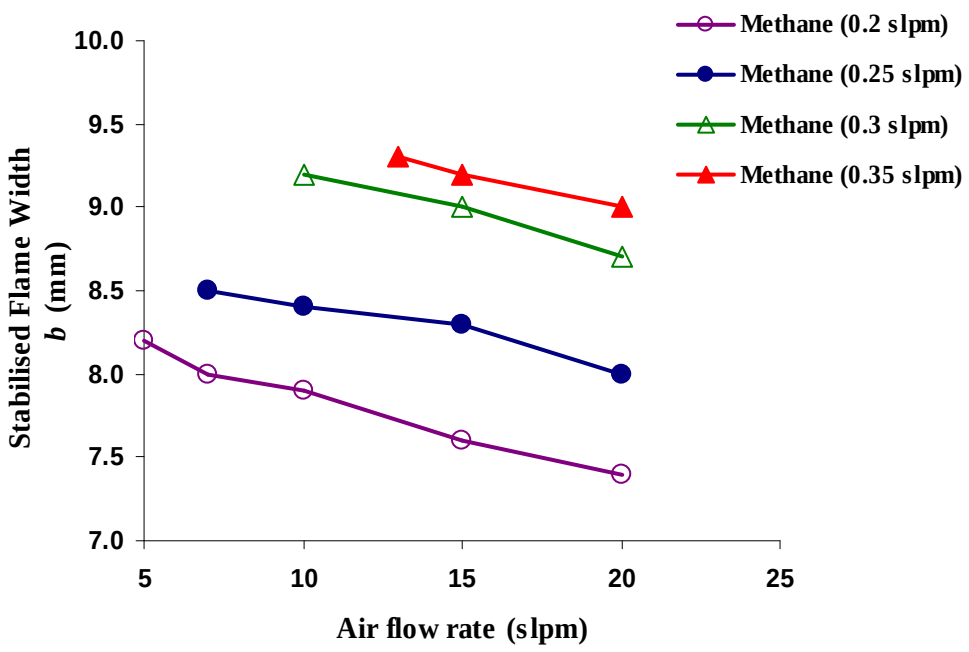

Figure 5-13: Maximum width of the stabilised flame (*b*) shows almost a linear decrease by increase at co-flow air flow rate.

The graphs of mean pixel intensity (MPI) of the flame high speed images versus time and the corresponding Fast Fourier Transform (FFT) analysis of the data for frequency measurement at methane (0.3 slpm)-air (0, 3, 5, 7, and 10 slpm) flames are shown in Figure 5-14. The MPI as an arbitrary unit (a.u.) was measured by image processing using MATLAB®. The maximum of this value corresponds to the maximum light emission of flame; similarly, a minimum refers to the minimum flame emission after burning out of the detached part. Interestingly, two major effects of increase in co-flow air on flame dynamics can be observed from these set of graphs.

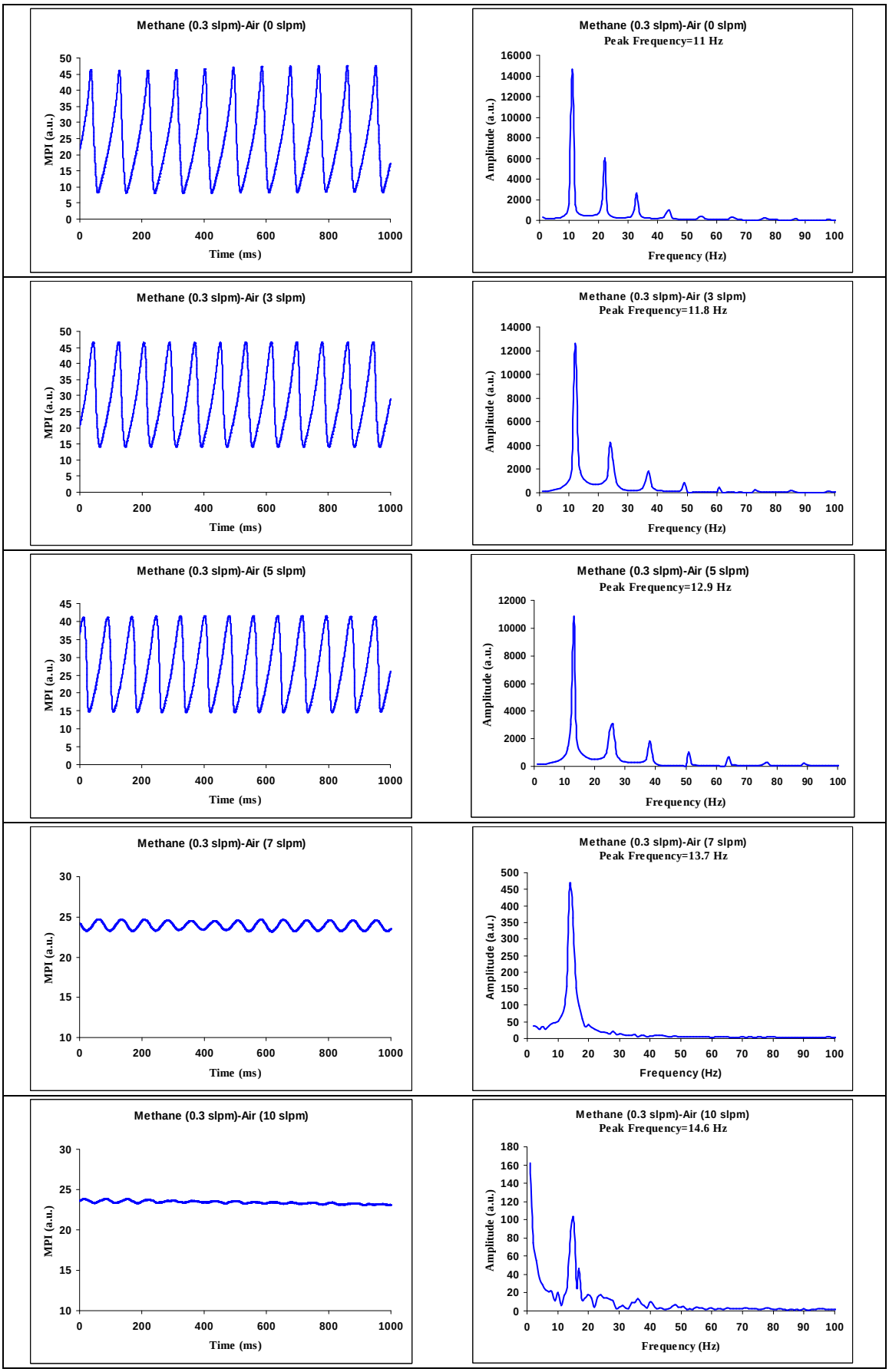

Figure 5-14: Mean Pixel Intensity (MPI) and the corresponding oscillation frequencies of methane (0.3) slpm flame at different co-flow air flow rates.

Suppression of the oscillations appears from MPI graphs and increase in the peak flickering frequencies while decreasing in the frequency amplitude, from FFT graphs (see Figure 5-14). The Maximum of MPI (MPI_max) shows a decreasing trend by co-flow air, the minimum of MPI (MPI_min), however, shows a rapid increase. The differences between these two parameters (dI) are decreasing by co-flow air from its maximum at zero co-flow to its minimum at air suppression flow rate and onwards (see Figure 5-15).

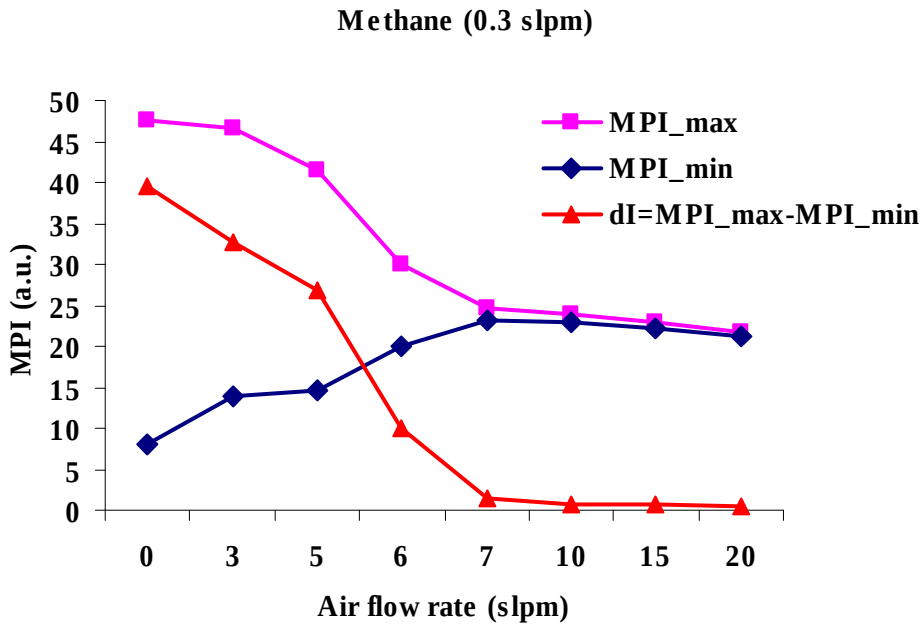

Figure 5-15: Maximum and minimum values of mean pixel intensity (MPI) from the flame high speed images in a whole cycle of the flame oscillation (for methane (0.3 slpm) at different air flow rates). The subtraction of these two parameters (dI) decreases towards zero at the suppression air flow rate (10 slpm) and onwards.

The average of MPI values in a full data-range of high speed images coupling with the standard deviation (σ) of MPI are shown in Figure 5-16. The standard deviation (σ) of MPI, measured from the intensity variation in the flame high speed images, tends to be another indicator of the flame fluctuations. The average of MPI, which is an indicator of the average flame luminosity, increases first by increasing the air flow rate, then

decreases with the further increase in co-flow air. The standard deviation (σ) of MPI, however, in a whole cycle of the flame oscillation, decreases continuously with the increase of co-flow air towards zero. This may be considered as another indicator of flame flickering suppression by the co-flow air. It has to be noted that in our previous study [10] the standard deviation (σ) of MPI was also found to be a good indicator of the trends of flame oscillation wavelength (λ) and magnitude (L_f), in the study of diffusion flames at elevated pressures.

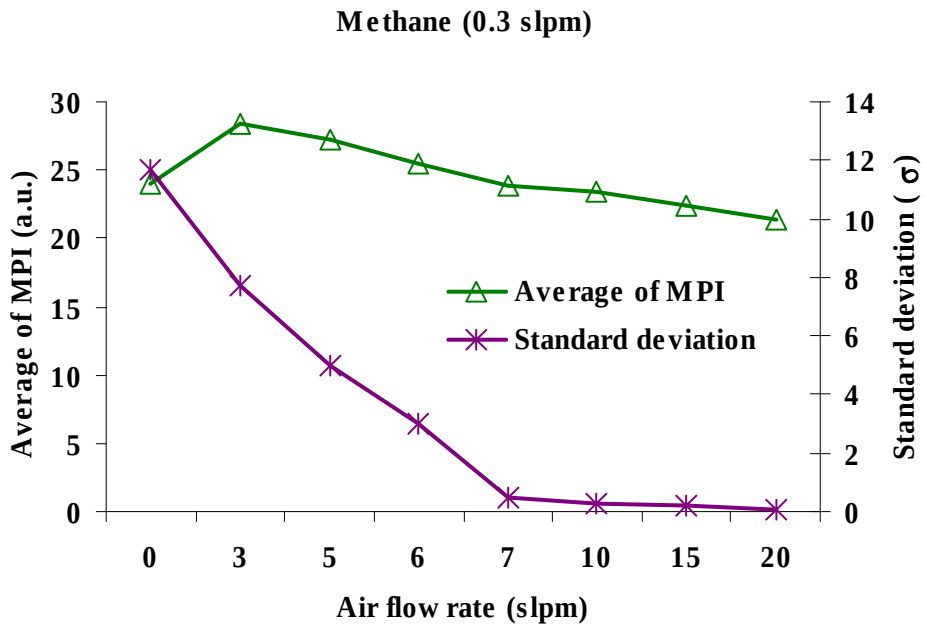

Figure 5-16: Average of mean pixel intensity (MPI) increases first by co-flow air then decreases with further increases in air flow rate. The standard deviation (σ) of MPI in a whole cycle of flame oscillation continuously decreases by co-flow air towards zero as a sign of suppression of the flame oscillations.

In the previous chapter it was found that the increase in fuel flow rate increases the magnitude of oscillation (L_f). The flickering frequency, however, remains almost constant at each pressure. It means the flickering frequency is not a function of fuel flow rate despite pressure. The power spectra of the flame emissions, by collecting the radiation spectrum at OH* and CH* emission bands using interference filters, are

shown in Figure 5-17. The frequency spectra of methane (0.3 slpm) flame at zero co-flow (see Figure 5-17-a) shows that the methane flame flicker with one dominant frequency and as many as six harmonic modes. The flame has a dominant (peak) frequency of 10.75 Hz and six noticeable harmonics peak frequencies at 21.5, 32, 42.75, 53.5, 64, 74.75 Hz, each with lower amplitude than the previous frequency. This methane flame at 3 slpm of co-flow (see Figure 5-17-b) clearly exhibits an enhanced flickering with the higher peak frequency spectra of 12 Hz. By adding more co-flow (at 5 slpm) the peak frequency increased to 12.75 Hz (see Figure 5-17-c). The co-flow rate of 7 slpm (see Figure 5-17-d) was found to be almost a transient mode between flickering flames and stabilised one. Although the peak flickering frequency still is increasing at this flame but lower numbers of harmonics were noticeable. This is however, at some instances flame tend to show a decrease in flickering magnitude (L_f), maintaining the same flickering frequency.

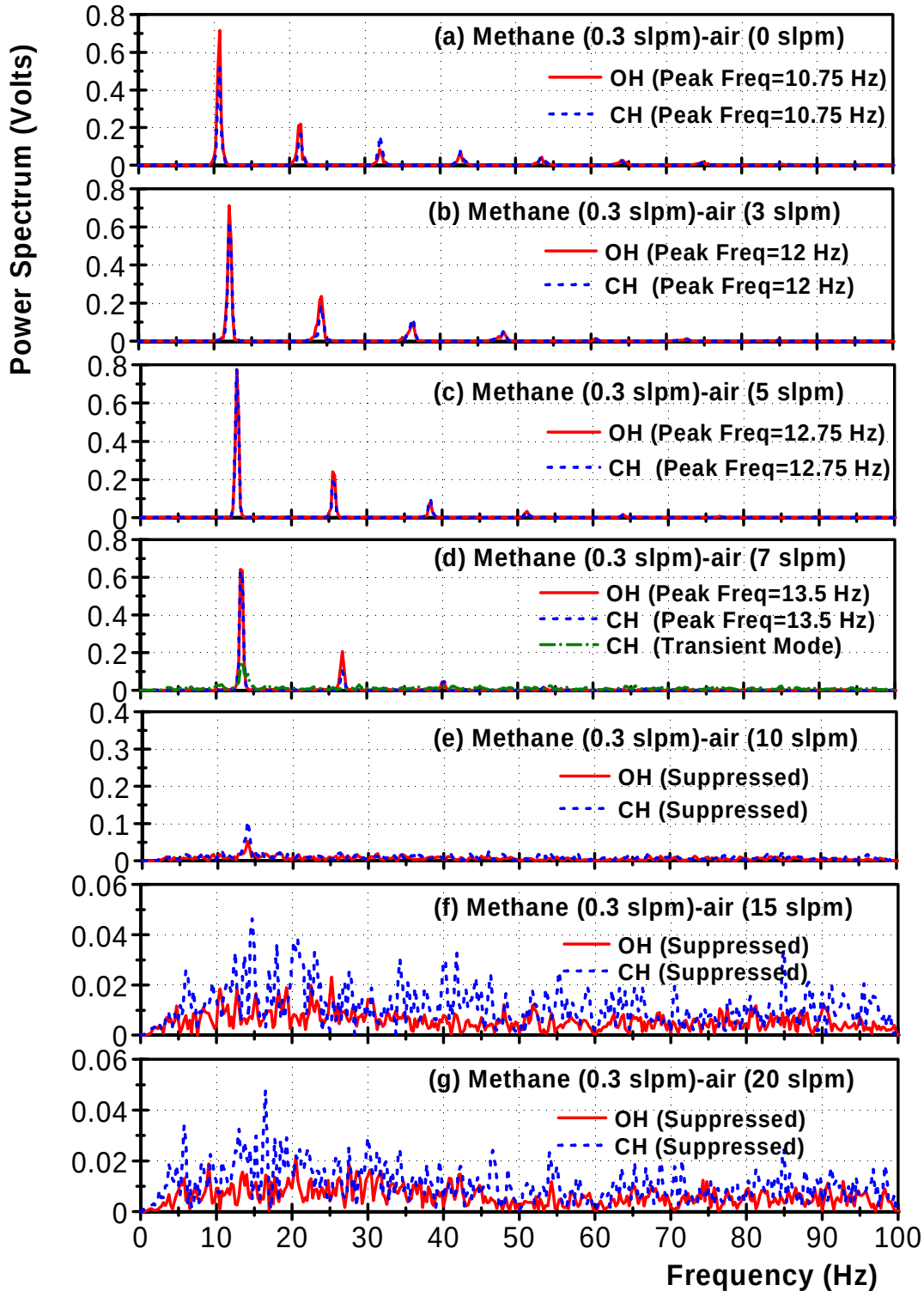

Figure 5-17: Frequency spectra for methane (0.3 slpm) diffusion flames with co-flow air at 0, 3, 5, 7, 10, 15 and 20 slpm flow rates (from (a) to (g) respectively). The increase at peak frequency by co-flow and suppression of oscillation at higher flow rates of air are evident from graphs.

The stabilised (suppressed oscillation) flame was found at co-flow rate of 10 slpm for methane flow rate at 0.3 slpm (see Figure 5-17-e). In this flame the flickering is stopped since the effect of buoyancy is decreased for higher Froude numbers. A steady flame structure is indicated, with some weak buoyancy-induced motion appearing in the post flame region. The frequencies of flame have very small amplitudes (power spectra). Also no more harmonics are observable. Increase in co-flow makes the flame even more stable and the captured frequencies seem to be mainly some noises (see Figures 5-17-f and g for co-flow rates of 15 and 20 slpm respectively).

The frequency spectra of the flame from FFT analysis of mean pixel intensity (MPI) of the flame high-speed photographs and chemiluminescence results are greatly in agreement, however, the photomultipliers failed to measure the very low amplitude frequency of the flames after suppression. The important observation is that the dominant (peak) frequency of flame flicker linearly increases with co-flow air flow rate. This is however, the frequency amplitude was observed to decrease fast by co-flow particularly near the air suppression flow rate (see Figure 5-18). It has been confirmed that, the flickering frequency is not a function of fuel flow rate but it increases linearly with the co-flow air. Figure 5-18 shows that the dominant flickering frequency of a methane diffusion flame at different fuel and air flow rates which follows a best line fit with the slope of 0.33 and the Y-intercept of 11 ($f=0.33\ a+11$). Where 'f' indicates the peak frequency (Hz) and 'a' indicates co-flow air flow rate (slpm).

The experimental results clearly demonstrate that the co-flow air has various strong effects on diffusion flame dynamics. In this study a comprehensive experimental data of methane diffusion flame at different flow conditions are compared. Since the evolution of a large scale structure is governed by Kelvin–Helmholtz instabilities and buoyant acceleration, the frequency, mutual interaction and energy distribution are controlled by the conditions of the flow.

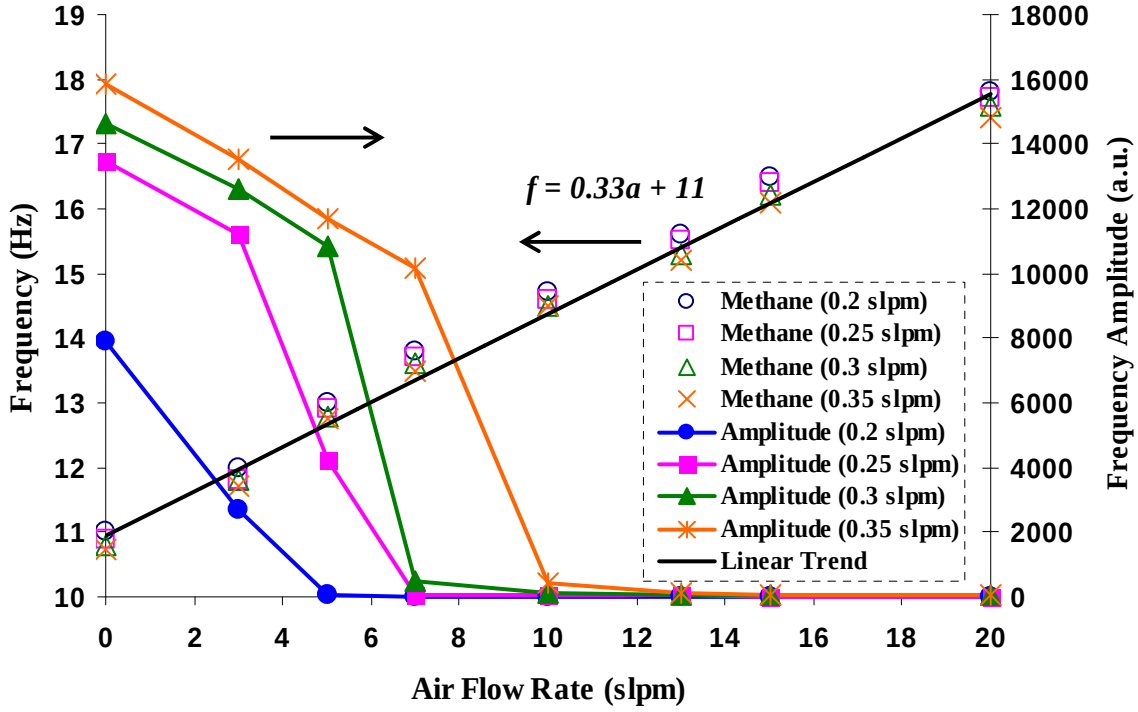

Figure 5-18: The linear increase of dominant flickering frequency of methane-air flames with increase of co-flow air and the corresponding frequency amplitudes.

5.5 CONCLUSION

Experiments were conducted on a co-flow diffusion flame burner to investigate the effects of co-flow air flow rate (velocity) on the flickering behaviour of methane-air diffusion flames. The buoyant acceleration of hot gases outside the diffusion flame surface can cause shear-layer rollup, leading to the formation of toroidal vortex rings, which then interact with the flame surface or the hot plume downstream of the flame, depending upon the value of the Froude and Reynolds number. The instability behaviour of the flame was observed to be strongly sensitive to the co-flow air velocity. The high-speed images help to visualise the structure of the outer toroidal vortices outside the luminance flame and the subtraction of two consecutive images show how the luminance boundaries of the flame is growing at the base and tip of the flame. The

schlieren images reveal how the outer vortices interact with flame surface and hot plume of gases.

The most striking observation is that, when the co-flow air flow rate (velocity) is increased to a certain level, the flame oscillation is completely suppressed (stabilised). From schlieren images it can be seen that Kevin Helmholtz instability was initiated at the very beginning of the fuel nozzle when there is no co-flow air. With increase of air co-flow flow rate, the instability initiation point was found to move downstream gradually. It then reaches a stage when outer toroidal vortices interact only with hot plume of gases farther downstream of the visible flame. Obviously, the visible flame will become stable if the outer instability initiation point is well downstream of the visible flame position. It is found that higher flow rates of co-flow air are needed to suppress flickering of the flames at higher fuel flow rates. Therefore the ratio of the air velocity to the fuel velocity, γ, is a stability controlling parameter. The velocity ratio, γ, of co-flow methane flame as a stability controlling parameter was found to be 0.72 for the range of tested flow rates.

The oscillation magnitude (L_f) and the oscillation wavelength (λ) were observed to decrease by increase in the co-flow air. Whereas the average oscillating flame height behaviour was bimodal with an initial stretch by increase of co-flow air then it starts to be decrease by adding more co-flow, up to its stabilised (suppressed) level. By adding more co-flow air to the stabilised flame, the flame height was observed to remain almost constant but the maximum width of the visible flame (b) was decreased slightly.

The average of mean pixel intensity (MPI), which is an indicator of the average flame luminosity, increases first with the co-flow air flow rate then decreases with the further increase of co-flow air flow rate. However, the standard deviation (σ) of MPI in a whole flame oscillation cycle decreases all the way towards zero with the increase of co-flow air.

The dominant flickering frequencies measured from FFT analysis of high speed imaging data and chemiluminescence results increase linearly by increase in co-flow air. The frequency amplitudes, however, show rapid decreases particularly at co-flow rates close to the suppression flow rate. It has been confirmed that, the flickering frequency is not a function of fuel flow rate but it is improving with co-flow air with a linear trend. The dominant flickering frequency (f) of a methane diffusion flame varies linearly with the air co-flow rate (a) as $f=0.33\ a+11$.

"In earlier times, smoke from the factory smokestack was a sign of prosperity. In time it became a nuisance and finally a health concern."

J. Warnatz (1944-2007)

CHAPTER 6

PRESSURE EFFECTS ON SOOT TEMPERATURE IN DIFFUSION FLAMES

6.1 ABSTRACT

This study addresses the influence of elevated pressures up to 10 bar on the flame geometry and two-dimensional soot temperature distribution of ethylene-air laminar co-flow diffusion flame. Narrow band photography and two-colour pyrometry in the Near Infra-red (NIR) region have been used to gain a better understanding on effects of pressure on these parameters. Theoretical background, discreet considerations in the choice of two narrow band filters at 780 nm and 1064 nm and calibration of the instrument factor are also described. It has been observed that the flame properties respond very sensitively to the pressure. As the pressure is increased, the flame diameter decreased at all flame heights and soot formation dramatically increased. The flame luminosity at the flame centreline increases, first by axial position from the fuel nozzle.

Then the flame became less intense with height due to cooling of the soot particles by radiative losses, leading to a smoking flame at pressures of 2 bar and above. The soot temperature results obtained by applying two-colour method in the NIR region are shown to be consistent with the pyrometry results. Soot temperature measurements show that in ethylene diffusion flame the overall temperatures decreases with increasing pressure. It is shown that the rate of temperature drop is greater for a pressure increase at lower pressures in comparison with higher pressures. The average temperature drop of about 177 K is recorded along the flame centreline for a pressure increase from atmospheric to 2 bar and also from 2 bar to 4 bar. However, at higher pressures the rate of temperature drop decreases to 1/3 of the previous temperature drop. It is found that, applying two-colour pyrometry method in the NIR region, utilising a commercial digital camera, is capable of nonintrusive measurement of two-dimensional soot temperatures with a simple and relatively high accuracy technique. The maximum recorded error of the method was found to be about 8%. It mainly occurred at the regions with the lowest concentration of soot particles.

Keywords: *Diffusion flames; Soot temperature; Two-colour method; Near infra-red.*

6.2 INTRODUCTION

Accurate and reliable measurements of soot temperature and distribution in the flame by nonintrusive means are highly desirable to achieve in-depth understanding of combustion and pollutant formation processes. The most widely applied methods use physical probes such as thermocouples or gas-sampling probes. These techniques have obvious disadvantages, such as intrusive sensing, degradation in a harsh environment, and single point measurement. The presence of soot makes such measurement of temperature particularly difficult, with deposition of soot particles on thermocouple probes obscuring the interpretation of thermocouple readings, although such probes are

still useful in non-sooting regions [130]. Even rapid-insertion techniques fail at the very high soot loadings found in high-pressure laminar diffusion flames. Consequently, a variety of optical methods such as LIF (laser-induced fluorescence) [131] and LSM (laser scattering of molecules) [132] have been developed in recent years. However, due to the complication of the measurement principles and system structures and using external light sources, these techniques are unsuitable for routine operations in industrial furnaces. Optical techniques based on the natural luminosity of the object do not require the use of additional light sources and are thus generally easier to implement, especially in field measurements outside the laboratory [133]. The two-colour method is an established optical technique for the temperature measurement of sooting flames. This technique makes use of two narrow band wavelengths in the visible or near infra-red emission.

The present study focuses on the influence of elevated pressures up to 10 bar, on soot temperature distribution of ethylene-air laminar co-flow diffusion flame. Experimental work is carried out in a high-pressure combustion chamber and two-colour pyrometry technique has been applied in the near infra-red (NIR) region, utilising a commercial CMOS (Complimentary metal-oxide semiconductor) digital camera. To the best knowledge of the author, applying two-colour method in the NIR region with a commercial digital camera has been not reported in existing literature. The two-colour method theory, discreet considerations in the choice of wavelengths and calibration of the instrument factor are also described.

The literature related to this part of the study is presented in Chapter 2, session 2.3. The obtained results in this chapter have been published in the *Proceedings of 48th AIAA Aerospace Sciences Meeting* [134].

6.3 TWO-COLOUR METHOD THEORY

The two-colour technique relies on the measurement of the emission intensity from incandescent soot particles in the flame. The wavelength dependent monochromatic radiation intensity of a blackbody is governed by Planck radiation law [135, 136].

$$I_{\lambda}^{b} = \frac{C_1}{\lambda^5.(e^{C_2/\lambda T} - 1)} \qquad 6.1$$

where $I^{b}{}_{\lambda}$ is the monochromatic blackbody radiation emitted intensity in energy per unit area per unit time (W/m^2/µm), λ is the wavelength of the radiation (µm), T is absolute temperature (K) and C_1 and C_2 are the first and second Planck constants respectively.

A blackbody emitter is a perfect emitter with an emissivity $\varepsilon_{\lambda}^{\ b}$ of unity at all wavelengths. If the flame emitted like a blackbody, it would be straightforward to calculate the flame temperature, T, using Planck's distribution shown in Equation 6.1 [106]. However, the soot has an unknown emissivity, ε_{λ}, which causes it to emit less than a blackbody at the same temperature. Single soot particles and thick soot clouds show near blackbody behaviour with $\varepsilon_{\lambda} \approx 1$, but thinner soot clouds can have non-blackbody characteristics [133].

I_{λ}, monochromic radiation of a gray body (i.e. soot particles) deviates by the spectral monochromic emissivity of the body ($0 \leq \varepsilon_{\lambda} \leq 1$) [133, 135, 137, 138].

$$I_{\lambda} = \varepsilon_{\lambda} \cdot I_{\lambda}^{b} = \varepsilon_{\lambda} \frac{C_1}{\lambda^5.(e^{C_2/\lambda T} - 1)} \qquad 6.2$$

The wavelength and temperature concerned in this study range from 0.78 to 1.064 µm and from 1000 to 2500 K respectively. Since $C_2/\lambda T >> 1$ within these ranges, Planck's law can be replaced by Wien's radiation law [97, 135]:

$$I_{\lambda} = \varepsilon_{\lambda} \frac{C_1}{\lambda^5.e^{C_2/\lambda T}} \qquad 6.3$$

It can be proven that the output of the imaging system, namely the grey level (I_λ), is proportional to the existence of the measured object and dependent on the spectral sensitivity S_λ of the imaging system (CCD or CMOS sensors), i.e.,

$$I_\lambda = k.S_\lambda.\varepsilon_\lambda \frac{C_1}{\lambda^5.e^{C_2/\lambda T}} \quad 6.4$$

where *k* is called the instrument constant which is independent of wavelength and reflects the effects of various factors including radiation attenuation due to the optical system and atmosphere, observation distance, lens properties and signal conversion [97].

The ratio between the grey levels at wavelengths λ_1 and λ_2 is given by:

$$\frac{I_{\lambda 2}}{I_{\lambda 1}} = \frac{S_{\lambda 2}}{S_{\lambda 1}} \cdot \frac{\varepsilon_{\lambda 2}}{\varepsilon_{\lambda 1}} \cdot (\frac{\lambda_1}{\lambda_2})^5 \cdot \exp\left[\frac{C_2}{T}.\left(\frac{1}{\lambda_1} - \frac{1}{\lambda_2}\right)\right] \quad 6.5$$

Rearranging Equation 6.5 yields:

$$T = C_2 \cdot \left(\frac{1}{\lambda_1} - \frac{1}{\lambda_2}\right) \Bigg/ \left[\ln\frac{I_{\lambda 2}}{I_{\lambda 1}} + \ln\frac{S_{\lambda 1}}{S_{\lambda 2}} + \ln\frac{\varepsilon_{\lambda 1}}{\varepsilon_{\lambda 2}} + \ln\left(\frac{\lambda_2}{\lambda_1}\right)^5\right] \quad 6.6$$

The ratio between the spectral sensitivities ($S_{\lambda 1}/ S_{\lambda 2}$) is called instrument factor and is known from calibration using a tungsten lamp as a standard temperature source. A crucial point here is how to deal with the ratio between the spectral emissivities $\varepsilon_{\lambda 1}$ and $\varepsilon_{\lambda 2}$. Normally, grey body behaviour is assumed for the detected object (i.e., $\varepsilon_{\lambda 1}/\varepsilon_{\lambda 2}=1$), when the wavelengths are very close to each other [97, 133, 139]. Another method of dealing with the ratio of emissivities is to consider the relation suggested by Flower [140]. When assuming the soot particles in the flame are homogeneous, optically thin and small relative to the used wavelength, the spectral emissivity is inversely proportional to the wavelength ($\varepsilon_\lambda \propto 1/\lambda$). Lee et al. [141] reported that the primary soot particles from diesel engines are nearly spherical, and have diameters ranging from 20–

50 nm with an average diameter of about 30 nm. Bruce et al. [142] reported a range of 30–70 nm for the primary particle diameter. For gaseous flames, the size of particles ranges from 5 to 100 nm according to the results of Char and Yeh [143] is much smaller than the wavelength of observation. Also according to the results of Flower and Bowman [32, 144] there was no significant effect of pressure on the size of the soot particles. The increase in the soot volume fraction results predominantly from an increase in the number density of particles and the local volumetric rate of soot production which is observed to increase with pressure. Consequently the proportion of $\varepsilon_{\lambda 1}/\varepsilon_{\lambda 2} \propto \lambda_2/\lambda_1$ exists and the soot temperature can be calculated by substitution of this ratio in Equation 6.6:

$$T = C_2 \cdot \left(\frac{1}{\lambda_1} - \frac{1}{\lambda_2}\right) \Bigg/ \left[\ln\frac{I_{\lambda 2}}{I_{\lambda 1}} + \ln\frac{S_{\lambda 1}}{S_{\lambda 2}} + \ln\left(\frac{\lambda_2}{\lambda_1}\right)^6\right] \qquad 6.7$$

Equation 6.7 indicates that the two-colour method measures temperature based on the signal ratios at two different wavelengths without the prior knowledge of the real existence intensities at those wavelengths. It also infers that the two-dimensional temperature can be obtained by calculating the signal ratios of the two images pixel by pixel. The wavelengths for the two-colour method for two narrow band filters must be selected carefully for accurate temperature measurements [12, 100, 101].

6.3.1 Choice of the Wavelengths

Several factors must be considered for the choice of the wavelengths [97, 98, 145]. Firstly, the wavelengths should be selected to avoid the radiation from gas molecules such as CO_2 and H_2O and intermediate free radicals like OH*, CH*, C_2* and CN*. It must be noted that the two-colour method only measures the temperatures of the soot particles within a flame, because Planck's radiation law only fits the continuous spectra from the solid particles [146] rather than the band spectra of gas molecules or free

radicals. Secondly, the wavelengths should be in a region where the outputs of the digital camera can be expected to vary sufficiently in view of sensitivity and signal-to-noise ratio. Thirdly, the choice of the wavelengths should be expected to prevent the camera from saturation. Finally, the two wavelengths should be chosen close to each other so that the differences between the emissivities and optical transmission effects are negligible. Despite achieving higher sensitivity and signal-to-noise ratio in visible wavelengths, the NIR region has been selected in this study due to less gas molecules or free radicals radiations, non-saturated photos and relative novelty of the approach. Compromising the factors addressed above has given rise to choose the two wavelengths at λ_1=780 nm and λ_2=1064 nm with a central wavelength tolerance of ±2 nm.

During combustion, strong band emissions from gaseous species can be present as well as the thermal radiation from soot particles. In the reaction zones of flames, many radicals, such as OH, CH, C_2, HCO, NH and NH_2 may be formed and give appreciable emission in the visible and near ultraviolet regions. In the infrared region, wavelengths must be chosen carefully to avoid radiation or absorption from $C0_2$, CO, water vapour and fuel vapour. Figure 6-1 shows the spectra from various gaseous species in the near infra-red region [102].

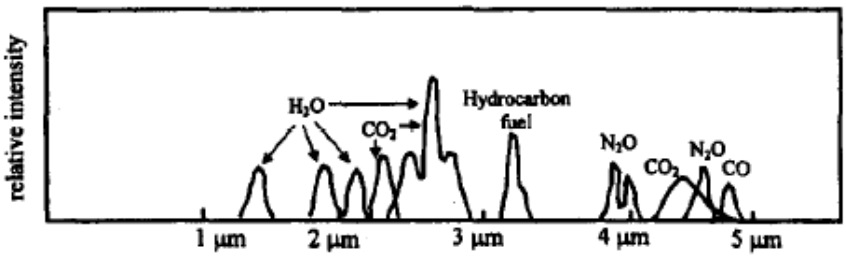

Figure 6-1: Emission in the near infra-red region for various gas molecules [102].

6.3.2 Calibration of the Instrument Factor

To calibrate the instrument factor (*S*) a pre-calibrated tungsten ribbon lamp [12] was used as a standard temperature source. The tungsten ribbon lamp was placed the same

distance from the camera as the flame. The instrument factor *S* can be derived by rearranging the Equation 6.6:

$$S = \frac{S_{\lambda 1}}{S_{\lambda 2}} = \frac{e^{\frac{C_2(\frac{1}{\lambda_1}-\frac{1}{\lambda_2})}{T}}}{\frac{I_{\lambda 2}}{I_{\lambda 1}} \cdot \frac{\varepsilon_{\lambda 1}}{\varepsilon_{\lambda 2}} \cdot (\frac{\lambda_2}{\lambda_1})^5} \qquad 6.8$$

The ratio of intensities ($I_{\lambda 2}/ I_{\lambda 1}$) at two wavelengths can be shown by *R*. The emissivity of tungsten ribbon ($\varepsilon_{\lambda 1}$ and $\varepsilon_{\lambda 2}$) is by its turn a function of the wavelength and of the true temperature T according to the equations proposed by Larrabee [147] at different wavelength regions from 450 nm to 800 nm. Dmitriev and Kholopov [148] presented the emissivity of tungsten in near infra-red region from 1000 to 5100 nm and temperature range of 1244-2441 K. The most complete investigation of tungsten ribbon emissivity in the 230-2700 nm wavelength region and at temperatures from 1600-2800 K was conducted by De Vos [149]. According to these studies the average emissivity of tungsten ribbon at 780 nm and 1064 nm wavelengths were found to be 0.43 and 0.37 respectively.

The calibration of instruments (camera with filters) was performed on a certified tungsten ribbon lamp [12]. The lamp was connected to a 12 V battery, a rheostat and a shunt resistor (0.01 Ω) connected in series. The voltage flowing across this resistance was an indication of the current through the lamp. The camera was placed in front of the lamp and focused on the tungsten ribbon and has been kept at a constant distance and position in all imaging. Two narrow band interference filters (780 nm and 1064 nm) were applied, in front of the digital camera lens. The calibrated temperature for the lamp ranged from 1300 to 2200°C and emits a range of light radiation temperature at different levels of applied amperes (9.345-19.04A). The detail of this calibration setup can be found in Figure 6-2.

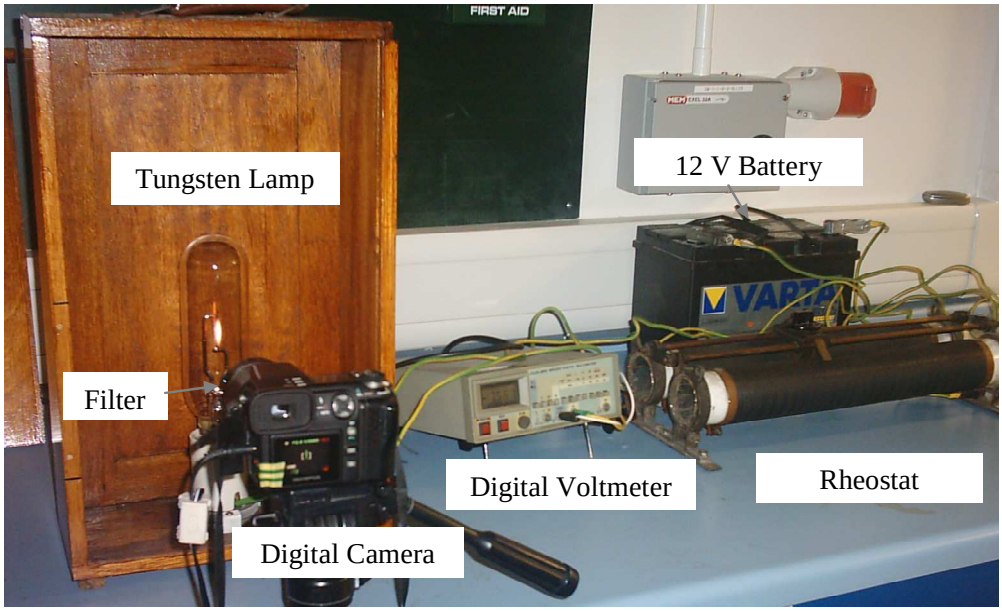

Figure 6-2: Camera calibration setup with tungsten ribbon lamp.

The ratio between the two average intensity levels (Iλ2/ Iλ1) was tabulated against the instrument factor (S). The calibration results are shown in Figure 6-3, where the data points marked with '▪' yields the following inverse power relationship, as indicated by the dotted line.

$$S = 1.5R^{-1.7} \tag{6.9}$$

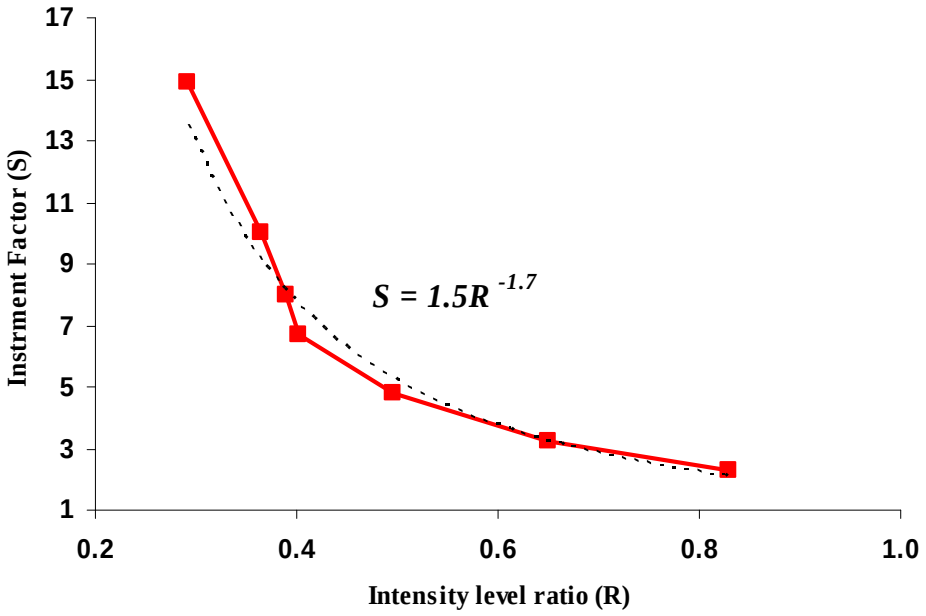

Figure 6-3: Instrument factor (S) versus the ratio of intensity levels (R).

6.4 EXPERIMENTAL SETUP

The co-flow ethylene (C_2H_4) diffusion flame was studied with the optical diagnostic method over the pressure range of 1 to 10 bar. A classic over ventilated Burke-Schumann [117] laminar co-flow diffusion flame is produced which is stabilised on a tapered nozzle with an exit diameter of 4.5 mm. A tapered fuel nozzle reduces recirculation from the burner tip and improves stability of the fluid-ambient interface. The flames exhibited long-term stability for all pressures. The high pressure burner used in this work is described in details in sections 3.3 and 4.3. The mass flow rate of ethylene (0.15 slpm) was kept constant at all pressures. Co-flow air is supplied from a compressed air bottle into the burner with a constant mass flow rate of 15 slpm. Table 6-1 shows the physical properties of fuel and air streams during the experiments. The region of Reynolds number (*Re*) indicates that all flows were in laminar mode during the experiments. Increasing the pressure within the vessel was achieved by increasing the flow rate of nitrogen and simultaneously decreasing the flow rate of the exhaust by adjusting the back-pressure regulating valve which can maintain the chamber pressure anywhere between 1 and 10 bar.

Table 6-1: Fuel and air parameters in soot temperature experiments.

Fuel Type	Volume Flow Rate		Mass Flow Rate [mg/s]	Velocity [m/s]	Re No.	Fr No.
	slpm [l/min]	[m^3/s]				
Ethylene (C_2H_4)	0.15	2.5E-06	2.95	0.172	91.7	0.703
Air	15	2.5E-04	301	0.230	513.82	0.171

Optical access into the chamber is possible through four viewing ports oriented so that line-of-sight as well as 90° scattering and imaging experiments are possible. Each window provides a 45 mm viewing diameter; two are made from fused silica (quartz) and two from high-resistivity float-zone silicon (HRFZ-Si). This study makes use of the quartz windows which provide optical access in the visible and NIR band.

The schematic of the experimental setup is shown in Figure 6-4. The optical set up is consist of a commercial CMOS digital camera (Canon EOS-30D), which was utilised to capture the colour photographs and also the narrow band (780 nm and 1064nm) photos of the flame and an Infratherm pyrometer with less than ± 1.0 % accuracy of measuring value. The digital single-lens reflex (SLR) Canon EOS-30D is a colour camera which uses CMOS technology. The camera provides the maximum effective resolution of 3,504 × 2,336 (8.2 Megapixels). The shutter speed range of this camera is 1/8000 to 30 s and with the light sensitivity (ISO) from 100 to 1600. It is worth mentioning that CMOS technology is one of the key advantages of new cameras with noise reduction circuitry at each pixel site. Also CMOS sensors have lower noise and lower power consumption characteristics than CCD sensors. The two narrow band filters were applied in front of the camera lens. Due to the lower sensitivity of commercial camera sensors to NIR band, the exposure time of 1 s with the maximum light sensitivity (ISO) of 1600 were selected to capture the narrow band photographs. The normal images of the flames were captured at an exposure time of 1/100 s and ISO of 100. Also the aperture was set to be *f*/ 5.6.

To verify the temperature results obtained by the two-colour method in NIR region, a digital noncontact temperature measurement instrument was utilised during the experiments. This Infratherm pyrometer (INFRATHERM IS 5/F) ascertains the temperature of glowing (sooty) flames by using two-colour temperature measurement method with ±1.0 % accuracy of the measuring value. These two colours have been selected in IR spectral range between 0.7~1.15 μm. The spot diameter of this pyrometer is 1.5 mm for a minimum distance of 250mm. Via integrated control panel and standard software (InfraWin) it is possible to read measuring temperature as well as changing the devise parameters. A full specification of this pyrometer is listed in Appendix A.

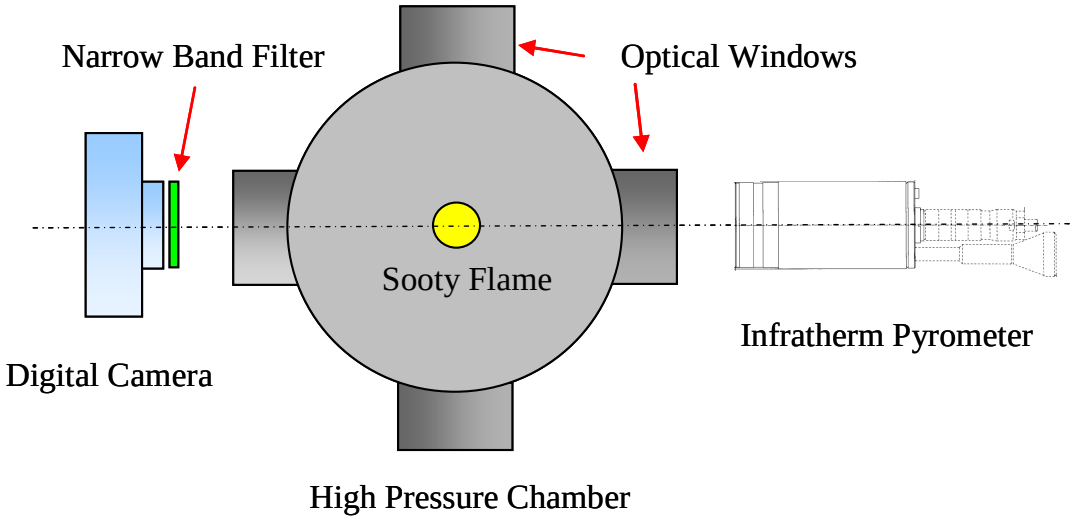

Figure 6-4: Schematic of experimental setup for two-colour pyrometry.

6.5 RESULTS AND DISCUSSION

The normal pictures captured by Canon EOS 30D (aperture: 5.6, exposure time: 1/100 sec and ISO: 100) from ethylene (0.15 slpm) – air (15 slpm) diffusion flame at different pressures are presented in Figure 6-5.

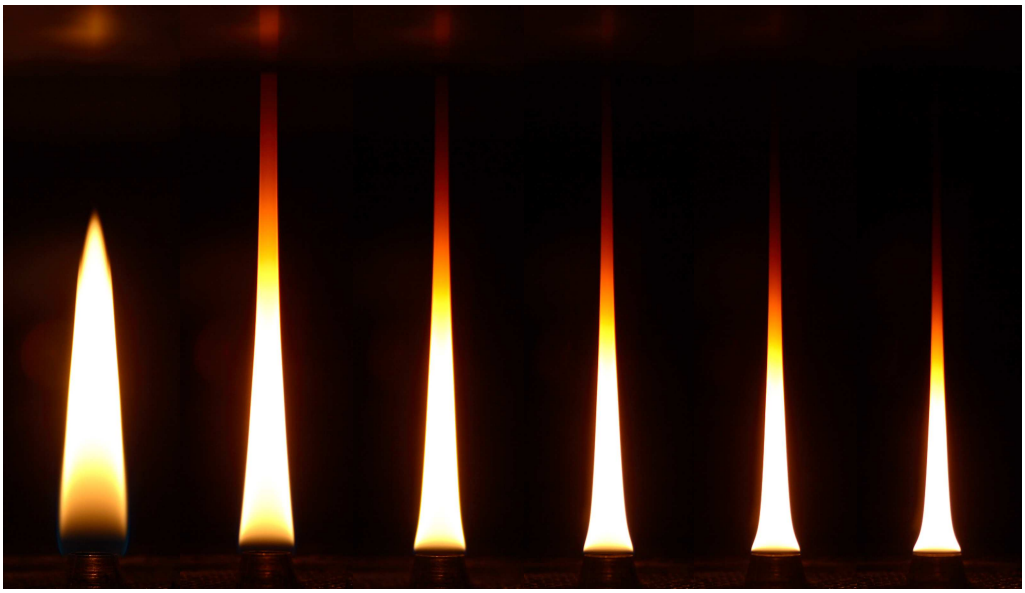

1 bar 2 bar 4 bar 6 bar 8 bar 10 bar

Figure 6-5: Normal pictures of ethylene (0.15 slpm)-air (15 slpm) diffusion flame at different pressures.

At atmospheric pressure, the base of the flame had a bulbous appearance and is wider than the burner nozzle exit diameter. Higher up the flame came to a relatively sharp tip where all luminosity ceased, corresponding to the vertical position where all the soot had been oxidized. As the pressure was increased, axial flame diameters decreased, giving an overall stretched appearance to the flame as noted by Flower and Bowman [19] and Thomson et al. [8]. This may explain the significant change in flame shape with the increase of pressure. Soot particles are higher in density than other combustion products, and cannot diffuse away from the primary flame region as easily as a gaseous product might. Combustion must therefore be maintained by oxygen diffusing inward to the primary flame region, resulting in a narrowing flame structure [17]. In other words, as pressure (P) increases, the density (ρ) will increase as well ($\rho \propto P$). By keeping the fuel exit velocity (U) and as a result the mass flow rate constant ($\rho U A_{cs} = const.$), at high pressures the mass conservation equation leads to a narrower flame cross section area (A_{cs}) at all heights within the flame [10]. The cross-sectional area (A_{cs}) of the flame (measured from the radius defined by the outer edges of the sooting region at each height) shows an average inverse dependence on pressure to the power of 0.8±0.2 ($1/P^{0.8\pm0.2}$) for ethylene flames [10].

The centre core of the flame near the nozzle tip has a mostly bluish colour up to 7 mm above the fuel nozzle exit (H=7 mm). The presence of the soot particles is mainly limited at the flame tip and in an annular band near the burner rim. By increasing pressure it was observed that the soot formation dramatically increases and the luminous carbon zone moved downward, closer to the burner rim, filling an increasingly larger portion of the flame. It means that near the mid-height of the flame, the annular distribution of soot remains pronounced, but soot also begins to appear in the core of the flame. At the tip of the flame, the soot annular and core soot distribution join to each

other and peak soot concentration is observed at the flame centre line. Bright luminosity from soot is visible for each flame. The increase in formation of luminous soot particles causes the heat loss from the flame by radiation to increase, thus lowering the flame temperatures. This leads to slower oxidation rates of soot, and eventually oxidation cannot keep up with soot production, leading to a smoking diffusion flame [19]. The decrease in soot luminosity suggests that temperature is affected by the presence of soot as a result of radiant energy transfer from the particles. Temperature, in turn, strongly influences soot-formation and soot-oxidation rates [33].

As pressure was increased the flame that did not emit smoke at atmospheric pressure began to smoke at higher pressures. Despite the flame being over-ventilated with co-flow air an extended line of soot (smoke) at the flame tip appears at a pressure of 2 bar (the point of incipient soot breakthrough) and onwards. For these flames, a significant amount of soot survives the oxidation region of the flame. The luminosity from soot becomes noticeably less intense with increasing height above the burner tip. As pressure increases, the decrease in soot luminosity moves to lower positions in the flame. The well defined luminous tip of the atmospheric pressure flame disappears as pressure increases, and a darkening orange column of soot rises from the flame. At fixed axial position, the diameter of the visible flame decreases with increasing pressure. Also, the opacity of the soot column increases with pressure, due to an increase in the integrated soot volume fraction across the flame diameter [19]. According to the results of Schalla and McDonald [18] the rate at which the fuels can be burned smoke free consistently decreases with increasing pressure. Furthermore the maximum smoke free fuel flow rate initially increases by air flow rate then remains almost constant for further increases in air flow rate. The smoking tendency is also found to be a strong function of fuel types as well [18]. The tendency of soot formation in ethylene-air diffusion flame was observed to be relatively higher than methane-air flame.

The two-colour technique relies on the measurement of the emission intensity from incandescent soot particles in the flame. In this method the two-dimensional intensity of every single pixel of the flame image, in the specific wavelength can be measured from the narrow band photos, captured by applying narrow band filters in front of the camera lens. Figure 6-6 and Figure 6-7 show a sequence of flames photograph at pressures 1, 2, 4, 6, 8 and 10 bar, taken by applying the 780 nm and 1064 nm narrow band filters respectively in front of the canon camera. Note that these pictures have been captured with an exposure time of 1 sec and at the maximum camera sensitivity (ISO 1600).

Through application of image processing techniques and derivation of a computer program (m-file) using MATLAB®, the two-dimensional monochromic normalized intensities ($I_{\lambda 1}$ and $I_{\lambda 2}$) of each flame has been measured by considering the value number in the HSV (Hue, Saturation and Value) model. The HSV is an alternative colour model derived from the RGB by looking down the greyscale/achromatic axis of the RGB space. The deficiency of the RGB method is that the colour and intensity parameters from a perceived scene are inseparably stored in the primary colour intensities (Red, Green and Blue). In contrast, the HSV method complements this by allowing the colour information to be presented independently from the intensity component. Within the cylindrical plane, hue and saturation (synonymous to colour and its brightness respectively) are measured as the angular coordinate and the radial distance from the achromatic axis respectively. Conversely, the normalized intensity component (value) is given by the depth along the achromatic line [150].

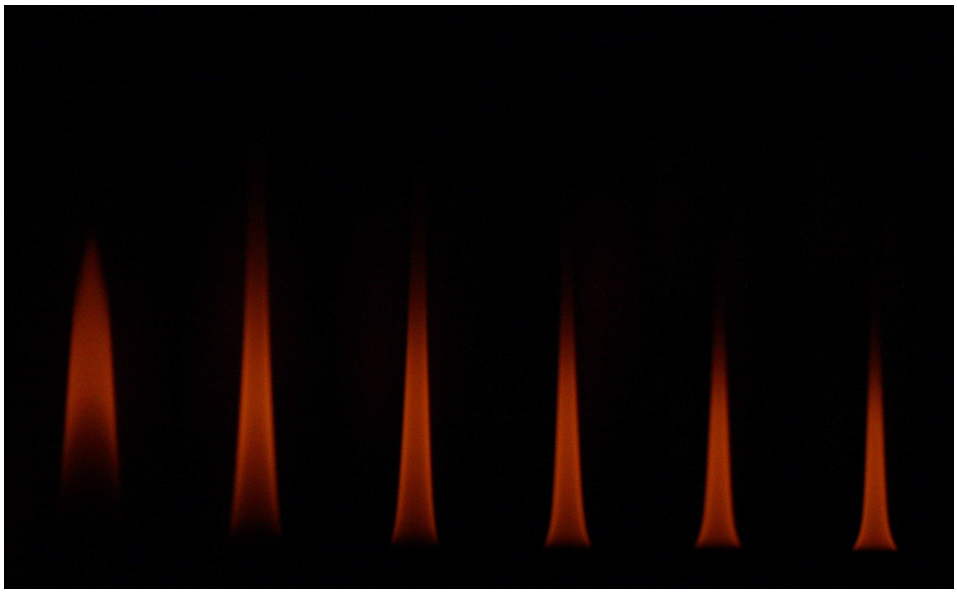

1 bar 2 bar 4 bar 6 bar 8 bar 10 bar

Figure 6-6: Narrow band (780 nm) images of ethylene (0.15 slpm)-air (15 slpm) diffusion flame at different pressures.

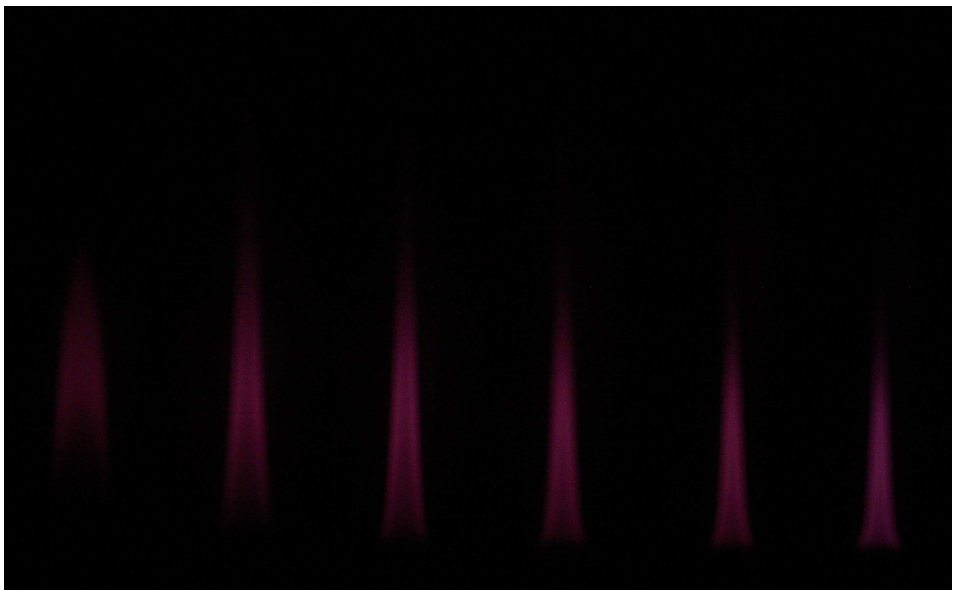

1 bar 2 bar 4 bar 6 bar 8 bar 10 bar

Figure 6-7: Narrow band (1064 nm) images of ethylene (0.15 slpm)-air (15 slpm) diffusion flame at different pressures.

The two-dimensional monochromic intensity distribution ($I_{\lambda 1=780\ nm}$) of the ethylene diffusion flame at 10 bar are presented in Figure 6-8. When there was no well defined flame tip and the flame luminosity became less intense with height due to cooling of the soot by radiative losses, the points with a normalized intensity smaller than 0.01 were

not considered as a part of the flame. These dark grey regions formed a long vertical column of non-fully oxidized carbon particles at the flame tip, which decreased in diameter only gradually with increasing height above the burner tip.

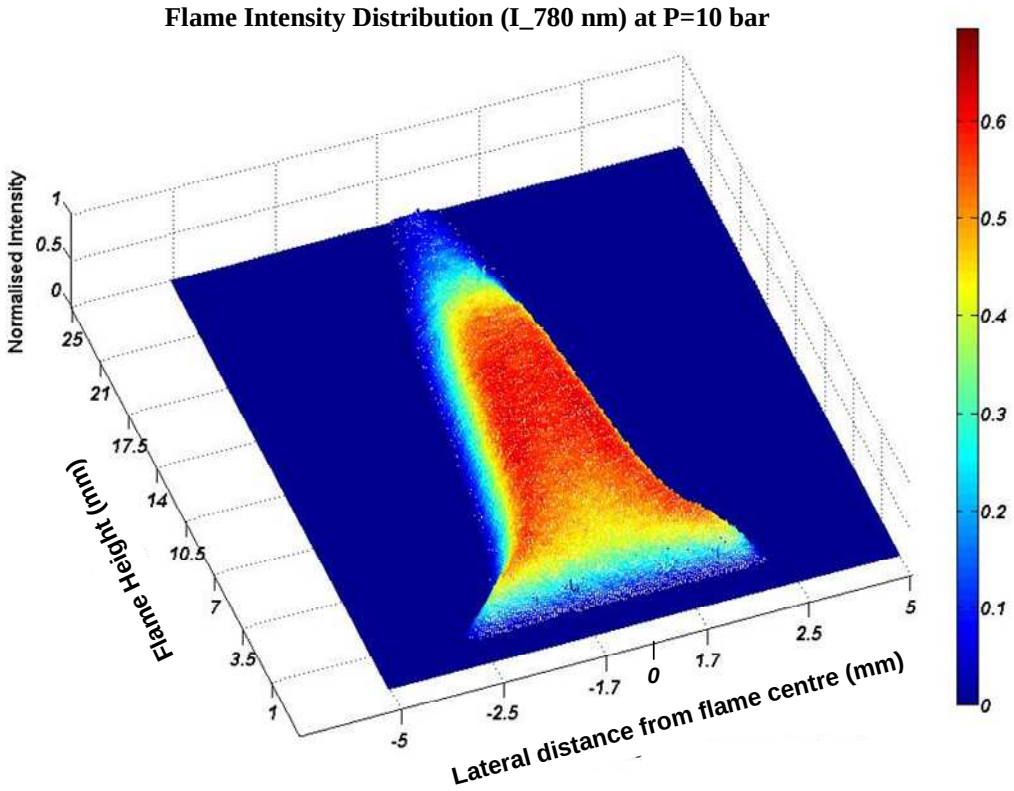

Figure 6-8: Monochromic (780 nm) intensity distribution of ethylene flame at 10 bar.

Figure 6-8 shows that the flame intensity is higher at regions with a higher concentration of luminous soot particles. The annular distribution of luminous soot particles is pronounced while the soot zone has moved down stream filling an increasingly larger portion of the flame due to high pressure. As it was predicted before the sensitivity of camera sensors to the 780 nm wavelength, which is closer to visible band, was found to be higher than the radiation at 1064 nm. This appears from the intensity distribution of flame pictures at these two wavelengths. The monochromic intensity distributions of the flame at 10 bar for 780 nm and 1064 nm wavelengths across the diameter of the flame, at different flame heights, are presented in Figure 6-9 and Figure 6-10 respectively.

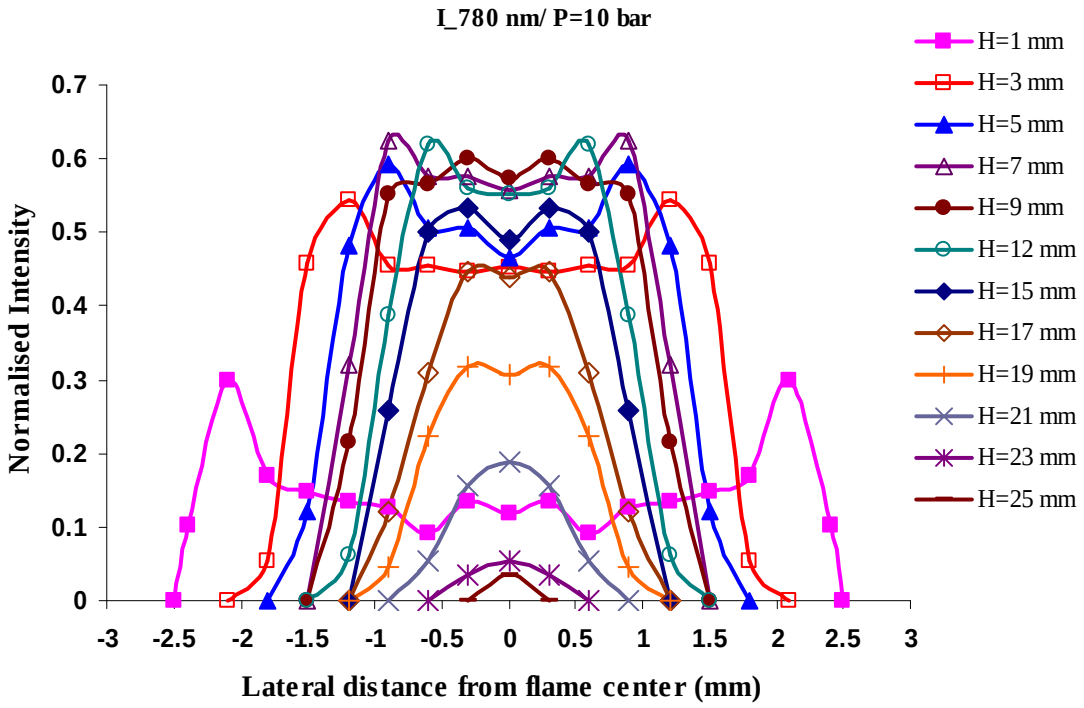

Figure 6-9: Monochromic (780 nm) intensity distribution at different heights of ethylene (0.15 slpm)-air (15 slpm) diffusion flame (P= 10 bar).

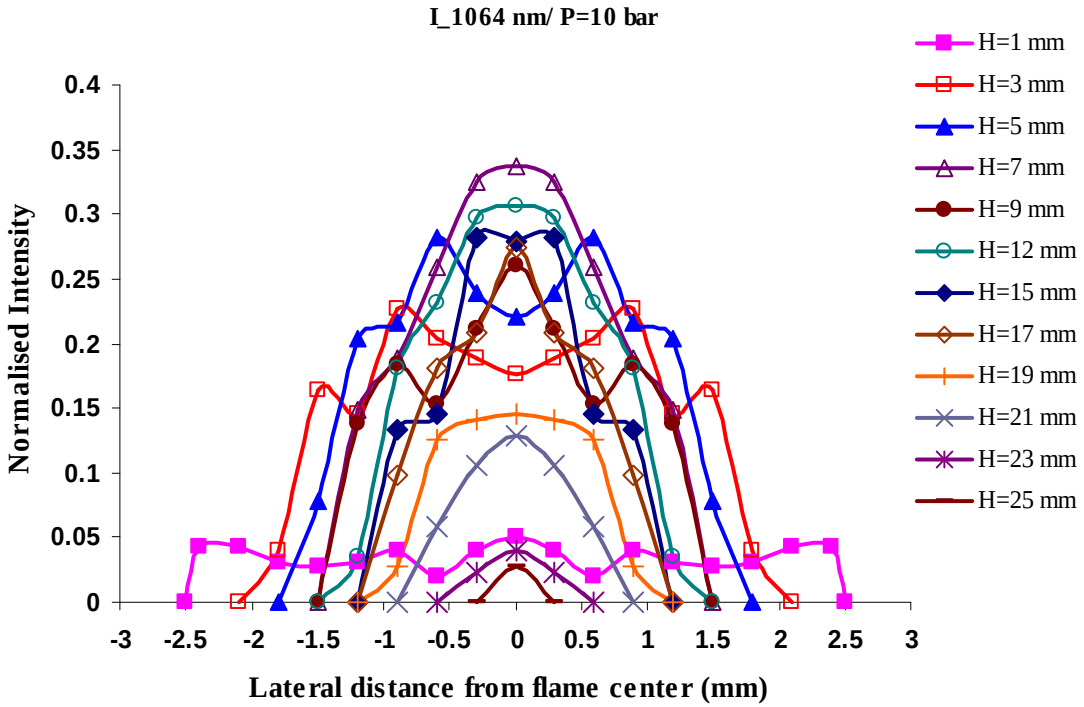

Figure 6-10: Monochromic (1064 nm) intensity distribution at different heights of ethylene (0.15 slpm)-air (15 slpm) diffusion flame (P= 10 bar).

Evolution of lateral intensity profiles with vertical position in Figure 6-9 and Figure 6-10 confirms that the flame is acceptably axisymmetric and narrows by increasing distance from the fuel nozzle exit. This radiation intensity, in the monochromic flame pictures, mostly belongs to the soot particles in the diffusion flame as grey bodies. Recall that we chose these two filters in NIR spectrum to avoid the radiation from other gas molecules and free radicals, in order to collect just the radiation of soot particles. Thus the trends of the intensity profiles are directly related to the soot concentration and temperature profiles. The redial profile of soot is typical of an ethylene diffusion flame. At the lower part of the flame soot is mostly distributed in an annular region, whereas the concentration is almost flat at higher flame heights above the fuel nozzle exit (H). The intensity is mostly higher at the outer band of the flame (in an annular region) and lower at the flame centreline core. This is believed to be due to a higher concentration of luminous soot particles at the outer band of the flame. In the middle part of the flame, soot concentration and emission increases, the sooty ring narrows and the profile evolves to a flat and then to a parabolic shape at the flame tip. Lower intensities at higher positions of the flame indicate the cooling of the soot particles by radiative losses.

The maximum soot emission at the flame centreline was observed to occur at H=18~19 mm and H=7 to 9 mm for the ethylene flames at P=1 bar and P=10 bar respectively (see Figure 6-11). Note that at atmospheric pressure the ethylene flame centreline, below H=7 mm is relatively free of soot particles. The first intensity is recorded at this height of the flame. However increasing the pressure to P=10 bar has extended the soot zone towards the burner rim. As a result the flame images, at both wavelengths, were recorded with the high intensities at the lower part of the flames. From H=19 mm of flame at P=10 bar to the flame tip, the intensity of the flame tends to be higher at the centreline in comparison with the annular band at the same height. This

is because the soot annular and core soot distribution are joining together and the peak soot concentration is observed on the flame centreline. Figure 6-11 also shows that the intensity at the centreline increases by distance from the fuel nozzle tip. This occurs up to a certain point and then it starts to decrease when the position increases further downstream of the flame. The diagrams also show the range of the flame heights at two pressures. The flame height at 1 bar is measured to be 31 mm and it is reduced to its minimum of 25 mm at 10 bar. This reduction of the flame height is believed to be due the extension of soot region further upstream towards the burner rim and also escaping of none-fully oxidized carbon particles (smoke) from the flame tip. These cause lowering the luminous flame tip position. The full range of the intensity results shows that the height of this diffusion flame increases, first by pressure up to 2 bar and then starts to decrease to its lowest level at 10 bar. The flame height at 1 bar was measured to be 31 mm and then it increased to 32 mm at 2 bar. By further increase of pressure, the flame heights were measured to decrease to 31, 28, 26 and 25 at pressures 4, 6, 8 and 10 bar respectively.

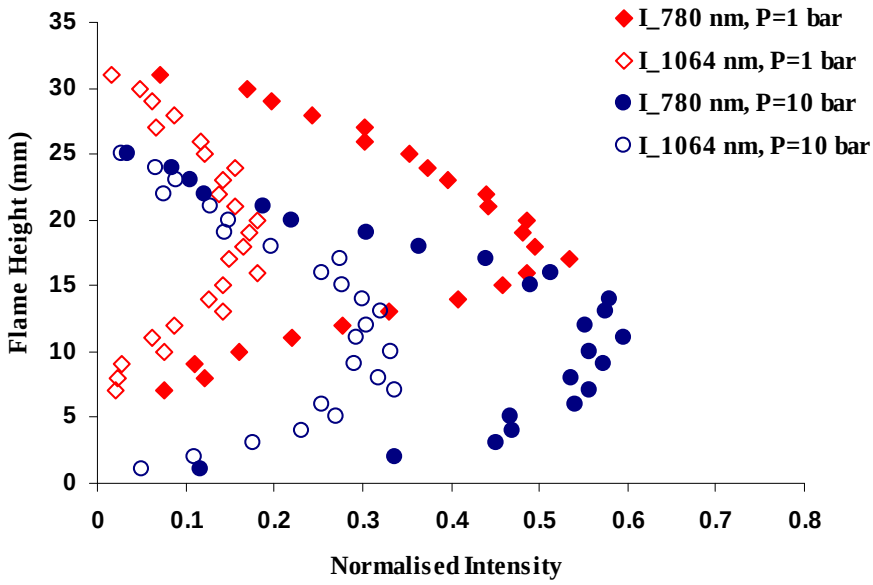

Figure 6-11: Two-colour intensity distribution along the flame centreline at P=1 bar and P=10 bar.

Radiative emission by flames is a useful source of information for nonintrusive combustion diagnostics as it carries characteristic information about the flame species such as combustion gases and soot.[151] Continuum emission sourced by flame soot can be detected and processed to extract information on the physical variables that govern the intensity of the emission, such as temperature and concentration of soot. In this study, measured intensities are utilised to infer soot temperature profile from two-colour pyrometry technique in the NIR region.

By means of a MATLAB® program, the integrated temperature at each point has been calculated by the intensity ratio of the two wavelengths. Equation 6.7 indicates that the two-colour method measures temperature based on the signal ratios at two different wavelengths without the prior knowledge of the real existence intensities at these wavelengths. To investigate solely the effect of intensity ratio (*R*), by considering an average for instrument factor (*S*) from the calibration curve (Figure 6-3), the trend of temperature as a function of the ratio of intensities is plotted in Figure 6-12.

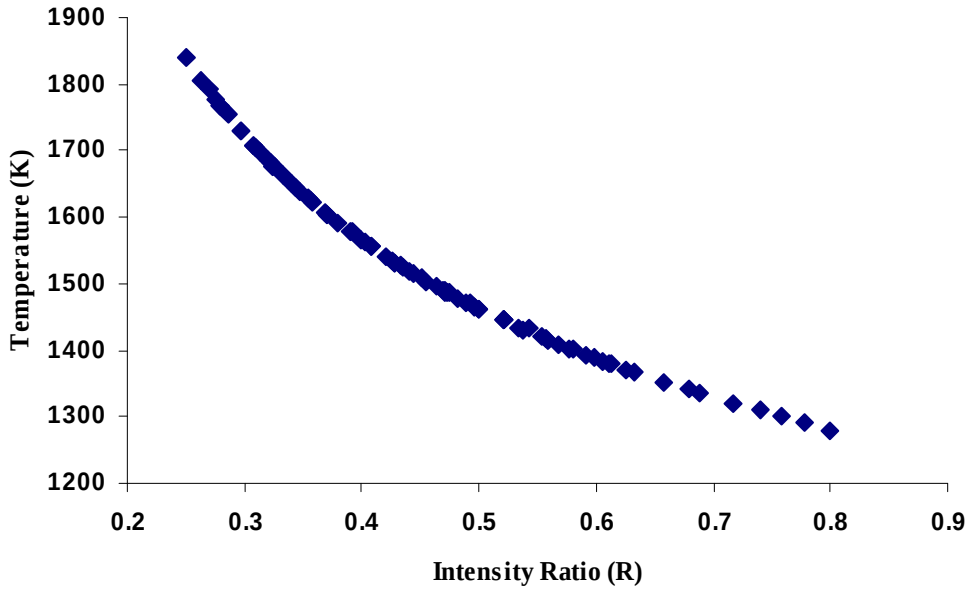

Figure 6-12: Two-colour temperature profile as a function of intensity ratio (R) by considering an average for instrument factor (S).

This graph suggests a series of hyperbola contour lines for different values of '*S*'. As the flame intensity at 1064 nm wavelength is mainly lower than the intensity at 780 nm, the intensity ratio (*R*) is found to be normally less than one. Figure 6-12 indicates that the two-colour temperature is higher at lower amounts of '*R*' and visa versa, by increase in '*R*' the soot temperature tends to be decreased.

The temperature results obtained by applying two-colour method in the NIR region have been shown to be consistent with the pyrometry results. Since two-colour data are based on measurements of soot emission, temperatures can only be determined in locations where sufficient soot exists to provide a resolvable signal. Soot temperature profiles along the flame centreline of an ethylene (0.15 slpm)–air (15 slpm) diffusion flame as a function of height along flame axis at different pressures are presented in Figure 6-13. The temperature plot at 1 bar starts from H=7 mm, as the flame at lower positions are relatively free of soot concentration. The temperature then slightly increases up to H=9 mm then drops off at H=9-14 mm, followed by a region where the temperature level slowly climbs up to H=19 mm. Then the temperature decreases at a constant gradient and the temperature profile finishes with a small climb of temperature at the flame tip. In this flame the maximum temperature of 1873 K was recorded at H=19 mm which has the maximum intensity level of the flame at 780 nm wavelength and the ratio of intensities (*R*) is also a minimum (see Figure 6-11). The minimum temperature was measured to be 1750 K near the flame tip (H=27 mm).

By increasing the chamber pressure from atmospheric pressure to 2 bar it was observed that the soot concentration dramatically increased. The flame was narrowed down by pressure and the soot region extended down towards the burner rim. Therefore, the flame intensity was increased at the lower flame heights. The soot temperature could be measured at the lower parts of the flame (from H=4 mm).

It was observed that a large temperature drop occurred at all the heights along the flame centreline. The maximum recorded temperature at this pressure was found to be 1789 K at H=7 mm whilst the minimum temperature was found to be 1350 K at the flame tip (H=32 mm). The lowest temperature drop was found to be 34 K at H=7 mm, however, the highest drop was measured to be 416 K at H=31 mm (the flame tip). A large temperature decrease at the flame tip is linked to the cessation of soot oxidation which leads to smoking flames. For these flames, a significant amount of soot survives the oxidation region of the flame. The temperature drop at H=27 mm, which is the last turning point on the temperature profile at atmospheric pressure, in comparison with the corresponding point in the flame at a pressure of 2 bar, is about 277 K. In the flame at 2 bar, the luminosity from soot becomes noticeably less intense with increasing height above H=27 mm. The average soot temperature drop between flames at 1 and 2 bar was measured to be about 175 K.

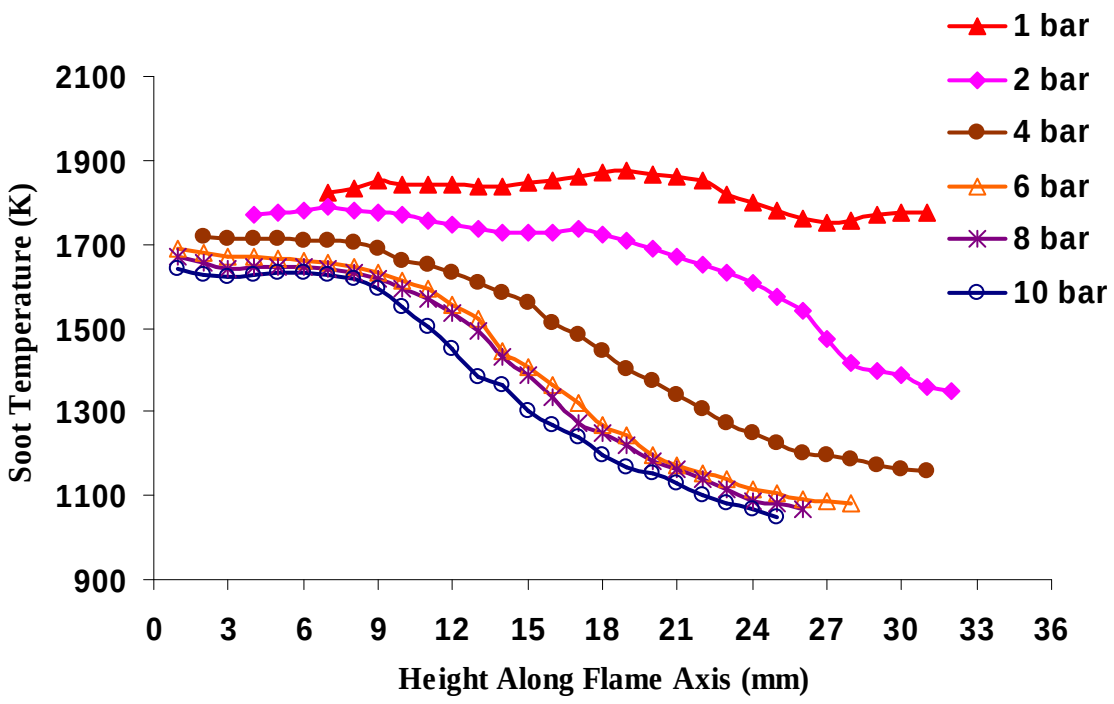

Figure 6-13: Soot temperature along the flame centreline as a function of flame height (axial location along the flame axis) at different pressures.

Ethylene flame under 4 bar pressure shows an initial high temperature of 1717 K at H=2 mm which decreases in the region, H=2-8 mm to 1701 K. This is followed by a zone in the middle of the flame where the temperature decreases with height at an almost constant gradient, up to H=26 mm. This gradient then decreases from this point up to the flame tip, where the minimum temperature at this pressure has been recorded (1158 K). The lowest temperature drop between flames at 2 bar and 4 bar was measured at H=4 mm to be 58 K and the highest drop is at H=23 mm which is 360 K. The average temperature drop between flames at 2 and 4 bar was found to be approximately179 K.

Similar curve trends are measured for the ethylene flame at higher pressures. In smoking flames at pressures higher than 2 bar (P=4~10 bar) plots typically show an initial high temperature at the base. The temperature then reduces by a small gradient at higher positions in the flame up to about 1/3 of the flame height. This is followed by a region in the middle of flame where the temperature decreases at a higher gradient along the flame axial position. Then the rate of temperature change, decline in the upper part of the flame. The temperature decrease at the top of the flame is linked to the cessation of soot oxidation and radiant heat loss of soot particles. The maximum soot temperature of ethylene flame along the flame centreline were measured at the base of the flames to be 1688 K, 1670 K and 1641 K at pressures of 6 , 8 and 10 bar, whilst the lowest temperatures were measured at the flame tips. The average temperature drop due to pressure increase from 4 to 6 bar was measured to be about 59 K. While this average drop was measured to be 9 K and 15 K due to pressure increase from 6 to 8 bar and 8 to 10 bar respectively.

Figure 6-14 compares the maximum, average and minimum temperatures along the ethylene flame centreline at different pressures. Soot temperature results show that in diffusion flames the overall temperatures decreased with increasing pressure. It is shown that the rate of temperature drop is greater for a pressure increase at lower

pressures in comparison with higher pressures. The decrease in flame temperature with increased pressure is believed to occur because of a combination of several factors. First, the significant amount of carbon converted to soot reduces the energy available from oxidation of the fuel. Secondly, this soot leads to significant heat loss from the flame by radiation to the environment. Finally, heat conduction to the core of the flame is much higher in the highly sooting, higher pressure flames [8].

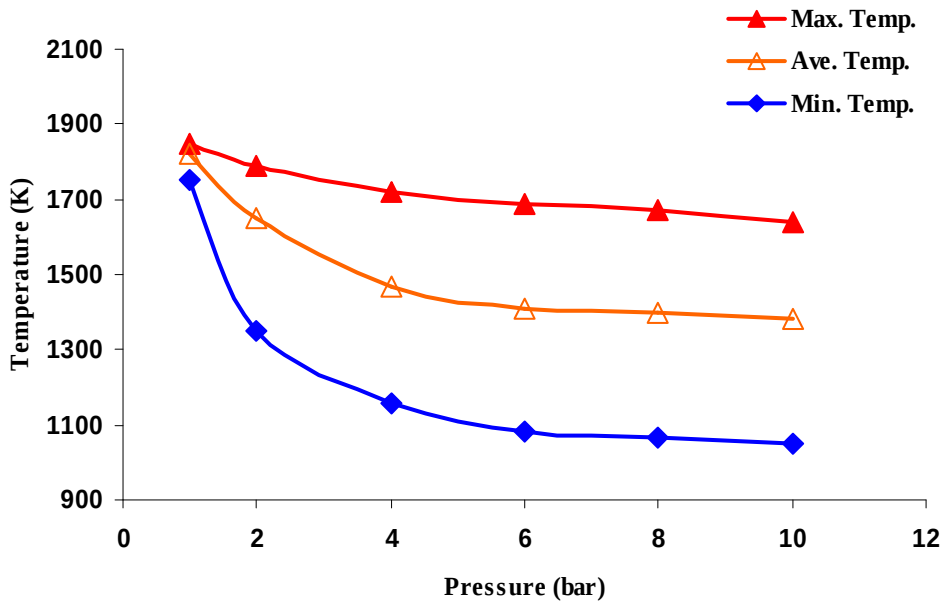

Figure 6-14: Maximum, average and minimum soot temperatures along the flame centreline at different pressures.

The temperature results obtained by applying two-colour method in the NIR region have been shown to be consistent with the pyrometry results. Since two-colour data is based on measurements of soot emission, temperatures can only be determined in locations where sufficient luminous soot exists to provide a resolvable signal. The maximum recorded error of the method was found to be about 8%. It mainly occurred at the regions with the lowest concentration of soot particles (at the flame base) or in none-fully oxidized soot clouds (flame tip). It is believed that the increased uncertainties in temperature in the lower core of the flame and on the flame tip is linked to optical limitations in recording NIR radiation when the intensity of flame is relatively low.

The temperature results of this study are consistent with the line-of-sight averaged soot temperatures results of Flower [33] in ethylene non-premixed flames. Flower [33] determined the temperatures from line-of-sight measurements of light emission, where the average soot particle temperature at the flame centre decreased with height in the upper half of the flame, except at a pressure of 1 bar. The reason for this behaviour was that all flames, except that at 1 bar, were sooting flames; therefore, soot is not completely oxidized and it escapes from the flame tip. From the reported plots, it is observed that the soot temperature drops with increasing pressure at all heights. Conversely, the increase of temperature in the lower to middle portion of the flame is enhanced by pressure, bringing the values of temperature measured at various pressures into closer agreement at about the mid height of the flames [33]. The experimental results of Thomson et al. [8] applying line of sight attenuation (LOSA) and soot spectral emission (SSE) measurements through the methane-air flame centre at pressures up to 40 bar are similar to those of Flower [33]. In flames studied by Thomson et al. [8] no soot escaped from the flame tip; therefore, all soot was oxidized within the visible yellow/orange flame region. For this reason, the average temperatures displayed an increase with downstream distance along the flame axis and the temperature curves converge at the tip of the flame. The overall temperature drop of diffusion flames by pressure, which is attributed to increased thermal radiation heat loss through increased soot volume fraction has also been reported by Bento et al. [9] and Liu et al. [20] It is reasonable to suggest that the decreased removal of soot by oxidation, observed at higher pressures in this study, results from a drop in temperature due to the increased radiative loss from the larger volume of soot formed at high pressure.

Figure 6-15 shows the soot temperature profiles at different heights above the burner exit as a function of radial location from the ethylene flame centreline at P=10 bar. An initial small axial increase in temperature from H=3 mm to H=6 mm is followed

by a general axial temperature drop at higher axial positions. The temperature profiles show radial temperature gradients across the soot annulus to a peak temperature. The temperature then decreases with more increase in the radial distance. The position of the maximum radial temperature moves towards the flame centreline at higher flame axial positions. The rate of temperature decrease with axial position increases with increasing pressure. However, the overall temperature drop with increasing pressure was observed at all flame heights, most significantly in the upper half of the flame. As the pressure increases, the visible flame gets narrower resulting in steeper radial temperature gradients. The temperature plots of Bento et al. [9] and Thomson et al. [8] generally show similar trends of temperature change as a function of radial distance. The exception to this is a steeper radial temperature gradient across the soot annulus at lower axial positions (near the burner rim). This may relate to the differences in fuel, soot loading, radiant heat loss, and pressure considered in these studies.

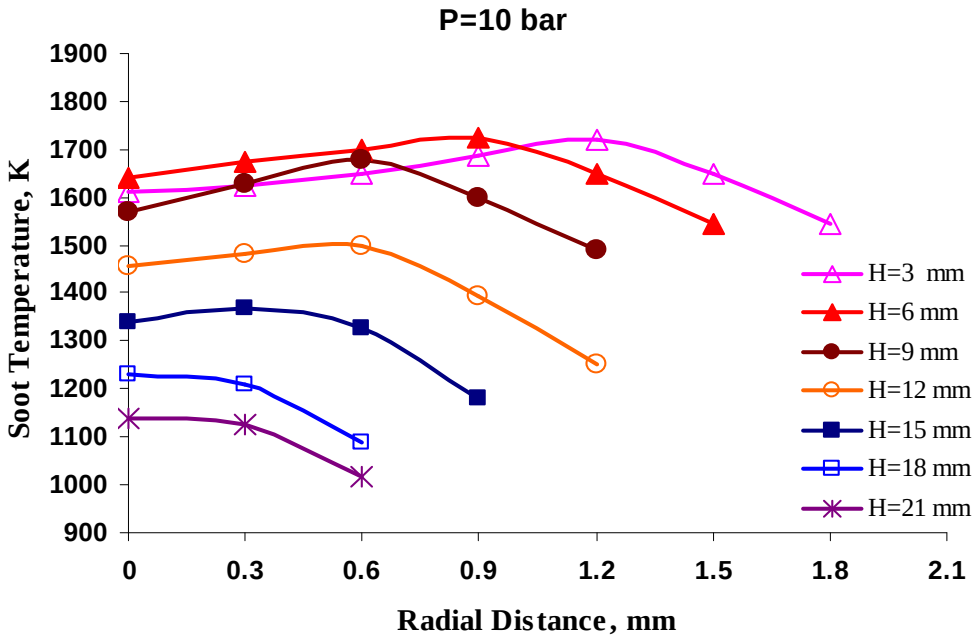

Figure 6-15: Soot temperature profiles at different heights above the burner exit as a function of radial location from the ethylene flame centreline at P=10 bar.

6.6 CONCLUSIONS

Experiments were conducted in a high-pressure burner to determine the influence of elevated pressures of up to 10 bar on the soot temperature distribution in an axisymmetric co-flow ethylene-air diffusion flame. Soot particle temperatures have been determined based on two-colour measurement of the emission of near infra-red radiation by soot particles. Two narrow band filters, of 780 nm and 1064 nm, have been chosen due to less gas molecules and free radicals radiation in these wavelengths. They also produce non-saturated photos and it is a relatively novel approach.

It was observed that flame properties are very sensitive to elevated pressures. The shape of the flame changes dramatically with increasing pressure. When the pressure increases, the axial flame height increases initially and then starts to decrease with further increases in pressure. The average cross-sectional area of the flame shows an inverse dependence on pressure. By increasing pressure it was observed that the soot formation dramatically increased and the luminous carbon zone moved downward, closer to the burner rim, filling an increasingly large portion of the flame. Also the flame that did not emit smoke at atmospheric pressure began to smoke at higher pressures. The soot emission (intensity) along the flame centreline, at two selected wavelengths in NIR, increases with distance from the fuel nozzle tip up to a certain point. It then starts to decrease when position increases farther downstream of the flame. The intensity profiles as a function of lateral distance from the flame centre at different heights showed that at the lower part of the flame, luminous soot is mostly distributed in an annular region. At higher axial heights above the fuel nozzle exit the concentration is pronounced at the flame centre, where the intensity profile is almost flat.

The temperature results obtained by applying two-colour method in the NIR region have been shown to be consistent with the pyrometry results. Since two-colour data are

based on measurements of soot emission, temperatures can only be determined in locations where sufficient luminous soot exists to provide a resolvable signal. Soot temperature measurements show that in ethylene diffusion flames the overall temperature decreased with increasing pressure, which is attributed to increased thermal radiation heat loss through increased soot volume fraction. It is shown that the rate of temperature drop is greater for a pressure increases at lower pressures in comparison with higher pressures. The average temperature drop of about 177 K is recorded along the flame centreline for a pressure increase from atmospheric to 2 bar and also from 2 bar to 4 bar. However, at higher pressures the rate of temperature drop decreases to 1/3 of the previous temperature drop. It is found that, applying two-colour pyrometry method in the NIR region, utilising a commercial digital camera, is capable of nonintrusive measurement of two-dimensional soot temperatures with a simple and relatively high accuracy approach. The maximum recorded error of the method was found to be about 8%. It mainly occurred at the regions with the lowest concentration of soot particles. To the best knowledge of the authors, applying two-colour method in the NIR region by utilising a commercial digital camera has not been reported in existing literature.

CHAPTER 7

CONCLUSIONS AND SUGGESTIONS FOR FURTHER WORK

7.1 INTRODUCTION

Experiments were conducted in a high-pressure burner to investigate the influence of elevated pressure, fuel type and fuel flow rate on the shape and buoyancy induced instabilities in the co-flow diffusion (sooty) flames. A wide range of the chamber pressure range (1 to 16 bar) and different hydrocarbon fuels (ethylene, methane and propane) were analysed. The results show that the flame structure and dynamics are strongly dependent on the pressure, fuel type and fuel flow rates. Global flame emission dynamics (Chemiluminescence) and high speed imaging have been applied to study the diffusion flame dynamics at different fuel type and flow rates and at elevated pressures.

The experiments were also conducted on methane co-flow diffusion flame at atmospheric pressure to investigate the effects of co-flow air flow rate (velocity) on the

flickering behaviour of diffusion flames. The instability behaviour of the flame was observed to be strongly sensitive to the co-flow air velocity. The most striking observation is that, when the co-flow air flow rate (velocity) is increased to a certain level, the flame oscillation is completely suppressed (stabilised). The high-speed images help to visualise the structure of the outer toroidal vortices outside the luminance flame and the subtraction of two consecutive images show how the luminance boundaries of the flame is growing at the base and tip of the flame. The schlieren images reveal how the outer vortices interact with visible flame and hot plume of gases.

Finally the experiments were conducted in the high-pressure burner to determine the influence of elevated pressures of up to 10 bar on the soot temperature distribution in an axisymmetric stable laminar ethylene-air diffusion flame. Soot particle temperatures have been determined based on two-colour measurement of the emission of near infra-red (NIR) radiation by soot particles. Narrow band photography and two-colour pyrometry have been used to gain a better understanding on effects of pressure on soot temperature distribution and quantitative understanding of soot concentration.

In the following a summary of the achievements of this PhD research in all above areas are concluded and the recommendations for future work are provided.

7.2 CONCLUSIONS

- **Fuel effects on diffusion flames at elevated pressures**

1. The results show that the flame structure and dynamics are dependent to the fuel type and very sensitive to elevated pressures.
2. The shape of the flame changes dramatically with increasing pressure. When the pressure increases, the axial flame height increases initially and then starts to decrease with further increases in pressure.

3. The average cross-sectional area of the flame (A_{cs}) shows an inverse dependence on pressure to the power of n ($A_{cs} \propto P^{-n}$), where $n=0.8\pm0.2$ for ethylene flames, $n=0.5\pm0.1$ for methane flames and $n=0.6\pm0.1$ for propane flames.
4. It was observed that the region of stable combustion was markedly reduced as pressure was increased.
5. The experiments confirm that a linear dependency between the dominant flickering frequency of the flame and pressure exists.
6. Harmonic frequencies were observed for both methane and ethylene at elevated pressures. In particular, for the ethylene flame a complex power spectrum was observed consisting of at least three peak frequency modes with their corresponding harmonics.
7. In contrast, methane flames at elevated pressures flicker with one dominant frequency and as many as six harmonic modes at elevated pressures.
8. High-speed images illustrate that the flickering and break-up of the methane flame for the tested flow rate at elevated pressures is uniform (periodic, regular and reproducible) with a pair of vortex rings at the base of flame bulge which breaking away a bulk of the flame tip with further split of this bulk, as it is burning out.
9. In contrast, ethylene flame at elevated pressures flickers and the flame tip breaks away in a more turbulent manner which can be split into at least three dominant coherent structures. Each has its own harmonics that are most likely formed as the vortices break up towards the tip of the flame as confirmed in the power spectra. Relatively high smoking tendency of the ethylene flame was found to modify the flickering behaviour of this flame.

- **Fuel flow rate effects on diffusion flames at elevated pressures**

1. The experimental results clearly demonstrate that both pressure and fuel flow rate have a strong effect on the diffusion flame dynamics.
2. The pressure is observed to change the flame shape, structure, flickering magnitude and frequency due to enhancement in the formation and growth of outer toroidal vortices.
3. The mass flow rate effects on oscillation magnitude and structure of vortices emerge from high speed images. The flickering frequency, however, remains almost constant at each pressure despite increase in fuel flow rate.
4. High-speed images have shown that the periodic break-up of the methane flame at higher flow rates (0.2 and 0.25 slpm) and elevated pressures is almost symmetric, with a pair of equal size pockets of flame highlighting the structure of the outer toroidal vortices with further separation at the tip of the breakaway flame part and it then splits into at least two wrinkled coherent flame structures.
5. However, the methane flames at lower flow rates (0.1 and 0.15 slpm) oscillate in a more waving manner and the flame tip is burnt out consisting of one portion of flame tongue.
6. The average of mean pixel intensity (MPI) values in a full sequence of flame images (proportional to the flame emission intensity) at all methane flow rates has been found to increase with pressure up to 6 bar then it starts to decrease with the further increase of pressure.
7. For methane flame at lower flow rates the maximum oscillation wavelength (λ) and maximum standard deviation (σ) of MPI have been observed to occur at 8 bar. However at higher flow rates these parameters were a maximum at 4 bar.

8. The increase in fuel flow rate increases the magnitude of flame oscillation (L_f). The flickering frequency, however, remains almost constant at each pressure.
9. It has been observed that methane flames flicker with one dominant frequency and as many as six harmonic modes at elevated pressures. The peak flickering frequency of a methane diffusion flame generally varies with the chamber pressure as a function of P^n ($f=15.7P^{0.17}$).

- **Co-flow air effects on diffusion flame dynamics**

1. The buoyant acceleration of hot gases outside the diffusion flame surface can cause shear-layer rollup, leading to the formation of toroidal vortex rings, which then interact with the flame surface or the hot plume of gasese downstream of the flame, depending upon the value of the Froude and Reynolds number.
2. The instability behaviour of the flame was observed to be strongly sensitive to the co-flow air velocity.
3. The most striking observation is that, when the co-flow air flow rate (velocity) is increased to a certain level, the flame oscillation is totally suppressed (stabilised).
4. From schlieren images it can be seen that Kevin Helmholtz instability was initiated at the very beginning of the fuel nozzle when there is no co-flow air. With the increase of air co-flow flow rate, the instability initiation point was found to move downstream gradually as outer toroidal vortices interact only with hot plume of gases father downstream of visible flame. Obviously, the visible flame will become stable if the outer instability initiation point is well downstream of the visible flame position.

5. It is found that higher flow rates of co-flow air are needed to suppress flickering of the flames at higher fuel flow rates. Therefore the ratio of the air velocity to the fuel velocity, γ, is a stability controlling parameter. The velocity ratio, γ, of co-flow methane flame as a stability controlling parameter was found to be 0.72 for the range of tested flow rates.
6. The oscillation magnitude (L_f) and the oscillation wavelength (λ) were observed to decrease by increase in the co-flow air.
7. The average oscillating flame height behaviour was bimodal with an initial stretch by increasing co-flow then starts to be decreasing by adding more co-flow, up to its completely stabilised (suppressed) level.
8. By adding more co-flow air to the stabilised flame, it was observed that the maximum width of the visible flame (b) decrease slightly.
9. The average of mean pixel intensity (MPI), which is an indicator of the average flame luminosity, increases first with the co-flow air flow rate then decreases with the further increase of co-flow air flow rate.
10. However, the standard deviation (σ) of MPI in a whole flame oscillation cycle decreases fast towards zero with the increase of co-flow air.
11. The peak flickering frequencies measured from FFT analysis of high speed imaging data and chemiluminescence results increase linearly by increase in co-flow air. However, the frequency amplitude shows a rapid decrease particularly at co-flow rates close to the suppression flow rate.
12. The dominant flickering frequency (f) of a methane diffusion flame generally varies linearly with the air co-flow rate (a) as $f=0.33\,a+11$.
13. It has been confirmed that, the flickering frequency is not a function of fuel flow rate but it is improving with co-flow air.

- **Pressure effects on soot temperature in diffusion flames (two-colour method)**

1. Soot particle temperatures have been determined based on two-colour measurement of the emission of near infra-red radiation by soot particles. Theoretical background, discreet considerations in the choice of two narrow band filters and calibration of the instrument factor are also described.
2. Two narrow band filters, of 780 nm and 1064 nm, have been chosen due to less gas molecules and free radicals radiation in these wavelengths. They also produce non-saturated photos and it is a relatively novel approach.
3. It was observed that flame properties are very sensitive to elevated pressures. The shape of the stable flame changes dramatically with increasing pressure.
4. By increasing pressure it was observed that the soot formation dramatically increased and the luminous carbon zone moved downward, closer to the burner rim, filling an increasingly large portion of the flame.
5. The flame luminosity at the flame centreline increases, first by axial position from the fuel nozzle. Then the flame became less intense with height due to cooling of the soot particles by radiative losses.
6. Despite the flame being over-ventilated with co-flow air an extended line of soot (smoke) at the flame tip appears at a pressure of 2 bar and above. Heat loss from the luminous soot particles causes by radiation leads to slower oxidation rates of soot, and eventually oxidation cannot keep up with soot production, leading to a smoking diffusion flame.
7. The intensity profiles as a function of lateral distance from the flame centre at different heights showed that at the lower part of the flame, luminous soot is mostly distributed in an annular region. At higher axial heights above the fuel

nozzle exit the concentration is pronounced at the flame centre, where the intensity profile is almost flat.

8. The temperature results obtained by applying two-colour method in the NIR region have been shown to be consistent with the pyrometry results.
9. Since two-colour data are based on measurements of soot emission, temperatures can only be determined in locations where sufficient luminous soot exists to provide a resolvable signal.
10. Soot temperature measurements show that in ethylene diffusion flames the overall temperature decreased with increasing pressure, which is attributed to increased thermal radiation heat loss through increased soot volume fraction.
11. It is shown that the rate of temperature drop is greater for a pressure increases at lower pressures in comparison with higher pressures. The average temperature drop of about 177 K is recorded along the flame centreline for a pressure increase from atmospheric to 2 bar and also from 2 bar to 4 bar. However, at higher pressures the rate of temperature drop decreases to 1/3 of the previous temperature drop.
12. It is found that, applying two-colour pyrometry method in the NIR region, utilising a commercial digital camera, is capable of nonintrusive measurement of two-dimensional soot temperatures with a simple and relatively high accuracy approach.
13. The maximum recorded error of the method was found to be about 8%. It mainly occurred at the regions with the lowest concentration of soot particles.
14. To the best knowledge of the author, applying two-colour method in the NIR region by utilising a commercial digital camera has not been reported in existing literature.

- **Summary**

The present PhD research study has provided a broad and comprehensive dataset on diffusion (sooty) flame properties under pressures from atmospheric to 16 bar as well as different fuel and flow conditions. Three major gaseous hydrocarbon fuels (methane, ethylene, and propane) were examined and the obtained data were compared.

The obtained results on flame dynamics and instabilities confirmed the low frequency oscillation of buoyant laminar jet diffusion flames at atmospheric pressures obtained by other researchers (e.g. Toong et al. [37], Kimura [38] Chen et al. [40], Chamberlin and Rose [39], Albers and Agrawal [24] and Durox et al. [23]). This research, however, presents an original research work on coupling of chamber pressure and fuel type or fuel flow rate. The peak frequencies and harmonics were found to be functions of both fuel type and pressure. Mapping the stability region of the high pressure burner and highlighting the differences between flickering structures of diffusion flames according to the type of fuel are obtained thanks to high speed photography, Chemiluminescence and image processing techniques. The obtained empirical formulation for the frequency variations by pressure as well as the oscillation magnitude and wavelength data were found to be of much interest to the combustion community due to the practical application of these results. Despite pressure, the weak dependence of the flame oscillation frequency on fuel exit velocity was confirmed.

Study of co-flow effects on buoyant jet diffusion flames flicker and stabilisation mechanism also enhanced the level of knowledge on the flame/vortex interactions and frequencies of flame flicker presented in the previous studies (e.g. Shu et al. [3], Lingens et al. [43, 45], Toong et al. [37], Kimura [38] Chen et al. [40], Gu et al. [88], Takeno and Kotani [75], Montgomery et al. [73] and Hermanson et al. [85]). This research, however, reported the complete suppression of a non-lifted oscillating diffusion flame by co-flow of air and experimentally illustrated the physical

interpretation of this interesting phenomenon. The linear increase of the flicker frequency by co-flow and the empirical formulation of its trend (for the first time) are reported.

The obtained temperature results are consistent with the findings of other researchers (e.g. Flower and Bowman [19], Flower [33], Thomson et al. [8] and Bento et al. [9]), who carried out other experimental methods including SSE and line-of-sight measurements of emission and absorption. However, in the present research it was found that applying a two-colour pyrometry method in the NIR region, utilising a commercial digital camera, is capable of non-intrusive measurements of two-dimensional soot temperatures with a simple, low cost and relatively high accuracy system. Moreover, the trends of stable flames height variations by pressure were traced and empirical relationships between pressure and cross-sectional area of these flames were proposed according to the fuel type.

As was expected, a significant understanding of combustion dynamics and instabilities and soot temperature distribution, at atmospheric, high pressure and sooty conditions was gained from the presented results.

7.3 SUGGESTIONS FOR FURTHER WORK

From the findings in this research work, the following insights have been suggested for future research:

- **Further research on the fuel variability effects on diffusion flames dynamics at elevated pressures:** Further investigation on the coupling effects of pressure and fuel type and flow rate on diffusion flame dynamics, flickering behaviour and instabilities are highly recommended. Lack of knowledge in these fields motivates the study of the diffusion flame dynamics in different gaseous hydrocarbon fuels (e.g. methane, ethylene, propane and butane) as well as biogas

and biomass fuels. The mixture of these fuels (fuel variability effects) at high pressures is also of great interest in practical combustion devices. Subsequently, the full mapping of the stability regime in the high pressure burner should be investigated for each fuel at different flow rates and co-flow conditions. Part of this investigation might also include the effects of the burner configuration and different fuel nozzle geometry, material and size. In addition to the optical diagnostic methods, other measurement instruments can also be applied including; a hot wire anemometer for the velocity fluctuation measurement and a sound pressure level meter for the pressure fluctuation measurement.

- **Further study on the interaction mechanism of the flame and the vortices in the non-lifted co-flow diffusion flames utilising different visualisation techniques:** The exact mechanism of flame flickering in diffusion flames as a buoyancy-induced instability is not fully understood. The flickering of a laminar diffusion flame is known to be caused by the interaction of the flame and the vortices, both inside and surrounding the flame jet as discussed previously. The vortex dynamics are believed to play a vital role in the formation of different flickering modes in oscillating flames. Therefore the study of these vortices and their interactions with the flame, particularly at elevated pressures, is of great importance to the understanding of the instability mechanism of oscillating laminar and turbulent flames. Utilising different visualisation techniques such as high speed schlieren (to visualise the outer flame vortex dynamics and their interaction with the co-flow air) and laser-based diagnostic techniques such as Laser Sheet Tomography (LST), Planar Laser Induced Fluorescence (PLIF) and Mie-scattering (to correlate between the invisible flow field and the visible flame) are highly recommended. In addition, employing image processing

techniques such as subtraction of consecutive high speed images and flame colour characterisation techniques may provide more insight in to the generation, growth, movement and interactions of these vortices.

- **Numerical study of instabilities in oscillating co-flow diffusion flames:** The general problem of instability in high pressure combustion systems affects all measurements and flame properties. For the present research the flame became more unstable at higher flow rates and pressures. Also increase at co-flow air modified the instability of the flame by a linear increase in flickering frequency and stabilisation at a certain air flow rate. These results show the influence of these parameters on buoyancy induced instabilities (e.g. Kelvin-Helmholtz and Rayleigh-Taylor) on different gaseous flames. Further insight on the roots, effects and prevention methods of the combustion instabilities may be gain from numerical (simulation) study using commercial (e.g. Fluent and CHENKIN) and domestic software. The chemistry of combustion, reaction processes and species may be considered in more details by using commercial CHENKIN software in conjunction with Fluent to investigate the effects of chemistry on flickering behaviour of sooty flames. To date, detailed explanations for high-pressure mechanisms and how they may differ from atmospheric pressure mechanisms is still quite obscure. Therefore, further research into the mechanisms under pressurised conditions is important to help establish a greater degree of knowledge on this matter.

- **Online measurements of soot temperature and concentration in a flickering flame:** In the present study, two-colour pyrometry method in the NIR region, utilising a commercial digital camera, was shown to be a capable and accurate approach for achieving two-dimensional soot temperatures in a stable flame.

Soot radiation at two different wavelengths was found to be proportional to both soot temperature and concentration. During the experiments with the propane flame, it has also been observed that soot can influence the flame flicker to such an extent that the oscillation is completely suppressed. Furthermore, the temperature drop in ethylene diffusion flame by increased pressure modified the flame structure by producing an extended line of soot at the flame tip (smoking flame). Thus simultaneous study on soot formation, concentration and oxidation along with the temperature distribution in a flickering diffusion flame will also enhance understanding of the impact of soot on the flame flicker. In practical systems, investigation of combustion phenomena under actual operating conditions at high pressure is of critical importance. Online and continuous, two or three dimensional measurements of soot volume fraction and temperature distribution are highly desirable in modern combustion systems, such as gas turbines. In order to utilise two-colour method for this purpose, it is important to collect both narrow band images simultaneously. This is due to point-to-point nature of the measurements in optical soot diagnostics methods. Stereo imaging technique, using beam splitter or prism, or utilising two digital cameras with a synchronising system in addition to a proper calibration procedure may be considered as the main solutions.

REFERENCES

1. Bassi, J., *Terahertz time domain spectroscopy of high-pressure flames*, in *School of Mechanical, Aerospace and Civil Engineering*. 2007, University of Manchester: Manchester, UK.

2. Davis, R. W., et al., *Preliminary results of a numerical-experimental study of the dynamic structure of a buoyant jet diffusion flame.* Combustion and Flame, 1991. **83**(3-4), p. 263-270.

3. Shu, Z., Aggarwal, S. K., Katta, V. R., and Puri, I. K., *Flame-vortex dynamics in an inverse partially premixed combustor: The Froude number effects.* Combustion and Flame, 1997. **111**(4), p. 276-286.

4. Gaydon, A. G. and wolfhard, H. G., *Flames, Their Structure, Radiation and Temperature*. 4th ed. 1979, London: Chapman and Hall Ltd.

5. Haynes, B. S. and Wagner, H. G., *Soot formation.* Progress in Energy and Combustion Science, 1981. **7**(4), p. 229-273.

6. Shurupov, S. V., *Some factors that govern particulate carbon formation during pyrolysis of hydrocarbons.* Symposium (International) on Combustion, 2000. **28**(2), p. 2507-2513.

7. Thomson, K. A., *Soot formation in annular non-premixed laminar flames of methane-air at pressures of 0.1 to 4.0 MPa*, in *Mechanical Engineering* 2005, PhD. Thesis, University of Waterloo: Waterloo, Canada.

8. Thomson, K. A., et al., *Soot concentration and temperature measurements in co-annular, non-premixed CH4/air laminar flames at pressures up to 4 MPa.* Combustion and Flame, 2005. **140**(3), p. 222-232.

9. Bento, D. S., Thomson, K. A., and Gülder, O. L., *Soot formation and temperature field structure in laminar propane-air diffusion flames at elevated pressures.* Combustion and Flame, 2006. **145**(4), p. 765-778.

10. Gohari Darabkhani, H., Bassi, J., Huang, H. W., and Zhang, Y., *Fuel effects on diffusion flames at elevated pressures.* Fuel, 2009. **88**(2), p. 264-271.

11. Faraday, M., *The Chemical History of a Candle,* ed. F.C.S. William Crookes. 1908, London: Chatoo and Windus.

12. Cheung, K. Y., *3D diagnostics based on optical and digital image processing*, in *School of Mechanical, Aerospace and Civil Engineering*. 2006, The University of Manchester: Manchester. p. 253.

13. Bassi, J., Naftaly, M., Miles, B., and Zhang, Y., *The investigation of sooty flames using terahertz waves.* Flow Measurement and Instrumentation, 2005. **16**(5), p. 341-345.

14. EHI-UUJAMHAN, A. O., *Chemiluminescence studies and flame dynamics of simulated biogas,* in *MACE*. 2008, The University of Manchester: Manchester. p. 219.

15. Charwath, M., Hentschel, J., Bockhorn, H., and Suntz, R., *Behavior of moderately oscillating sooting methane-air diffusion flames.* Flow, Turbulence and Combustion, 2009. **82**(4), p. 1-17.

16. McCrain, L. L. and Roberts, W. L., *Measurements of the soot volume field in laminar diffusion flames at elevated pressures.* Combustion and Flame, 2005. **140**(1-2), p. 60-69.

17. Miller, I. M. and Maahs, H. G., *High-Pressure Flame System for Pollution Studies with Results for Methane-Air Diffusion Flames*. 1977, NASA Technical Report.

18. Schalla, R. L. and McDonald, G. E., *Mechanism of smoke formation in diffusion flames.* Proceedings of the Combustion Institute, 1955. **5**, p. 316-324.

19. Flower, W. L. and Bowman, C. T., *Soot production in axisymmetric laminar diffusion flames at pressures from one to ten atmospheres.* Proceedings of the Combustion Institute, 1986. **21**(1), p. 1115-1124.

20. Liu, F., Thomson, K. A., Guo, H., and Smallwood, G. J., *Numerical and experimental study of an axisymmetric coflow laminar methane-air diffusion flame at pressures between 5 and 40 atmospheres.* Combustion and Flame, 2006. **146**(3), p. 456-471.

21. Joo, H. I. and Gülder, Ö. L., *Soot formation and temperature field structure in co-flow laminar methane-air diffusion flames at pressures from 10 to 60 atm.* Prococeedings of Combustion Institute, 2009. **32**(1), p. 769-775.

22. Lee, W. and Na, Y. D., *Soot study in laminar diffusion flames at elevated pressure using two-colour pyrometry and Abel inversion.* JSME Int. J., Series B: Fluids and Thermal Engineering, 2000. **43**(4), p. 550-555.

23. Durox, D., Yuan, T., and Villermaux, E., *The effect of buoyancy on flickering in diffusion flames.* Combustion Science and Technology, 1997. **124**(1-6), p. 277-294.

24. Albers, B. W. and Agrawal, A. K., *Schlieren analysis of an oscillating gas-jet diffusion flame.* Combustion and Flame, 1999. **119**(1-2), p. 84-94.

25. Turns, S. R., *An Introduction to Combustion: Concepts and Applications* 2Rev ed. 2000, Boston ; london: McGraw-Hill, p. 676.

26. Mandatori, P. M. and Gülder, Ö. L., *Complete conversion of ethane to soot in a coflow laminar diffusion flame at 3.65 MPa.* Combustion and Flame, 2007. **150**(4), p. 400-403.

27. Roper, F. G., Smith, C., and Cunningham, A. C., *The prediction of laminar jet diffusion flame sizes: Part 11. Experimental verification.* Combustion and Flame, 1977. **29**(C), p. 227-234.

28. Kitano M. and Otsuka Y., *Suppression effects of stretching flow on soot emission from laminar diffusion flames.* Combustion Science and Technology, 1985. **42**(3), p. 165 - 183.

29. Glassman, I., *Soot formation in combustion processes.* Symposium (International) on Combustion, 1989. **22**(1), p. 295-311.

30. McArragher, J. S. and Tan, K. J., *Soot Formation at High Pressures: A Literature Review*. Combustion Science and Technology, 1972. **5**(1), p. 257 - 261.

31. Kuhn, G. and Tankin, R. S., *Spectroscopic measurements to determine temperature and carbon particle size in an absorbing propane diffusion flame.* Journal of Quantitative Spectroscopy and Radiative Transfer, 1968. **8**(6), p. 1281-1292.

32. Flower, W. L. and Bowman, C. T. *Measurments of the structure of sooting laminar diffusion flames at variable pressure*. in *Western States Section, Combustion Institute (Paper)*. 1983.

33. Flower, W. L., *Soot particle temperatures in axisymmetric laminar ethylene-air diffusion flames at pressures up to 0.7 MPa.* Combustion and Flame, 1989. **77**(3-4), p. 279-293.

34. Lee, W. and Na, Y. D. *Determination of the soot temperature in laminar diffusion flames at elevated pressures using two-wavelength pyrometry with Abel inversion*. in *International Symposium on Combustion Abstracts of Accepted Papers*. 2000.

35. Coats, C. M., *Coherent structures in combustion.* Progress in Energy and Combustion Science, 1996. **22**(5), p. 427-509.

36. Glassman, I., *Sooting laminar diffusion flames: Effect of dilution, additives, pressure, and microgravity*. Proceedings of the Combustion Institute, 1998. **1**, p. 1589-1596.

37. Toong, T.-Y., Richard F, S., John M, S., and Griffin Y, A., *Mechanisms of combustion instability.* Proceedings of the Combustion Institute, 1965. **10**(1), p. 1301-1313.

38. Kimura, I., *Stability of laminar-jet flames.* Proceedings of the Combustion Institute, 1965. **10**(1), p. 1295-1300.

39. Chamberlin, D. S. and Rose, A., *The flicker of luminous flames.* Proceedings of the Combustion Institute, 1948. **1-2**, p. 27-32.

40. Chen, L. D., Seaba, J. P., Roquemore, W. M., and Goss, L. P., *Buoyant diffusion flames.* Proceedings of the Combustion Institute, 1989. **22**(1), p. 677-684.

41. Ellzey, J. L. and Oran, E. S., *Effects of heat release and gravity on an unsteady diffusion flame.* Proceedings of the Combustion Institute, 1991. **23**(1), p. 1635-1640.

42. Katta, V. R. and Roquemore, W. M., *Role of inner and outer structures in transitional jet diffusion flame.* Combustion and Flame, 1993. **92**(3), p. 274-282.

43. Lingens, A., Neemann, K., Meyer, J., and Schreiber, M., *Instability of diffusion flames.* Proceedings of the Combustion Institute, 1996. **26**(1), p. 1053-1061.

44. Buckmaster, J. and Peters, N., *The infinite candle and its stability--A paradigm for flickering diffusion flames.* Proceedings of the Combustion Institute, 1988. **21**(1), p. 1829-1836.

45. Lingens, A., Reeker, M., and Schreiber, M., *Instability of buoyant diffusion flames.* Experiments in Fluids, 1996. **20**(4), p. 241-248.

46. Cetegen, B. M. and Ahmed, T. A., *Experiments on the periodic instability of buoyant plumes and pool fires.* Combustion and Flame, 1993. **93**(1-2), p. 157-184.

47. Papadopoulos, G., Bryant, R., and Pitts, W., *Flow characterization of flickering methane/air diffusion flames using particle image velocimetry.* Experiments in Fluids, 2002. **33**(3), p. 472-481.

48. Sunderland, P. B., Mendelson, B. J., Yuan, Z. G., and Urban, D. L., *Shapes of buoyant and non-buoyant laminar jet diffusion flames.* Combustion and Flame, 1998. **116**(3), p. 376-386.

49. Yuan, T. and Durox, D., *The effects of ambient pressure upon global shape and hydrodynamic behaviour of buoyant laminar jet diffusion flames.* Combustion Science and Technology, 1993. **92**(1-3), p. 69-86.

50. Arai, M., Sato, H., and Amagai, K., *Gravity effects on stability and flickering motion of diffusion flames.* Combustion and Flame, 1999. **118**(1-2), p. 293-300.

51. Durox, D., Yuan, T., Baillot, F., and Most, J. M., *Premixed and diffusion flames in a centrifuge.* Combustion and Flame, 1995. **102**(4), p. 501-511.

52. Sato, H., Amagai, K., and Arai, M., *Flickering frequencies of diffusion flames observed under various gravity fields.* Proceedings of the Combustion Institute, 2000. **28**(2), p. 1981-1987.

53. Sato, H., Amagai, K., and Arai, M., *Diffusion flames and their flickering motions related with Froude numbers under various gravity levels.* Combustion and Flame, 2000. **123**(1-2), p. 107-118.

54. Thomson, K. A., Snelling, D. R., Smallwood, G. J., and Liu, F., *Laser induced incandescence measurements of soot volume fraction and effective particle size in a laminar co-annular non-premixed methane/air flame at pressures between 0.5-4.0 MPa.* Applied Physics B: Lasers and Optics, 2006. **83**(3), p. 469-475.

55. Yilmaz, N., Burl Donaldson, A., and Edward Lucero, R., *Experimental study of diffusion flame oscillations and empirical correlations.* Energy Conversion and Management, 2008. **49**(11), p. 3287-3291.

56. Durao, D. F. G. and Whitelaw, J. H. *Instantaneous Velocity and Temperature Measurements in Oscillating Diffusion Flames*. in *Proceedings of the Royal Society of London. Series A, Mathematical and Physical Sciences (1934-1990).* 1974.

57. Hamins, A., Yang, J. C., and Kashiwagi, T., *An experimental investigation of the pulsation frequency of flames.* Proceedings of the Combustion Institute, 1992. **24**(1), p. 1695-1702.

58. Grant, A. J. and Jones, J. M., *Low-frequency diffusion flame oscillations.* Combustion and Flame, 1975. **25**(C), p. 153-160.

59. Davis, R. W., et al., *A numerical/experimental study of the dynamic structure of a buoyant jet diffusion flame.* Theoretical and Computational Fluid Dynamics, 1994. **6**(2-3), p. 113-123.

60. Chen, L. D., Roquemore Wrdci, W. M., Goss, L P. and Vilimpoc, V., *Vorticity Generation in Jet Diffusion Flames.* Combustion Science and Technology, 1991. **77**, p. 41-57.

61. Agrawal, A. K., Cherry, S. M., and Gollahalli, S. R., *Effects of Buoyancy on Steady Hydrogen Gas-jet Diffusion Flames.* Combustion Science and Technology, 1998. **140**(1-6), p. 51-68.

62. Davis, R. W., Moore, E. F., Santoro, R. J., and Ness, J. R., *Isolation of Buoyancy Effects in Jet Diffusion Flame Experiments.* Combustion Science and Technology, 1990. **73**(4), p. 625 - 635.

63. Ghoniem, A. F., Lakkis, I., and Soteriou, M., *Numerical simulation of the dynamics of large fire plumes and the phenomenon of puffing.* Proceedings of the Combustion Institute, 1996. **26**(1), p. 1531-1539.

64. Williams, T. C., Shaddix, C. R., Schefer, R. W., and Desgroux, P., *The response of buoyant laminar diffusion flames to low-frequency forcing.* Combustion and Flame, 2007. **151**(4), p. 676-684.

65. Katta, V. R., et al., *Impact of soot on flame flicker. Proceedings of the Combustion Institute,* 2009. **32**(1), p. 1343-1350.

66. Mishra, D. P. and Kiran, D. Y., *Experimental studies of bluff-body stabilized LPG diffusion flames.* Fuel, 2009. **88**(3), p. 573-578.

67. Sato, H., Amagai, K., and Arai, M., *Flickering frequencies of diffusion flames observed under various gravity fields.* Proc.Combust. Instit., 2000. **28**(2), p. 1981-1987.

68. Bahadori, M. Y., Zhou, L., Stocker, D. P., and Hegde, U., *Functional dependence of flame flicker on gravitational level.* AIAA Journal, 2001. **39**(7), p. 1404-1406.

69. Chen, L. D., et al., *Time evolution of a buoyant jet diffusion flame.* Proceedings of the Combustion Institute, 1992. **24**(1), p. 303-310.

70. Chen, Y.-C. and Bilger, R. W., *Stabilization mechanisms of lifted laminar flames in axisymmetric jet flows.* Combustion and Flame, 2000. **123**(1-2), p. 23-45.

71. Eickhoff, H. and Winandy, A., *Visualization of vortex formation in jet diffusion flames.* Combustion and Flame, 1985. **60**(1), p. 99-101.

72. Karim, G. A., Wierzba, I., and Hanna, M., *The blowout limit of a jet diffusion flame in a coflowing stream of lean gaseous fuel-air mixtures.* Combustion and Flame, 1984. **57**(3), p. 283-288.

73. Montgomery, C. J., Kaplan, C. R., and Oran, E. S., *Effect of coflow velocity on a lifted methane-air jet diffusion flame.* Proceedings of the Combustion Institute, 1998. **1**, p. 1175-1182.

74. Dahm, W. J. A. and Dibble, R. W., *Coflowing turbulent jet diffusion flame blowout.* Proceedings of the Combustion Institute, 1989. **22**(1), p. 801-808.

75. Takeno, T. and Kotani, Y., *An experimental study on the stability of jet diffusion flame.* Acta Astronautica, 1975. **2**(11-12), p. 999-1008.

76. Vanquickenborne, L. and van Tiggelen, A., *The stabilization mechanism of lifted diffusion flames.* Combustion and Flame, 1966. **10**(1), p. 59-69.

77. Terry, S. D. and Lyons, K. M., *Turbulent lifted flames in the hysteresis regime and the effects of coflow.* Energy Resources Technology, 2006. **128**(4), p. 319-324.

78. Chen, Y. C., Chang, C. C., Pan, K. L., and Yang, J. T., *Flame lift-off and stabilization mechanisms of non-premixed jet flames on a bluff-body burner.* Combustion and Flame, 1998. **115**(1-2), p. 51-65.

79. Chung, S. H. and Lee, B. J., *On the characteristics of laminar lifted flames in a nonpremixed jet.* Combustion and Flame, 1991. **86**(1-2), p. 62-72.

80. Lee, B. J. and Chung, S. H., *Stabilization of lifted tribrachial flames in a laminar nonpremixed jet.* Combustion and Flame, 1997. **109**(1-2), p. 163-172.

81. Lee, B. J., Cha, M. S., and Chung, S. H., *Characteristics of laminar lifted flames in a partially premixed jet.* Combustion Science and Technology, 1997. **127**(1-6), p. 55-70.

82. Lee, B. J., Kim, J. S., and Chung, S. H., *Effect of dilution on the liftoff of non-premixed jet flames.* Symposium (International) on Combustion, 1994. **25**(1), p. 1175-1181.

83. Lee, J., Won, S. H., Jin, S. H., and Chung, S. H., *Lifted flames in laminar jets of propane in coflow air.* Combustion and Flame, 2003. **135**(4), p. 449-462.

84. Thring, M. W. and Newby, M. P., *Combustion length of enclosed turbulent jet flames.* Proceedings of the Combustion Institute, 1953. **4**(1), p. 789-796.

85. Hermanson, J. C., Sangras, R., Usowicz, J. E., and Johari, H., *Effects of coflow on turbulent flame puffs.* AIAA Journal, 2002. **40**(7), p. 1355-1362.

86. Ghosal, S. and Vervisch, L., *Theoretical and numerical study of a symmetrical triple flame using the parabolic flame path approximation.* Journal of Fluid Mechanics, 2000. **415**, p. 227-260.

87. Eickhoff, H., Lenze, B., and Leuckel, W., *Experimental investigation on the stabilization mechanism of jet diffusion flames.* Proceedings of the Combustion Institute, 1984. **20**(1), p. 311-318.

88. Gu, X., Zang, S. S., and Ge, B., *Effect on flow field characteristics in methane–air non-premixed flame with steam addition.* Experiments in Fluids, 2006. **41**, p. 829-837.

89. Beér J. M. and Chigier, N. A., *Combustion Aerodynamics*. 1983: In: Robert E. Krieger Publishing Company, FL, p. p. 68.

90. Huerre, P. and Monkewitz, P. A., *Absolute and convective instabilities in free shear layers.* Journal of Fluid Mechanics, 1985. **159**, p. 151-168.

91. Huerre, P. and Monkewitz, P. A., *Local and global instabilities in spatially developing flows.* Annual Review of Fluid Mechanics, 1990. **22**(1), p. 473-537.

92. Hamins, A., Yang, J. C., and Kashiwagi, T., *An experimental investigation of the pulsation frequency of flames.* Proceedings of Combustion Institute, 1992. **24**(1), p. 1695-1702.

93. Shaddix, C. R. and Smyth, K. C., *Laser-induced incandescence measurements of soot production in steady and flickering methane, propane, and ethylene diffusion flames.* Combustion and Flame, 1996. **107**(4), p. 418-452.

94. Lee, K.-O., et al., *Soot formation effects of oxygen concentration in the oxidizer stream of laminar coannular non-premixed methane/air flames.* Combustion and Flame, 2000. **121**(1-2), p. 323-333.

95. Katta, V. R., Blevins, L. G., and Roquemore, W. M., *Dynamics of an inverse diffusion flame and its role in polycyclic-aromatic-hydrocarbon and soot formation.* Combustion and Flame, 2005. **142**(1-2), p. 33-51.

96. Hottel, H. C. and Broughton, F. P., *Determination of true temperature and total radiation from luminous gas flames: Use of special two-colour optical pyrometer.* Industrial and Engineering Chemistry, 1932. **4**(2), p. 166-175.

97. Huang, Y. and Yan, Y., *Transient two-dimensional temperature measurement of open flames by dual-spectral image analysis.* Transactions of the Institute of Measurement and Control, 2000. **22**(5), p. 371-384.

98. Gang Lu, Yong Yan, Steve Cornwell, and Riley, G. *Temperature profiling of pulverised coal flames using multi-colour pyrometric and digital imaging techniques*. in *Instrumentation and Measurement Technology Conference*. 2005. Ottawa, Canada: IEEE.

99. Matsui, Y., Kamimoto, T., and Matsuoka, S., *Study on the application of the two-colour method to the measurement of flame temperature and soot concentration in diesel engines.* SAE Preprints, 1980(800970).

100. Zhou, H.-C., Han, S.-D., Sheng, F., and Zheng, C.-G., *Visualization of three-dimensional temperature distributions in a large-scale furnace via regularized reconstruction from radiative energy images: numerical studies.* Journal of Quantitative Spectroscopy and Radiative Transfer, 2002. **72**(4), p. 361-383.

101. Zhou, H.-C., et al., *Experimental investigations on visualization of three-dimensional temperature distributions in a large-scale pulverized-coal-fired boiler furnace.* Proceedings of the Combustion Institute, 2005. **30**(1), p. 1699-1706.

102. Zhao, H. and Ladommatos, N., *Optical diagnostics for soot and temperature measurement in diesel engines.* Progress in Energy and Combustion Science, 1998. **24**(3), p. 221-255.

103. Cashdollar, K. L., *Three-wavelength pyrometer for measuring flame temperatures.* Applied Optics, 1979. **18**(15), p. 2595-2597.

104. Levendis, Y. A., Estrada, K. R., and Hottel, H. C., *Development of multicolour pyrometers to monitor the transient response of burning carbonaceous particles.* Review of Scientific Instruments, 1992. **63**(7), p. 3608-3622.

105. Panagiotou, T., Levendis, Y., and Delichatsios, M., *Measurements of particle flame temperatures using three-color optical pyrometry.* Combustion and Flame, 1996. **104**(3), p. 272-287.

106. Svensson, K. I., *Effects of fuel molecular structure and composition on soot formation in direct-injection spray flames*, in *Mechanical Engineering* 2005, Brigham Young, Provo, Utah.

107. GIBSON, A. F., *A two-colour infra-red radiation pyrometer.* Scientific Instruments, 1951. **28** p. 153-155.

108. Gomes, G. C. F., *Temperature analysis of high-speed photographs of diesel combustion by the two-colour method*, in *Institute of Science and Technology*. 1995, The University of Manchester Manchester.

109. Kobayashi, S., Sakai, T., Nakahira, T., Komori, M., Tsjimura, K., *Measurement of flame temperature distribution in d.i. diesel engine with high pressure fuel injection*, in *SAE Paper, 920692.* 1992.

110. Kadota, T., Hiroyasu, H., and Farazandehmehr, A., *Soot formation by combustion of a fuel droplet in high pressure gaseous environments.* Combustion and Flame, 1977. **29**, p. 67-75.

111. Maahs, H. G. and Miller, I. M., *Pollutant emissions from flat-flame burners at high pressures*, in *NASA Technical Paper*. 1980, NASA Technical Paper.

112. Fischer, B. A. and Moss, J. B., *The influence of pressure on soot production and radiation in turbulent kerosine spray flames.* Combustion Science and Technology, 1998. **138**(1-6), p. 43-61.

113. Heidermann, T., Jander, H., and Wagner, H. G., *Soot particles in premixed C2H4-air-flames at high pressures (P = 30- 70 bar).* Physical Chemistry Chemical Physics, 1999. **1**(15), p. 3497-3502.

114. Renard, P. H., Thevenin, D., Rolon, J. C., and Candel, S., *Dynamics of flame/vortex interactions.* Progress in Energy and Combustion Science, 2000. **26**(3), p. 225-282.

115. Ferguson, D. H., Straub, D. L., Richards, G. A., and Robey, E. H. *Impact of Fuel Interchangeability on dynamic Instabilities in Gas Turbine Engines* in *5th U.S. National Combustion Meeting*. 2007. San Diego, CA: Western States Section of the Combustion Institute.

116. Straub, D., Ferguson, D., Casleton, K., and Richards, G. *Effects of Propane/Natural Gas Blended Fuels on Gas Turbine Pollutant Emissions*. in *5th U.S. National Combustion Meeting*. 2007. San Diego, CA: Western States Section of the Combustion Institute.

117. Burke, S. P. and Schumann, T. E. W., *Diffusion flames.* Proceedings of the Combustion Institute, 1948. **1**(2), p. 2-11.

118. Naftaly, M., Stringer, M. R., Miles, R. E., Bassi, J., and Zhang, Y. *Terahertz transmission spectroscopy of high-pressure flames*. in *The Joint 30th International Conference on Infrared and Millimeter Waves and 13th International Conference on Terahertz Electronics*. 2005. Williamsburg, VA.

119. Takahashi, F., Linteris, G. T., and Katta, V. R., *Extinguishment of methane diffusion flames by carbon dioxide in coflow air and oxygen-enriched microgravity environments.* Combustion and Flame, 2008. **155**(1-2), p. 37-53.

120. Lee, W. and Na, Y. D., *Soot study in laminar diffusion flames at elevated pressure using two-color pyrometry and Abel inversion.* JSME Int. J., Series B: Fluids and Thermal Engineering, 2000. **43**(4), p. 550-555.

121. Roper, F. G., *The prediction of laminar jet diffusion flame sizes: Part I. Theoretical model.* Combustion and Flame, 1977. **29**, p. 219-226.

122. Hottel, H. C. and Hawthorne, W. R., *Diffusion in laminar flame jets.* Symposium on Combustion and Flame, and Explosion Phenomena, 1949. **3**(1), p. 254-266.

123. Gohari Darabkhani, H. and Zhang, Y., *Methane diffusion flame dynamics at elevated pressures.* Combustion Science and Technology, 2010. **182**(3), p. 231-251.

124. Higgins, B., McQuay, M. Q., Lacas, F., and Candel, S., *An experimental study on the effect of pressure and strain rate on CH chemiluminescence of premixed fuel-lean methane/air flames.* Fuel, 2001. **80**(11), p. 1583-1591.

125. Clemens, N. T., Paul, P. H., and Mungal, M. G., *The structure of OH fields in high Reynolds number turbulent jet diffusion flames.* Combustion Science and Technology, 1997. **129**(1-6), p. 165-184.

126. De Leo, M., Saveliev, A., Kennedy, L. A., and Zelepouga, S. A., *OH and CH luminescence in opposed flow methane oxy-flames.* Combustion and Flame, 2007. **149**(4), p. 435-447.

127. Flower, W. L. and Bowman, C. T., *Short Communication.* Combustion Science and Technology, 1987. **53**(2), p. 217 - 224.

128. Gohari Darabkhani, H., Wang, Q., and Zhang, Y., *Impact of Co-flow Air on Buoyant Diffusion Flames Flicker.* Energy Conversion and Management, 2010. **under review**.

129. Turns, S. R., *An introduction to combustion: concepts and applications*. series in mechanical engineering, ed. 2000, Boston ; london: McGraw-Hill, p. 676.

130. Flower, W. L. and Bowman, C. T., *Measurements of the structure of sooting laminar diffusion flames at elevated pressures.* Symposium (International) on Combustion, 1985. **20**(1), p. 1035-1044.

131. Lee, M. P., McMillin, B. K., and Hanson, R. K., *Temperature measurements in gases by use of planar laser-induced fluorescence imaging of NO.* Applied Optics, 1993. **32**(27), p. 5379-5396.

132. Kampmann, S., Leipertz, A., Dobbeling, K., Haumann, J., and Sattelmayer, T., *Two-dimensional temperature measurements in a technical combustor with laser Rayleigh scattering.* Applied Optics, 1993. **32**(30), p. 6167-6172.

133. Vattulainen, J., Nummela, V., Hernberg, R., and Kytola, J., *A system for quantitative imaging diagnostics and its application to pyrometric in-cylinder flame-temperature measurements in large diesel engines.* Meas. Sci. Technol. , 2000. **11**, p. 103-119.

134. Gohari Darabkhani, H. and Zhang, Y. *Pressure effects on structure and temperature field of laminar diffusion flames*. in *48th AIAA Aerospace Sciences Meeting*. 4 - 7 January 2010. Orlando, Florida, USA: American Institute of Aeronautics and Astronautics.

135. Siegel, R. and Howell, J. R., *Thermal Radiation Heat Transfer*. 4th ed. 2002, New York: Taylor & Francis, p. 868.

136. Kerker, M., *The Scattering of Light and Other Electromagnetic Radiation*. 1969, New York: Academic press, p. 666.

137. Nguyen, D. and Honnery, D. *Soot and Temperature Measurement in Diesel Sprays* in *Fourth Australian Conference on Laser Diagnostics in Fluid Mechanics and Combustion*. 2005. The University of Adelaide, South Australia, Australia.

138. Jenkins, T. P. and Hanson, R. K., *Soot pyrometry using modulated absorption/emission.* Combustion and Flame, 2001. **126**(3), p. 1669-1679.

139. Tago, Y., Akimoto, F., Kitagawa, K., and Arai, N., *Measurements of surface temperature and emissivity by two-dimensional four-color thermometry with narrow bandwidth.* Energy, 2005. **30**(2-4 SPEC. ISS.), p. 485-495.

140. Flower, W. L., *Optical measurements of soot formation in premixed flames.* Combustion science and technology, 1983. **33**(1-4), p. 17-33.

141. Lee, K. O., et al., *Detailed characterization of morphology and dimensions of diesel particulates via thermophoretic sampling*, in *SAE Paper 2001-01-3572*. 2001.

142. Bruce, C. W., Stromberg, T. F., Gurton, K. P., and Mozer, J. B., *Trans-Spectral Absorption and Scattering of Electromagnetic Radiation by Diesel Soot.* Applied Optics - LP, 1991. **30**(12), p. 1537-1546.

143. Char, J. M. and Yeh, J. H., *The measurement of open propane flame temperature using infrared technique.* Journal of Quantitative Spectroscopy and Radiative Transfer, 1996. **56**(1), p. 133-144.

144. Flower, W. L. *The effect of elevated pressure on the rate of soot production in laminar diffusion flames* in *Western States Section, Combustion Institute (Paper)*. 1985. San Antonio, TX, USA; Code 8929.

145. Huang, Y., Yan, Y., and Riley, G., *Vision-based measurement of temperature distribution in a 500-kW model furnace using the two-colour method.* Measurement, 2000. **28**(3), p. 175-183.

146. Dewitt, D. P. and Nutter, G. D., *Theory and Practice of Radiation Thermometry*. 1989, New York: John Wiley & Sons Inc.

147. Larrabee, R. D., *spectral emissivity of tungsten.* JOSA, 1958. **49**(6), p. 619-625.

148. Dmitriev, V. D. and Kholopov, G. K., *Radiant emissivity of tungsten in the infrared region of the spectrum.* Journal of Applied Spectroscopy, 1966. **2**(6), p. 315-320.

149. De Vos, J. C., *A new determination of the emissivity of tungsten ribbon.* Physica, 1954. **20**(7-12), p. 690-712, IN1, 713-714.

150. Huang, H. W. and Zhang, Y., *Flame colour characterization in the visible and infrared spectrum using a digital camera and image processing.* Measurement Science and Technology, 2008. **19**(8), p. Article number 085406.

151. AyrancI, I., Vaillon, R., and Selçuk, N., *Near-infrared emission spectrometry measurements for nonintrusive soot diagnostics in flames.* Journal of Quantitative Spectroscopy and Radiative Transfer, 2008. **109**(2), p. 349-361.

APPENDIX A

Technical Specifications of IR Two-Colour Pyrometer (INFRATHERM IS 5/F**);**

Basic ranges:	800...2500 °C
Spectral range:	0.7...1.15 µm
Lens assembly:	Focusable, 250 mm and more
Spot diameter	1.5 mm for minimum distance (250mm)
Accuracy: (on black body source)	< 1500 °C ± 0.5 % of measuring value in °C ± 2 K > 1500 °C ± 1.0 % of measuring value in °C
Resolution:	< 1 °C
Temperature coeff.	± 0.25 K per K change of device case temperature
Repeatability:	0.2 % of measuring value / °C ± 2 K
Response time t90:	< 10 ms, adjustable up to 10 s
Soot factor, n:	n=0.50 ... 2.50(usually n=1.2 for sooty flames with unknown soot factor)
Switch off:	below minimum intensity (2% ... 50%, adjustable via interface)
Analog output:	Linear, switchable 0 or 4 ... 20 mA, burden: 0... 500 W
Power supply:	24 V DC ± 25 %, stabilised, ripple <50 mV
Power consumption:	Less than 3 VA (with laser pointer)
Serial interface:	RS 232 or RS 485 addressable

Parameters:	*adjustable at the converter's rear side:* soot factor, response time, 0 or 4-20 mA analog output, switch to one-channel intensity mode, online/offline *adjustable and readable via interface;* soot factor, response time, parametring the analog output, temperature sub-range, , clear time and external clear of the maximum value storage, address, bound rate *only readable;* measured value, optical thickness, spectral temperature and internal temperature of the instrument
Alignment:	non-parallax through-the-lens sighting
Peak memory:	Single or double storing peak memory clearing: timer, external clearing contact, automatically with new measuring object or via interface
Insulation:	pyrometer, analog output and serial interface are galvanically separated
Safety class:	I (according to VDE 0411)
Safety system:	IP 65 (according to DIN 40050)
Storage temperature:	-20...70 °C
Operating temperature:	0...70 °C (housing temperature)
Weight:	550 g

The spot diameter calculation in Infratherm pyrometer;

$$M_2 = \frac{a_2}{a}(M + D) - D \qquad M_1 = \frac{a_1}{a}(M - D) + D$$